Risk mapping of eMalahleni municipal area with focus on coal mining impacts

Schoeman, A.

22137122

Dissertation submitted in fulfilment of the requirements for the degree Magister Scientiae in Environmental Sciences at the Potchefstroom Campus of the North-West University

Supervisor: Me D Van Tonder

May 2016

Declaration

I, the undersigned, hereby declare that the work contained in this dissertation is my own original work and that I have not submitted in previously in its entirety or in part to any other university or intuition.

Signature:

Date: 10 December 2015

Abstract

TITLE: Risk mapping of eMalahleni municipal area with focus on coal mining impacts

KEYWORDS: Coal mining; coal fires; acid mine drainage; subsidence; air pollution; detection of coal mining impacts; environmental impacts.

Coal-mining in eMalahleni raises a number of environmental challenges, including coal fires, subsidence, acid mine drainage (AMD) and air pollution. Previous studies by a number of institutions, including the Council for Geoscience, have shown that the impact on the environment and on human health and safety in the Mpumalanga coalfields is threatening the very basic rights entrenched in the South Africa Constitution.

Coal fires and their by-products are major contributors to human health and safety problems such as respirational problems in humans, loss of productive land, etc. After the original underground board and pillar mining ceased and the mining operations abandoned the roof material between pillars sagged and collapsed. This resulted in a significant area becoming unsafe. Areas associated with subsidences cannot be used for infrastructural purposes. AMD forms when sulphides are exposed to oxygen and water. AMD can flow into drainage systems and cause heavy metals to become mobilized due to the low pH of the affected water. Air pollution in eMalahleni is generally associated with industrial smelters and coal fly ash. Air pollution can cause respiratory illnesses, cardiovascular illnesses and even death.

The focus of this study is the development of a practical method for identifying coal-mining risks. By identifying these risks, hazardous areas can be identified and human access to these areas restricted. By restricting these areas, tragic accidents can be prevented. The results that were obtained from this study can also be used by mining companies for rehabilitation purposes and for environmental risk management.

Aerial thermal infrared spectrometry is a technique which can be used to detect coal fires. The technique produces thermal infrared images which can be mosaicked in a GIS program and classified to indicate the localities of coal fires. Subsidence can be detected with Light Detection and Ranging (LIDAR). LIDAR indicates the slope elevation of objects with different colours, thus features such as subsidences can be detected. To identify the subsidences, the LIDAR image has to be analysed in a GIS program. AMD sources such as coal dumps can be located with aerial photos. However, AMD-producing minerals such as goethite have to be detected with hyperspectral satellite data. The AMD pathway can be determined by using an elevation map to identify the flow directions of rivers. Air pollution can be determined by analysing street dust

samples. Street dust can be used as a proxy for air quality impacts. Street dust results can be digitised and loaded onto ArcGIS to evaluate the data by means of Kriging estimation. A risk map of eMalahleni can be created to identify all hazardous areas with a risk rating for each potential hazard. The risk map completed for the study, successfully identified high, medium and low potential risk areas.

Uittreksel

Steenkool mynbou-aktiwiteite in die eMalahleni-omgewing veroorsaak talle omgewingsprobleme. Die omgewingsprobleme sluit onder andere in steenkoolvure, grondversakkings, suur mynwater en lugbesoedeling. Vorige studies deur verskillende instansies soos die Raad vir Geowetenskap het bewys dat die impak op die omgewing en die gesondheid en veiligheid van mense in die Mpumalanga steenkoolvelde bedreig die basiese regte in die Suid-Afrikaanse Grondwet.

Steenkoolvure en die neweprodukte van die vure is die oorsaak van enorme omgewingsprobleme soos respiratoriese siektes, verlies van produktiewe grond ens. Na die oorspronklike ondergrondse myn operasies gestop is, het die oorliggende materiaal tussen die steenkoolpilare ineen gestorte. Die ineengestorte materiaal vorm sinkgate wat die area baie onveilig maak en onbruikbaar vir infrastruktuur. Suur mynwater vorm wanneer sulfiede oksideer as gevolg van blootstelling aan water en suurstof. Suur mynwater kan in dreineringsisteme inbeweeg en swaar metale mobiliseer as gevolg van die suur mynwater se lae pH. Lugbesoedeling in eMalahleni word meestal geassosieer met industriële smelters en die vrystelling van steenkool-as. Lugbesoedeling kan asemhalingsiektes, kariovaskulêre probleme en selfs die dood veroorsaak.

Die fokus van die studie is om ŉ praktiese metode te ontwikkel om steenkoolmyn-verwante risiko's te identifiseer. Deur hierdie risiko's te identifiseer, kan gevaarlike areas geidentifiseer word en sodoende mense se toegang tot hierdie areas beperk. Deur toegang tot te beperk, kan tragiese ongelukke voorkom word. Die resultate wat verkry is vanaf die studie kan gebruik word deur mynmaatskappye vir rehabilitasie-doeleindes, sowel as vir omgewingsrisikobestuur.

Lug termiese infrarooi spektrometrie is ŉ tegniek wat gebruik kan word om steenkoolvure op te spoor. Wanneer die tegniek gebruik word, word infrarooibeelde verkry vanaf ŉ termiese infrarooi spektrometer. Hierdie beelde kan dan ge-mosaïek word in ŉ GIS-program. Die ge-mosaïekte beeld sal ŉ kaart vorm van die studie area wat die posisies van vure sal aandui. Grondversakkings kan geïdentifiseer word deur gebruik te maak van LIDAR. LIDAR dui die helling elevasie van voorwerpe aan sodat voorwerpe soos grondversakkings aangedui kan word deur gebruik te maak van kleure. Om die grondversakkings te identifiseer, moet die LIDAR data in n GIS-program geanaliseer word. Suur myn dreineringsbronne kan geïdentifiseer word deur gebruik te maak van lugfoto's. Maar suur mynwater produserende minerale soos goethite moet opgespoor word deur magnetiese en radiometriese tegnieke. Suur mynwater se vloeirigting kan bepaal word deur gebruik te maak van elevasiekaarte. Lugbesoedeling kan bepaal word deur straat-stofmonsters te analiseer. Straat-stofmonsters kan omgesit word as digitale data en gelaai word op ArcGIS. Die data kan ge-evalueer word deur Kriging. ŉ Riskiko kaart van eMalahleni kan gemaak word om al die gevaarlike areas te identifiseer met ŉ risiko gradering vir elke potensiële gevaar. Die

risiko kaart wat vir die studie gemaak is, dui die potensiële risko areas suksesvol aan as hoog, medium en laag.

Acknowledgements

This dissertation was completed with the support of different individuals and organizations.

The first person whom I wish to show appreciation to is my supervisor, Ms Danel van Tonder, who was always available when help was needed with the project. Ms Van Tonder was also part of the EOMINERS team.

I am grateful for Mr. Christopher, J. Roelofse who guided me through my research with his extensive knowledge in remote sensing research. Christopher also provided me with raw data.

Thanks to Hennie van den Berg for helping me with TNTmips with his wide-ranging understanding and experience with mosaicking in GIS.

My sincere thanks to Kopano Energy Resources and the North-West University for offering the funds that enabled the research to take place.

I would also like to express my appreciation to EOMINERS Project for providing data and equipment.

I feel a special gratitude to my parents who supported me financially and emotionally throughout the year.

Finally I would like to thank the Kent Trust Fund of the GSSA for a grant which enabled language-editing of the manuscript and preparation of high quality hard copies.

List of abbreviations

ABA	Acid-Base Accounting
AHS	Airborne Hyper Spectral imaging sensor
AMD	Acid Mine Drainage
ASTAR	Advanced Space-borne Thermal Emission and Reflectance Radiometer
ATSR	Along Track Scanning Radiometer
AVHRR	Advanced Very High Resolution Radiometer
BIRD	Bi-spectral Infrared Detection
CARA	Conservation of Agricultural Resources Act
CBFA	Coal / Biomass fly ash
DDC	Dynamic Deep Compaction
DEM	Digital Elevation Model
DInSAR	Differential Interferometric Synthetic Aperture Radar
DWA	Department of Water Affairs
EIA	Environmental Impact Assessment
EM	Electromagnetic Radiation
EOMINERS	Earth Observation for Monitoring and Observing Environmental and Societal Impacts of Mineral Resources Exploration and Exploitation
ETM	Enhanced Thematic Mapper
FFF	Fossil Fuel Foundation
GIS	Geographic Information System

GPS	Global Positioning System
ICP-MS	Inductive Coupled Plasma Mass Spectrometry
IS	Imaging Spectroscopy
LIDAR	Light Detection and Ranging
MA	Minerals Act
MODIS	Moderate Resolution Imaging Spectrometer
MPRDS	Mineral and Petroleum Resource Development Act
NEMA	National Environmental Management Act
NFA	National Forests Act
NHRA	National Heritage Resources Act
NWA	National Water Act
TDS	Total Dissolved Solids
TIR	Thermal Infrared Remote Sensing
TM	Thematic Mapper
SAR	Synthetic aperture radar
SAHRA	South African Heritage Resource Agency
SPOT	Probatoire d'Observation de la Terre
XRF	X-Ray Fluorescence

Table of contents

List of Tables

List of Figures

Chapter 1: Introduction

1.1 Background

Despite its importance as a resource, coal mining is increasingly perceived as an unsightly and environmentally damaging practice. Spontaneous combustion, subsidence, acid mine drainage (AMD) and air pollution in coal mines are historical problems which have left a legacy of environmental degradation around many South African mines (Bell *et al*., 2001:195). As environmental legislation has become more stringent, South African mining houses have been forced to take more decisive steps in controlling and managing all sources of pollution, including coal fires and subsidence on their mines (Coaltech Reasearch Association & Chamber of mines of South Africa, 2007:3).

The purpose of this study is to identify and detect environmental problems created by coal-mining practices. Once these problems have been identified and detected, rehabilitation actions can be proposed.

Pollution from traditional coal mining is a continuous threat to the environment. These threats include the emission of noxious gases, water and soil pollution, destruction of floral and faunal habitats and it is also the cause of human diseases and fatalities (Bell *et al*., 2001:195). Oxidation of pyrite and organic sulphur in coal result in the production of sulphates and sulphuric acid that can be toxic to vegetation and results in acid water infiltrating surface and ground water resources. Noxious gases such as carbon monoxide, sulphur dioxide and nitrogen oxides may be found in the surrounds of any active coal fire (Bell *et al*., 2001:202).

Coal mines in the eMalahleni area have been mined underground with board and pillar techniques which left the pillars to support the overlying roof material (Bell *et al*, 2001:197). In some areas the roofs have collapsed and allowed air to enter into old underground mines. The air caused the coal to oxidise which subsequently caused coal in the remaining pillars to spontaneously combust (Ochieng *et al*., 2010:3352).

In the eMalahleni area, underground coal fires resulting from spontaneous combustion can reach temperatures of up to 630 ˚C at the surface (Pone *et al*., 2007b:133). It is not only the toxic gases released, but also the extreme temperatures which are a risk to humans and the environment (Pone *et al*., 2007b:137).

Abandoned mining areas may potentially pose a health and safety risk due to the potential of collapsing ground. People from surrounding neighbourhoods tend to walk through these areas

where underground coal fires and voids occur, therefore these underground fires and voids need to be identified to protect the people and for rehabilitation purposes (Van Tonder, 2011:62).

According to Zhang (2004:25) there is limited knowledge of the specific geo-spatial characteristics of these underground coal fires, making rehabilitation a very dangerous undertaking. The rehabilitation is also an expensive and technically challenging endeavour. Furthermore, the monitoring requirement in these areas increases costs and risk.

The use of remote sensing techniques is becoming an increasingly valuable tool to monitor the impact of anthropogenic activities on the environment. Satellites are a source of regular and consistent data that allow for the investigation of variables changing both spatially and temporally. Satellite-derived remote sensing images are finding increased applications in the mining industry (Van Der Meer *et al*., 2012:122). However, the spatial resolution of satellite imaging is often not high enough for the monitoring of localised impacts. For this reason aerial remote sensing, using aircraft, is becoming a regular tool in the mining industry. This information could potentially provide mining houses with a management tool that is not only cost-effective, efficient and reliable, but also a regular means of monitoring potential impacts. The remote platform eliminates risk to the safety of mine personnel and allows for monitoring at relatively low costs since several monitoring variables can be accessed from a single image.

Coal fires can be detected through factors such as smoke, burnt pits and surface cracks. However, the fact that coal fires create elevated temperatures on the earth's surface makes them easy to identify through Thermal Infrared (TIR) Remote Sensing (Zhang, 2004:40).

Subsidence in eMalahleni causes substantial damage to infrastructure such as power lines and railways. It was noted during the field visit in 2013 that power lines at a site, Blesboklaagte, directly north of eMalahleni were damaged due to the occurrence of subsidence. Subsidence can be detected with various techniques such as aerial photos (Pazuniak, 1989:265), seismic investigations (Venkatanarayana & Rao, 1989:63), electromagnetic survey (Pazuniak, 1989:266), remote sensing (Engelbrecht *et al*., 2011:78) and LIDAR (Lillesand & Kiefer (1994:722). Aerial photos can be a useful source of information to identify subsidence and help obtain information about the development of the subsidence over time (Gutiérrez, *et al*., 2011:134). Remote sensing techniques can contribute to the detection and monitoring of subsidence as it provide the ability to obtain deformation measurements over large areas at reduced cost (Engelbrecht *et al*., 2011:78). A remote sensing technique known as LIDAR, can for instance be used in the detection of subsidence as it constructs a profile of elevation depths.

AMD can be detected with remote sensing techniques such as Airborne-Hyper Spectral imagining (AHS) (Banks *et al*., 2011:87).

Toxic gases released by mining activities at eMalahleni are higher than international standards (Pone *et al*., 2007a:10). Mining activities which contribute to air pollution includes: power generation, coal mining, primary metallurgical operations, secondary metallurgical operations and combustion of coal (Banks *et al*., 2011:58). The precise impact that these toxic gasses have on humans and the environment are unknown and needs advance investigation (Pone *et al*., 2007b:124). Air pollution associated with coal mining and related industries can be detected from street dust or dust traps (Zibret *et al*., 2013:4456).

1.2 Problem statement

Section 24 of South Africa's Constitution (Act 108 of 1996) stipulates that: "Everyone has the right to an environment that is not harmful to their health or well-being and the Government is required to act reasonably in order to protect the environment by preventing pollution, while promoting conservation and sustainable development, as well as building society and the economy." However, the eMalahleni coalfield does not comply with this act. The health and well-being of the community is at risk due to coal-mining impacts such as coal fires, associated industry impacts, subsidence, AMD and air pollution.

Before rehabilitation of the affected area can be done, coal fires must be detected, subsidence located, AMD traced and air pollution identified. The investigation examines techniques used in the detection of these coal-mining impacts in the eMalahleni municipal area and the application of risk mapping methods in identifying high risk areas.

This dissertation offers an object-based, multi-level, graded classification framework uniting shape, spectral, ordered and background information for the identification of coal-mining impacts. The study was undertaken to analyse the progression of human-induced landscape alteration in the coal mine affected areas around eMalahleni, Mpumalanga, South Africa by studying remote sensing data using the geographic information system. Remote sensing methods are employed in the detection of underground coal fires. Several levels of remote sensing data are used, from ground monitoring data to low altitude aircraft and satellite images. A comparison of these data sets allows for the identification of the areas where the fires occur.

The particular focus is on identification of underground coal fires by mosaicking thermal infrared images which have been obtained from an aerial thermal infrared spectrometer. Important information of the study area can then be obtained from the mosaicked images.

In previously mined areas subsidence can be seen from aerial photos; however, underground mining areas which are not visible from these photos pose a potential health and safety threat to residents due to surface collapse and subsidence formation (Bell *et al*., 2001:197). Surface

subsidence associated with coal mining activities in the eMalahleni coalfield resulted in changing the natural environment in several ways. Mining companies face challenges in the rehabilitation and the prevention of further degradation in previously mined areas. An understanding of what leads to subsidence development and the capability to predict subsidence hazards is critical to environmental management. Traditional field-based monitoring approaches to monitor and map the spatial and temporal evolution of surface subsidence, including GPS and spirit levelling, cannot be utilised safely at a number of locations. To address the safety issue of frequent visitations, remote sensing techniques such as LIDAR and satellite-borne synthetic aperture radar (SAR) can be employed. The current study applies LIDAR maps and ground stability maps in a GIS based risk assessment. By combining the aerial photos and maps, subsidence and potential subsidence can be accurately identified and the knowledge applied for remedial and rehabilitation purposes and for future infrastructure development decisions.

AMD and air pollution are not always visible. However, the impact can cause enormous environmental degradation and pose potential threats to human health. Acid water decants into the nearby Brugspruit which flows between the mine and the settlements of Kwa-Guqa and Vosman and eventually feeds into the Olifants River and the Loskop Dam. Information available from previous projects, such as the studies done by EOMINERS project, can be applied in the detection of possible air pollution and AMD.

Not only do coal-fired power stations produce air pollution, they also cause land degradation as the acidic air pollutants are deposited on the ground which then increases the acidity of the ground (WWW, 2011:3). The acidic ground is mostly not suitable for agricultural purposes.

1.3 Objectives

The main aim of the study is to detect, map and classify areas within the eMalahleni municipal area, which pose a potential risk from coal mining impacts to the environment. The objectives of the study are therefore:

- Conducting an extensive literature review on coal-mining impacts and the detection of these impacts.
- Detecting underground coal fires within eMalahleni municipal area.
- Locate potential subsidencewith in eMalahleni's municipal area.
- Identify AMD sources and pathways in drainage systems within the study area.
- Identify areas with high levels of air pollution
- Produce a risk map for the eMalahleni municipal area

1.4 Study area

eMalahleni, previously known as Witbank, is located in the Mpumalanga Province, South Africa (Figure 1). The study area will be referred to as the "eMalahleni municipal area" and is situated to the north-east of central eMalahleni and north of the N4 national road (Figure 2). The measured area of the eMalahleni municipal area is 93 km^2. Land use in the eMalahleni municipal area includes mining activities, residential housing, industrial activities and agricultural undertakings. Residential housing has developed within 500 metres of mining areas, which resulted into hazardous living conditions for the residents (EOMINERS, 2014b). The land use can be seen in Figure 3 which was constructed by means of GIS. As seen in Figure 3, agricultural and industrial activities appear to be the most dominant for land use in eMalahleni (Stewart & Troksie, 2006: 32). However, this is changing due to the amount of new mines being developed. According to an article of the Mpumalanga Province, 2013 (as mentioned by Van Tonder, (2011:20)) conflict arises between various land users, who all use the natural resources which impact negatively on each other. Examples of such conflict can be noted where mining activities impact on the agricultural sector through excessive air and water pollution and where forestry and mining threaten the conservation of biodiversity, which again impacts on the tourism potential of the area.

The land surface in the eMalahleni Municipal area is pockmarked due to the high occurrence of subsidence related to historic underground mining activities. The placement of residential and industrial areas around those areas affected by mining subsidence is clearly seen in Figure 4. These areas are dangerous due to the occurrence of underground coal fires with temperatures in excess of 400 ˚C and the regular occurrence of subsidence (Figure 4 and 5). People living in the informal settlements on the western border of eMalahleni's municipal area are exposed to health and safety threats, as footpaths pass over burning underground (Desk, 2004:13).

Coal-fired power plants and metal smelters were established in eMalahleni due to the availability of good quality coal which can be used as an inexpensive energy source (Zibret *et al*., 2013:4457). These industries contribute to the high levels of toxic gases in the atmosphere (Figure 6).

The elevation of eMalahleni is 1,500-1,700 m above sea level and forms the headwaters for three important rivers in South Africa, namely the Vaal River, Olifants River and the Pongola River (Zibret *et al*., 2013:4456). Mining activities in the region have been linked to the high levels of pollution in these river systems (Zibret *et al*., 2013:4458). Decanting AMD ponds in wooded areas can be seen in Figure 7.

Serious water quality problems exist in Mpumalanga and are mostly caused by sewerage pollution, intensive agricultural use of fertilizers and pesticides, industrial waste, mining and soil

erosion. Many of the water management areas contain high levels of toxic substances which exceed water quality guidelines for irrigated agricultural and industrial use and this can have a negative impact on crop production or increase the cost of water treatment before use (Janse Van Rensburg, 2003:10).

According to Janse Van Rensburg (2003:11) a decant point occurs at eMalahleni (located west in the study area). The point is decanting acidic brine water from old mine workings which is flooded (Figure 8). The decant point has been ponded in an effort to keep AMD from flowing into the Brugspruit (Janse Van Rensburg, 2003:11).

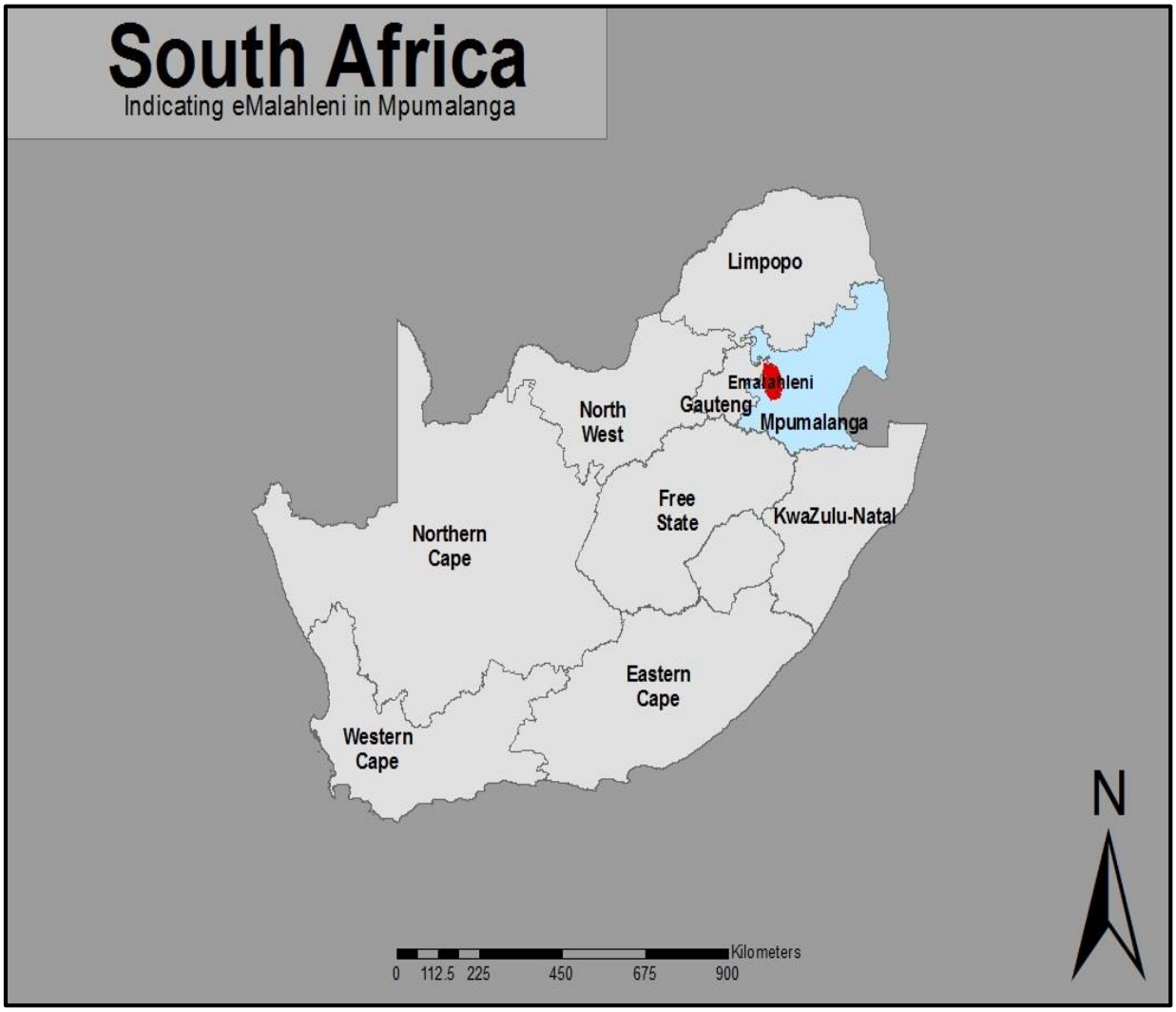

Figure 1: Location of eMalahleni in Mpumalanga.

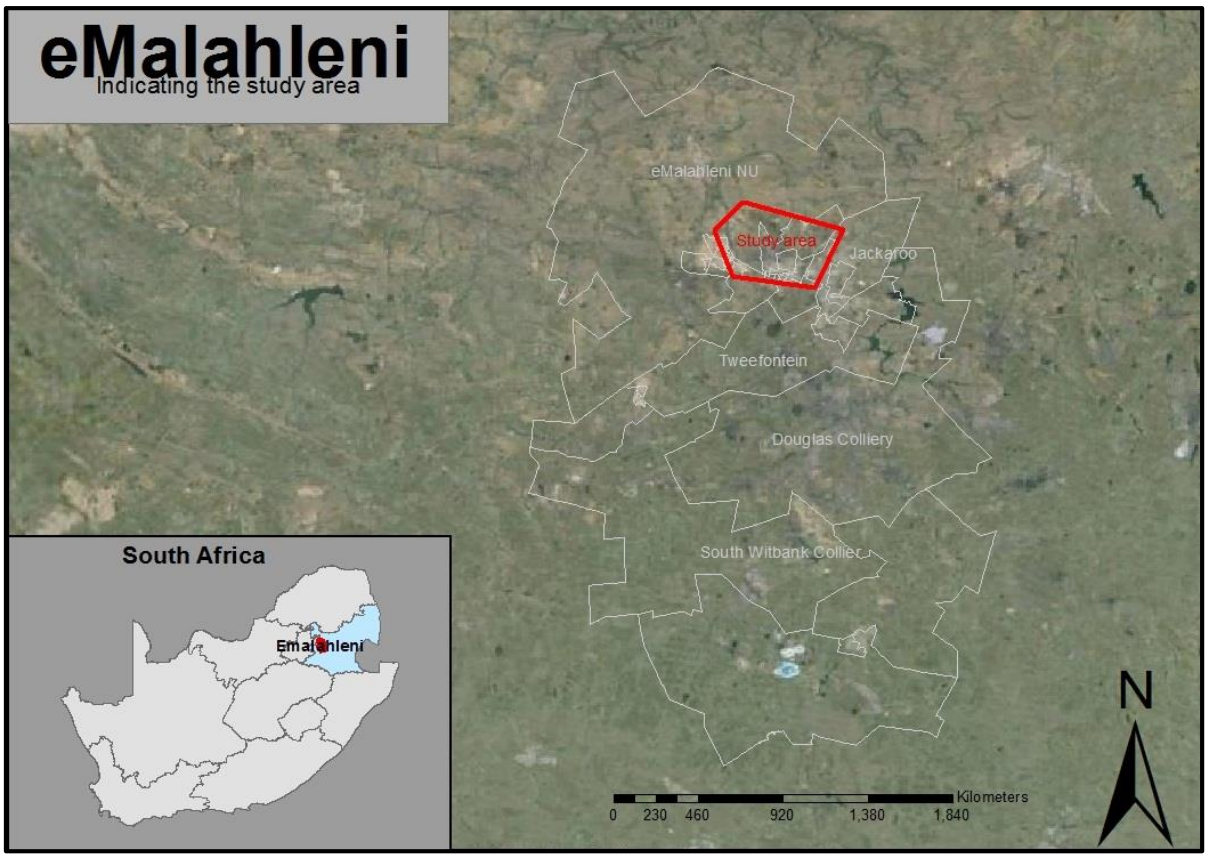

Figure 2: Location of study area in eMalahleni.

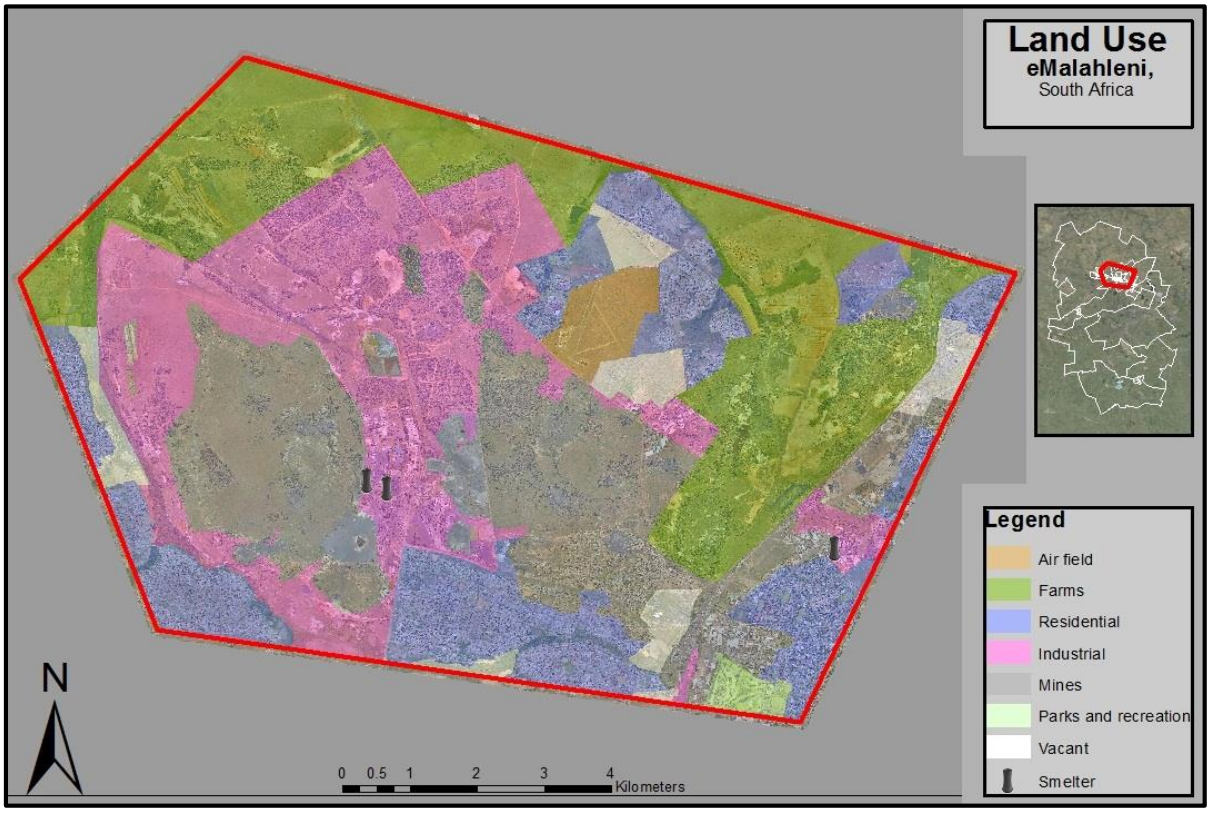

Figure 3: Map indicating the diverse land use in the eMalahleni municipal area.

Figure 4: Photo of subsidence from the air (Photo by A Schoeman, 2013).

Figure 5: Typical coal fire from a collapsed underground coal mine in eMalahleni municipal area (Photo by D van Tonder, 2011).

Figure 6: Air pollution caused by metal smelters (Photo by A Schoeman, 2013).

Figure 7: Decanting of AMD in wooded area (Photo by A Schoeman, 2013).

Figure 8: Decant point along the Brugspruit (Photo by A Schoeman, 2013).

1.5 Dissertation layout

The dissertation is structured according to the following chapters:

- **Chapter 1: Introduction**

Chapter 1 serves as the introductory chapter, and includes a background description of the dissertation, the problem statement and the objectives of the study. This chapter also includes a discussion on the study area.

- **Chapter 2: Literature review**

Chapter 2 provides a literature review based on existing research and information concerning the research objectives. The literature sources were peer reviewed articles, books and book chapters, legislation, guideline documents, reports, internet sources, newspapers and previous dissertations.

- **Chapter 3: Methodology**

This chapter provides the outline of the methodological design. It describes the research instruments and techniques used to collect the data. The methodology section furthermore describes the techniques used to analyses data to produce the final results.

- **Chapter 4: Results**

In this chapter the data analysis and results are interpreted in relation to the objectives of the study.

- **Chapter 5: Discussions**

Chapter 5 describes the results according to the following objectives:

  - Objective two: Detecting burning underground coal fires in eMalahleni municipal area.
  - Objective three: Locate potential subsidence in eMalahleni's municipal area.
  - Objective four: Identify AMD sources and pathways in drainage systems in the study area.
  - Objective five: Identify areas with high levels of air pollution
  - Objective six: Produce a risk map for the eMalahleni municipal area

- **Chapter 6: Conclusion and recommendations**

In the final chapter the outcomes of the research results are discussed in relation to the objectives of the study. Recommendations are made for further studies.

Chapter 2: Literature review

2.1 Introduction

Coal mining in eMalahleni makes a major contribution to South Africa's financial income (Pone *et al*., 2007:4a); however, these mines are responsible for a vast amount of environmental degradation and risks (Bell *et al*., 2001:195). Some of these risks include underground coal fires, subsidence, acid mine drainage (Bell *et al*., 2001:195) and air pollution (Zibret *et al.,* 2013:4455).

In this review, a systematic discussion for potential coal mining risks are discussed including the causes, the environmental problems associated with and the detection of each risk.

Finally risk mapping is discussed to ensure that all terms and the process is clearly understood.

2.2 Formation of coal

Coal accumulation occurs when peat layers (accumulations of organic matter) are formed and accumulated in swamps and marshes. For this process to occur, the climatic conditions must be ideal for rapid growth of plants. Peat is made up of 50% carbon and the rest consists of oxygen and hydrogen (McCarthy & Rubidge, 2005:201). When peat is compressed by overlaying material, the peat is heated. As peat is heated, oxygen and hydrogen are expelled and the carbon content increased. Finally, the process leads to the alteration of peat to coal through metamorphism (McCarthy & Rubidge, 2005:201). For the conversion process to take place there must be a deficiency of oxygen to restrict the oxidising of bacterial waste (Monroe *et al*., 2007:208). The amount of carbon in the coal depends on the temperature and pressure the peat has undergone (McCarthy & Rubidge, 2005:201).

The formation of coal is influenced by the following factors: tectonic and sedimentary environments, plant communities, prevailing climatic conditions and geochemical conditions such as water level, pH and salinity (Falcon, 1986a:1880). These factors influence the formation of coal by controlling the rate and degree of degradation of the plant matter (Falcon, 1986a:1880). Classification of coal is done by means of the rank, type and grade of the coal (Bruce, 2004:136). Coal rank is dependent on the degree of metamorphism the coal endured (Falcon, 1986b:1910). As the rank of the coal increases, the water content decreases and the carbon content increases (Table 1) (Bruce, 2004:137). As the peat changes into lignite, elements such as nitrogen and oxygen of the peat are driven off, and this enriches the residue with carbon (Monroe *et al*., 2007:208). As seen in Table 1, a decrease in moisture content leads to an increase in the amount of fixed carbon. The coal grade is based on the amount of inorganic impurities (clay minerals,

quartz and pyrite) in the coal. The coal type is determined by the type of organic materials present in the coal (Bruce, 2004:137).

Table 1: Coal ranks (Sherwood & Philips, 2012).

Rank	Moisture %	Volatile matter %	Fixed carbon	Original depth of burial (m)
Peat	80	9	5	
Lignite	55	20	17	Up to 1 000
Sub-bituminous	20	36	40	Up to 2 000
Bituminous	2	36	60	Up to 5 000
Semi-anthracite	1	9	87	More than 5 000

Factors which control the coal rank, includes temperature (enforced by depth of burial, igneous intrusions and geothermal influences), pressure (weight of overburden and tectonic stress) and time (Falcon, 1986a: 1880).

2.3 Coal in South Africa

2.3.1 Background

Coal is not only the most abundant fossil fuel in the world, but is also the most widely distributed (Moon *et al*., 2013:111). Coal was first discovered in KwaZulu-Natal in 1840 and has been commercially explored since the 1800s (Stratten, 1986:1868). South Africa is the fourth largest coal producer in the world (Pone *et al*., 2007a; 3). According to Mistry (2005:10) South Africa's recoverable coal assets are around 58 billion ton, equalling 10 percent of the world's total coal resources. This 10 percent excludes low-grade coal and coal with a high ash content which could increase the percentage to 35. The largest portion of South Africa's coal is bituminous grade and only two per cent is anthracite (Mistry, 2005:10). Most of the coal in South Africa is fairly shallow and can simply be extracted through open-cast mining methods (Bruce, 2004:137). Mistry (2005:10) has predicted that coal resources will be available for approximately 200 years at the present production levels.

There are 19 coalfields in South Africa spread over an area of 700 kilometres from north to south and 500 km from east to west (Hocking, 1995; Schmidt, 2008:3) (Figure 9). Generally the coal rank increases eastwards while the number of seams and their thickness decrease. Thus coal

occurring in Mpumalanga and Limpopo Provinces are usually high rank bitumin, occurring in thick seams, whereas KwaZulu-Natal coal is frequently anthracitic and found in somewhat thinner seams. The largest coal deposits are found in the Highveld and Mpumalanga Witbank coalfields. The Highveld and eMalahleni (Witbank) area is the most productive coal areas in South Africa (Hocking, 1995).

Most of the recovered coal in South Africa is used in the energy sector, as 77% of the country's energy is provided by coal (Universal coal plc., 2012). It is also said by the Fossil Fuel Foundation (FFF) (2013:16) that coal is the primary source of energy for South Africa and will continue to be so. The Witbank Coalfield produces 53% of South Africa's coal and 43% of South Africa's electricity (Pone *et al*., 2007a:5). Further, 69 million tons of coal is annually exported exported to other countries (Universal coal plc., 2012). These exports provide a sustainable source of income to South Africa. FFF (2013:8) predicts there will be a demand for coal export beyond 2040.

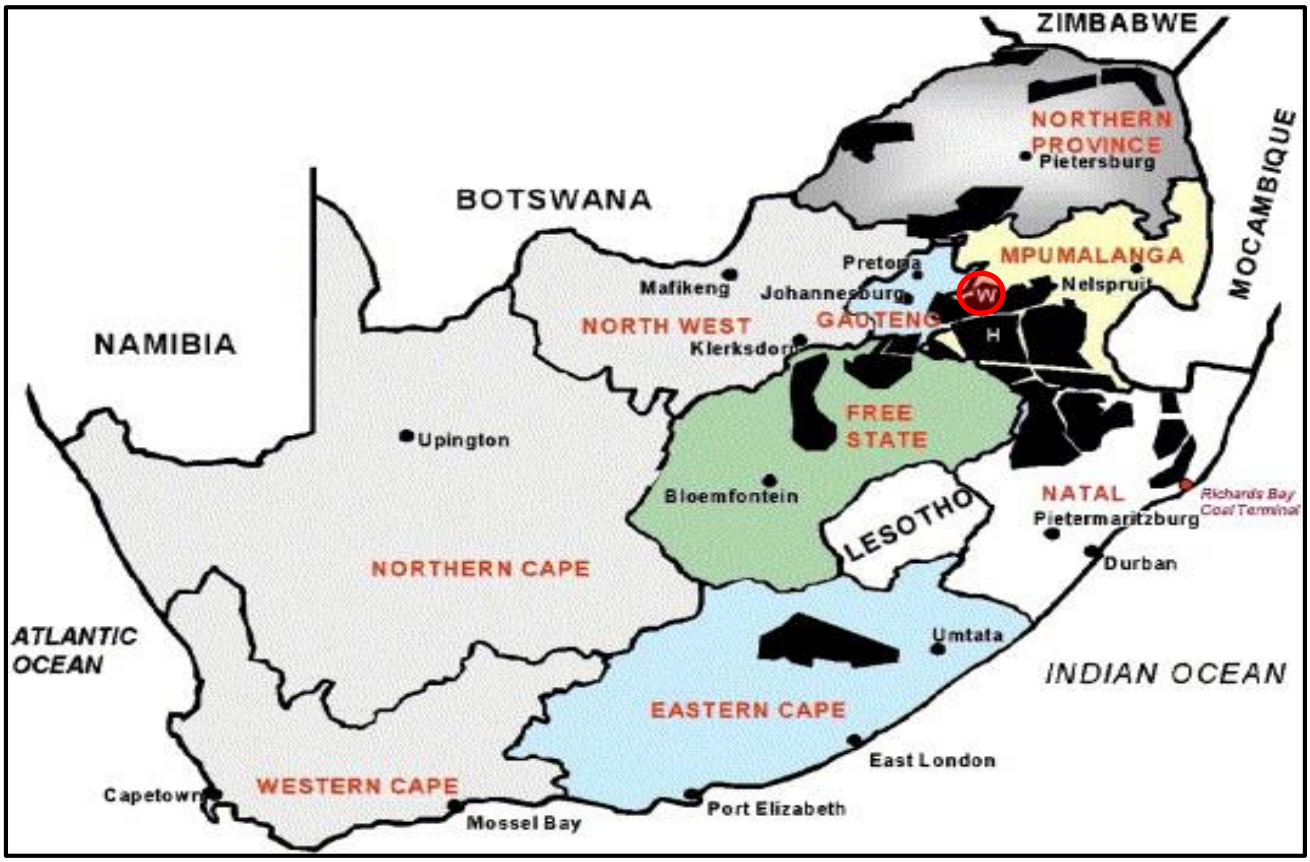

Figure 9: Coal fields of South Africa (Pinetown, *et al*., 2007:66).

2.3.2 South African geological context

Coal is found in the Karoo Supergroup and is known to be the most important deposit in this Supergroup (McCarthy & Rubidge, 2005:195; Stratten, 1986:1868). The Karoo Supergroup varies from glacial tillite at the base to sandstone and shale covered by basaltic and rhyolitic lavas at the top of the succession (Stratten, 1986:1863), which were deposited between 300 and 180 million years ago (Banks *et al*., 2011:16). The Karoo Basin is approximately 12 km thick and covers an area of 700 000 km^2 or two-thirds of South Africa (Johnson *et al.*, 2006:461; Schmidt, 2008:1). Outcrops of the Karoo Supergroup occur around the edges of the main basin, as seen in Figure 10. The Karoo Basin was formed as an inland marine environment due to sagging of the lithosphere which was caused by the heavy load of the Cape Fold Belt to the south. The Cape Fold Belt formed due to compression at a subduction zone to the south-west (McCarthy & Rubidge, 2005:193). In this period the southern portion of Gondwana was situated over the South Pole and was covered by thick ice sheets. Gondwana moved towards the north, which caused the ice sheets to melt and cause the deposition of the glacial sediment load as tillite, known as the Dwyka Group (McCarthy & Rubidge, 2005:186). The Dwyka Group contains tillite, shale, pebbly mudstone, stratified sandstone and granulated stone (Stratten, 1986:1864). Sedimentation in the Karoo Basin occurred approximately 310 to 182 million years ago (Figure 11) (McCarthy & Rubidge, 2005:195). The melting of the glaciers formed a large inland sea (main Karoo Basin) into which rivers drained, forming deltas and channels and extensive swamps. This sedimentary deposit overlying the Dwyka Group tillite is known as the Ecca Group (McCarthy & Rubidge, 2005:200). The Ecca Group mainly includes shale units and coal deposits (Stratten, 1986:1864). According to Schmidt (2008:1), coal in the Ecca Group accounts for a third of the coal resources in the Southern Hemisphere. Although rocks of the Ecca Subgroup are widespread across the centre of the country, conditions suitable for the formation of coal did not occur everywhere and the coal deposits are limited to the main Karoo Basin in an arc extending from Welkom in the Free State Province to Nongoma in KwaZulu-Natal (Banks, 2011:16). The environmental conditions these rivers offered, encouraged the rapid growth of plants, resulting in the accumulation of decaying vegetation (McCarthy & Rubidge, 2005:200). The accumulation resulted in the formation of coal (McCarthy & Rubidge, 2005:201). The Beaufort Group was deposited when the Karoo Sea was slowly filled with sediment from the Cape Mountains (McCarthy & Rubidge, 2005:186). The Stormberg Group was formed due to sedimentation and consists of the Molteno, Elliot and Clarens Formations. The Molteno Formation was formed by large braided rivers and contains local beds of coal (McCarthy & Rubidge, 2005:207; Stratten, 1986:1868), whereas the Clarens Formation was formed in a dry period and represents a desert deposit (McCarthy & Rubidge, 2005:208). The last unit of the Karoo Supergroup is the Drakensberg Group which consists of basaltic lava which ruptured from the crust approximately

182 million years ago. The large volumes of basaltic lava covered the Clarens Desert and the whole of southern Africa and portions of Gondwana. According to McCarthy & Rubidge (2005:209) the eruption started the beginning of the break-up of Gondwana and the scattering of its fragments, which gave rise to the formation of the continents as they are known today.

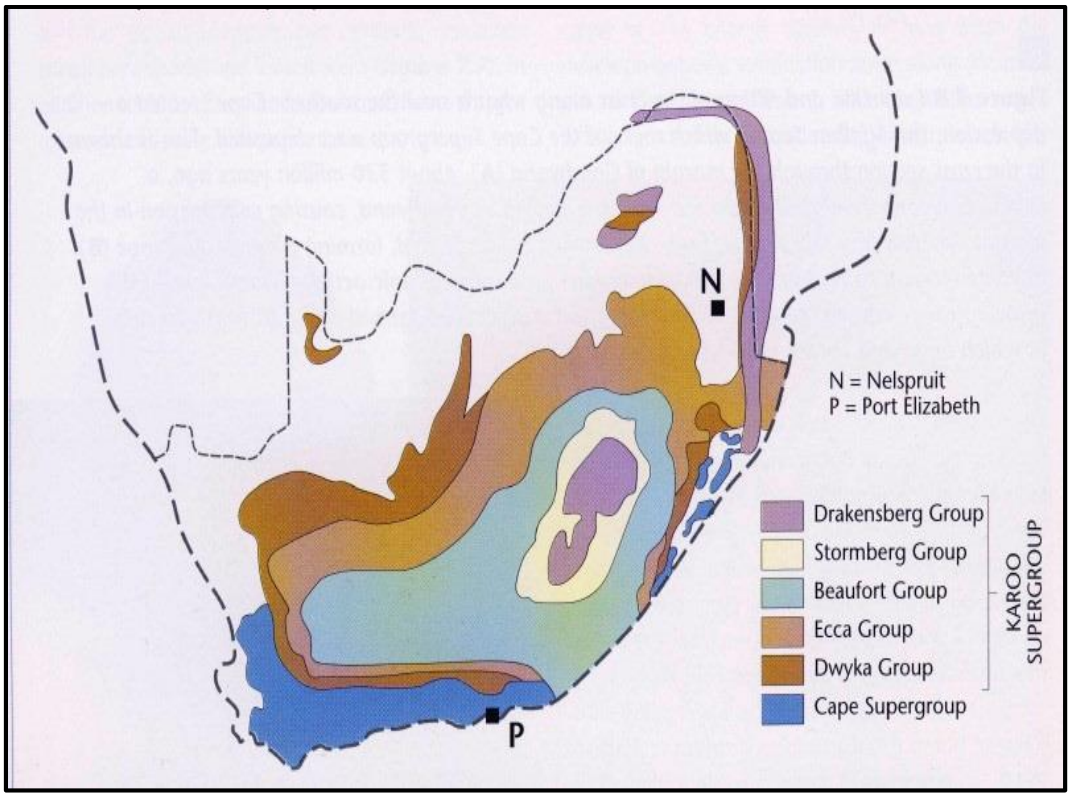

Figure 10: Distribution of Karoo Supergroup rocks (McCarthy & Rubidge, 2005:194).

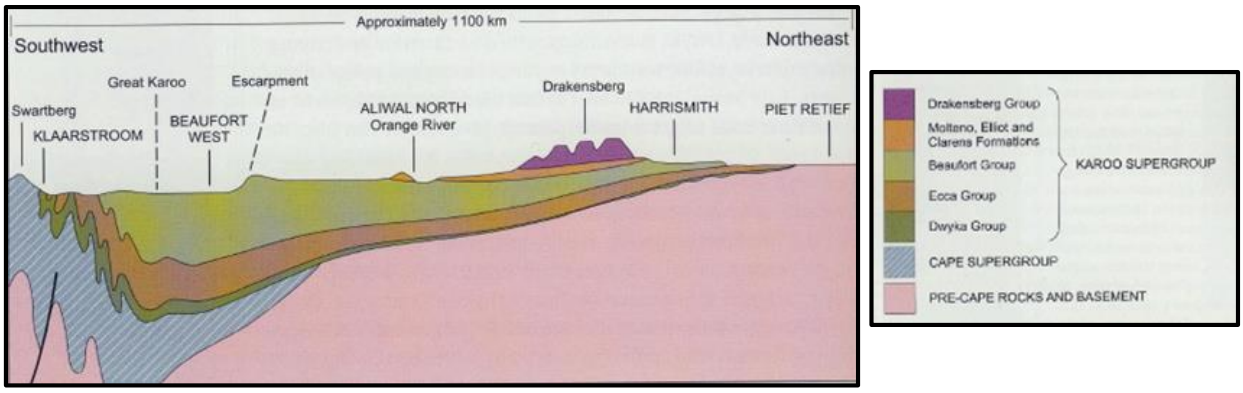

Figure 11: Cross-section of Karoo Supergroup in the main Karoo Basin (McCarthy & Rubidge, 2005:195).

The coal seams in South Africa are shallow, horizontal and have been intruded by many igneous dolerite intrusions. These intrusions affected the rank of the coal as they affected the temperature and pressure of the coal (Schmidt, 2008:2). These intrusions occur as sills or dykes and have caused major displacement of seams, which seriously affects mining activities (Falcon,

1986c:1974). According to Falcon (1986c:1974) the most prominent dyke known in the study area is the Ogies Dyke which has a strike length of roughly 100 km and an east-west strike direction.

2.4 The Witbank Coalfield

South Africa's coal seams are mainly concentrated around the northern border of the main Karoo Basin (Muaka, 2013:26; Schmidt, 2008:3). Most of the seams are concentrated around eMalahleni, Ermelo and Secunda (Schmidt, 2008:3). The Witbank Coalfield is indicated with a 55555555fvgred circle in Figure 9. Coal mining in this coalfield commenced in the 1890s, as small surface mines with at least four collieries operating in the area around 1889 (Banks *et al*., 2011:43). Underground collieries at the time used board and pillar mining with low coal recovery percentages, resulting in momentous amounts of coal being left in pillars and roofs. The bulk of the coal produced was used in the newly-discovered goldfields around Johannesburg (Banks *et al*., 2011:43). Coal production and export increased after 1907 with the development of railway infrastructures (Singer, 2010:30). Increased demand in the late 20th century resulted in larger mines and new techniques such as walking draglines operating on large surface strip mines.

EOMINERS (2014a) indicate there are 209 abandoned mines in the Witbank Coalfield, 118 of these being coal mines. Even though there are numerous abandoned mines, there are 5,000 applications for mining permits in the eMalahleni area (HOMEF, s.a.).

The Witbank Coalfield is situated in the Ecca Group of the Karoo Supergroup at the northern margin of the main Karoo Basin. This geological environment was a shallow marine and fluvial-delta and the deposit consisted of sandstone, siltstone, mudstone, shale and coal (Bell *et al.,* 2001:195). Smith and Whittaker (1986:1972) recognised the Witbank Coalfield as flat-lying to gently undulating with a southwards dip of 1 in 100. The Witbank Coalfield consists of five coal seams, with No. 2 seam being the most important, producing 60%, of the coalfield's coal (Pone *et al*., 2007a:5). The seams are numbered from 1 to 5, with 1 being at the bottom and 5 at the top (Muaka, 2013:11).

- The No. 1 coal seam has an average thickness between 1.5 and 3 m which is controlled by the paleo-floor (Muaka, 2013:11). The No. 1 coal seam is also known to be the least important of the five seams and consists of dull coal and shaly sandstone (Smith & Whittaker, 1986:1981).
- The No. 2 coal seam is roughly 6 m thick in the central part of the Witbank Coalfield and thins out to about 3 m to the east and west (Muaka, 2013:11). The No. 2 coal seam is divided into six coal quality zones and contains 69% of the coal resources of this coalfield (Muaka, 2013:11; Smith & Whittaker, 1986:1981).

- The No. 3 coal seam contains very high quality coal; however, this seam is thinner than 0.3 m which makes the No. 3 coal seam economically unviable to mine (Muaka, 2013:11).
- The No. 4 coal seam is between 2.5 and 6 m thick and provides nearly 26% of the coal resources from Witbank Coalfield (Muaka, 2013:11; Smith & Whittaker, 1986:1981).
- The No. 5 coal seam is nearly 1.8 m thick and extensively eroded and only contributes 4% of the coal resources in the Witbank Coalfields (Muaka, 2013:11; Smith & Whittaker, 1986:1981). The lower seam 5 is of high quality and used for exportation, whereas the top zone is of far poorer quality.

2.5 Coal fires

2.5.1 Causes of coal fires: spontaneous combustion

The phenomenon through which coal spontaneously ignites when coming into contact with oxygen in the atmosphere, without any external source of fire, is known as spontaneous combustion of coal. Coal mine fires are a major problem in the coal mining industry worldwide. It has been reported that the majority of existing fires in different coalfields are mainly due to spontaneous combustion of coal. Coal fires in China burn an about 120 million tons of coal a year, emitting 360 million metric tons of CO_2, amounting to 2-3% of the annual worldwide production of CO_2 from fossil fuels (Wenhua and Ruxiang, 2014:156). Spontaneous combustion of coal is a phenomenon which occurs during mining, storage, disposal and transportation.

All coal in contact with the atmosphere will eventually show signs of oxidation and weathering. When coal is exposed to air, it absorbs oxygen on the exposed surfaces. Some fraction of the exposed coal will absorb free oxygen at a faster rate than others. The resulting oxidation causes the formation of gases (CO, CO_2), water vapour and heat during the chemical reaction. The oxidation of coal is a strongly exothermic reaction. If the rate of heat dissipation is slow related to the evolution of heat by oxidation, there is a gradual build-up of heat and temperature will reach the point at which coal will ignite, causing open fires to occur. When under pressure, the chemical structure of coal breaks down, which causes free radicals such as methyl ($-CH_3$), methylene ($-CH_2$), carbonyl (C = O) and hydroxyl (−OH) to be released from the structure. These free radicals will react with oxygen (O_2), an oxide free radical which releases heat and increases the temperature of the coal (Wenhua & Ruxiang 2014:157). Wenhua and Ruxiang (2014:156) describe spontaneous combustion of coal as a free radical chain reaction (Figure 12). When the heat generated from spontaneous combustion is absorbed by the surrounding area, the phenomenon is called low-temperature oxidation. However, if the heat is not removed, the heated coal will increase the rate of the oxidation process. The oxidation process will increase the temperature even more, resulting in spontaneous combustion of the coal (Pone *et al.,* 2007b:128).

A 'hot spot' is created in the seam or stockpile. The rate of this reaction is therefore directly related to the rise temperature (Wenhua & Ruxiang 2014:157).

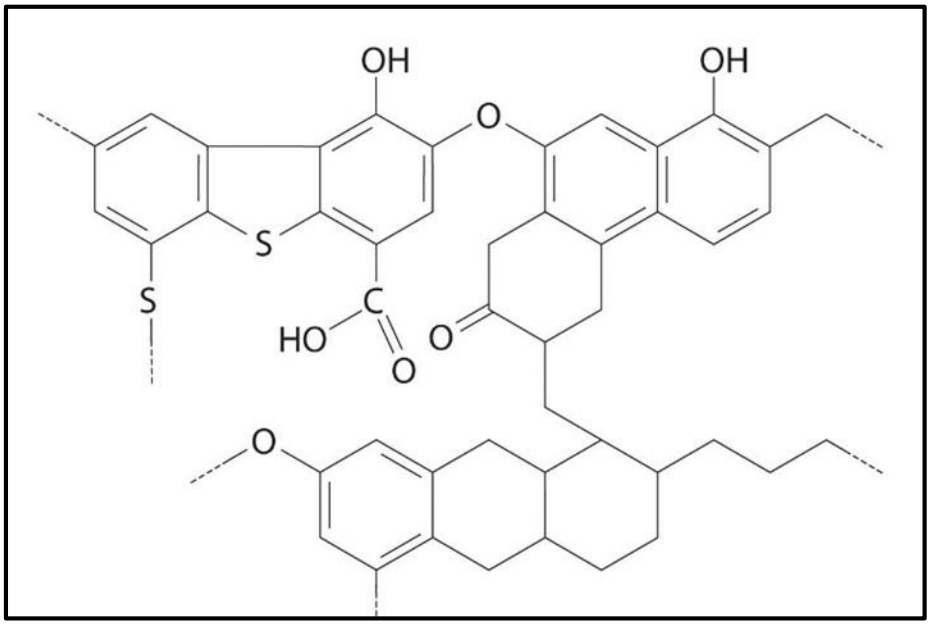

Figure 12: Chemical structure of coal (Averill & Eldredge, 2013).

According to Pone *et al.* (2007b:128), spontaneous combustion in underground coal mines starts when old mine workings are re-opened for further mining. When opened, air enters into the workings, resulting in chemisorption and oxidation of coal. Chemisorption is the process through which air moves through organic material, such as coal and increases the temperature. Chemisorption involves the following reactions (Pone *et al.,* 2007b:128):

Coal + Oxygen = oxycoal (1)

Oxycoal + heat = gas product (2)

The high temperature will increase the rate of coal oxidation which will eventually lead to spontaneous combustion of the coal. Open shafts are an acceleration factor for spontaneous combustion (Pone *et al.,* 2007b:128).

There are many factors which contribute to spontaneous combustion of coal. These factors include: coal rank, coal type, geomorphological setting, geological conditions (such as: strike, dip and pyrite content), geographical conditions, hydrological conditions (such as moisture content), exposed surface area and human interaction (Bell *et al.,* 2000:201-202; Zhang, 2004:29). However, Yang *et al*. (2014:385) highlight three factors which must be present in an environment for spontaneous combustion to occur: heat, oxygen and combustible materials such as pyrite or coal.

Two other sources of heat must be considered:

(1) Heat from oxidation of pyrite, and

(2) Heat from rewetting of dry or oxidized coal and pyrite.

The air-oxidation of pyrite has long been regarded as a contributory cause of the generation of heat in spontaneous combustion. Pyrite found in coal also contributes to spontaneous combustion when the pyrite is oxidised (USGS, 2009). The sulphur in pyrite reacts with oxygen and produces sulphates. This process is exothermic which releases heat (USGS, 2009). The heat which is released from the exothermic reaction heats up the coal, also contributing to spontaneous combustion.

2.5.2 Coal fires in eMalahleni

HOMEF (s.a.) describes the Witbank Coalfields as “the devil’s territory” due to the sulphuric smell emitted from coal fires. Spontaneous combustion of the Witbank Coalfield has been reported for over 50 years. Spontaneous combustion was first noticed in 1947 and affected coal production negatively (Bell *et al.,* 2001:201).

Pone *et al*. (2007b:133) investigated the coal fire vents at eMalahleni and found temperatures varying from 34 ˚C to 630 ˚C. Pone *et al*. (2007b:133) also identified the following coal-fire gas minerals: sulphur compounds and salammoniac and by-products such as mascagnite ($(NH_4)2SO_4$), illite ($(Al,Si)_4O_{10}[(OH)_2,H_2O]$), letovicite ($(NH_4)_3H(SO_4)_2$), phlogopite ($KMg_3(AlSi_3)O_{10}(F,OH)_2$), titanium dioxide ($TiO_2$), barite ($BaSO_4$), iron sulphate ($FeSO_4$), gypsum ($CaSO_4 \cdot 2H_2O$) and silicate. Heavy elements such as mercury, arsenic, lead, zinc and copper were also found to be present in the coal-fires gas. High concentrations of toluene, benzene and xylene were found and are known to possess carcinogenic properties (Pone *et al*, 2007b:137).

The old, abandoned Transvaal and Delagoa Bay colliery (T&DB) in eMalahleni is associated with in-situ combustion of coal (Cellania, 2013). The T&DB colliery, which lies between the township of Kwa-Guqa and the industrial area of Ferrobank, began operations in 1896 (Masondo & Lelliot, 2010). After the closure of the mine in 1953 (Cellania, 2013), many regions of the mine subsided which resulted in spontaneous combustion giving rise to additional formation of subsidence and air pollution. Even though the old mine shafts were covered and sealed, most of these seals failed or have been removed, and accelerated the spontaneous combustion of the coal. Footpaths crisscross the subsided underground mine, passing close to burning areas (Cellania, 2013). Attempts by authorities to prevent residents from passing over these dangerous areas vary from warning signs to fencing-off dangerous areas (Figure 13).

Numerous methods have been used to deal with spontaneous combustion in the Witbank Coalfield, but not one has proved successful over a period of time. Most methods involve cladding and dozing, where sand is dumped onto the burning coal seam to choke the fire, i.e. preventing oxygen from entering the mine workings. However, this was not successful due to the fast rate at which the fire spread (Pone *et al*., 2007a: 8).

Figure 13: Photo taken at T&DB Collier (Photo by Van Tonder, 2011).

2.5.3 Environmental problems associated with coal fires

Many environmental problems associated with coal fires occur in the study area. The first aspect is the impact on air quality through the release of harmful gases such as benzene, toluene, ethyl benzene, methane, xylene, methane, carbon dioxide and carbon monoxide by uncontrolled coal fires (Zhang, 2004:24; Pone *et al*., 2007a:6). These gases cause air pollution and are associated with environmental and human health problems (Finkelman, 2004:21). The health risks are discussed further in Chapter 2.8.3. Methane and carbon monoxide released by these fires are classified as green house gasses (GHGs) (Van Dijk *et al*., 2001:109). It is said by Iowa State University (ISU) (2008) that greenhouse gasses contribute to global warming as these gasses absorb infrared rays which are supposed to reflect back into space. Thus, the amount of greenhouse gasses in the atmosphere is directly related to the temperature of the atmosphere (ISU, 2008). Associated with the impact on air quality is the formation of coal fly ash that may pose a health risk to the community. The theory of fly ash is discussed in Chapter 2.8.3.

The second impact is related to the fires itself that may spread to wooded areas and even into residential areas (Zhang, 2004:21). This can be a major problem in the eMalahleni area as people live on hazardously undermined land very close to burning mine dumps (Mashaba, 2012). Illegal mining of coal from these burning mine dumps may lead to serious injuries and even death (Roelofse, 2013; Goldswain, 2015). Furthermore, the areas burning underground may collapse without warning as people are crossing these areas.

The most visible problem is that of land degradation due to collapse of land when coal fires burn underground pillars as fuel (Zhang, 2004:24). The subsidence causes damage to infrastructure such as roads, high voltage power lines and buildings, and could even claim the lives of people in areas where houses were built on areas mined with the board and pillar method.

Furthermore, the loss of coal as a non-renewable natural resource due to the spreading of underground coal fires will negatively impact the economy by lowering export volumes and also have a negative impact on the country's future energy resources, According to Pone *et al*. (2007a:4) more than 3 million tons of coal are lost annually in South Africa due to coal fires.

2.5.4 Detection and analysing of coal fires

Detection of coal fires can be done using geological investigation, remote sensing, geophysical investigation or chemical detection. However, it is stated by Qi *et al*. (2013:1916) that it is difficult to detect the exact position of fires due to the complexity of coal fires. Geological investigations can be expensive due to borehole costs, thus the most practical method used is remote sensing (Qi *et al*., 2013:1916).

2.5.4.1 Fundamentals of remote sensing

Various authors have defined remote sensing as the gathering and analysis of information about an object without being in the proximity thereof (Smith, 2012:3). Remote sensing includes interpretations of aerial and satellite derived information of the earth's surface and atmosphere (Smith, 2012:3). Remote Sensing techniques use a sensor which measures the electromagnetic radiation (EM) which has interacted with the Earth's (Target) surface (Smith, 2012:5).

According to Jensen (2007:2), the human eye is too insensitive to detect the difference in thermal infrared energy. Thermal Infrared Cameras can take high quality images of thermal infrared energy. By analysing these images, both surface and underground fires can be detected. Jensen (2007:2) states that this is done by taking images of the earth's surface at various wavelengths of the electromagnetic spectrum, allowing a practical way of obtaining the temperature images of the whole eMalahleni area.

Lillesand and Kiefer (1994:3) describes the process and elements involved in remote sensing (Figure 14). The two elementary processes involved in remote sensing are data acquisition and data analysis. The elements of acquisition include (Lillesand & Kiefer, 1994:3):

(a) Energy source- illuminates or provides electromagnetic energy to the target of interest.
(b) Propagation of energy through the atmosphere- energy (radiation) travels from its source to the target.
(c) Energy interaction with earth surface features- reflected and/or radiated energy from source target is transmitted through and interacts with the atmosphere. The degree of interaction depends both on atmospheric composition along the ray path and on the height of the sensor (e.g. satellite or airborne).
(d) Re-transmission through the atmosphere.
(e) Airborne and/or Spaceborne sensor- a sensor collects and records the electromagnetic radiation that has been transmitted through the atmosphere.
(f) Sensor data as pictorial and/or digital form- the data recorded by the sensor is received at a ground station where the data are processed into an image and distributed.

The data analysis process involves the following:

(g) Interpretation and analysis- the processed image is interpreted, visually and/or digitally, to extract information about the illuminated or emitting target.
(h) Information products- the interpreted data is then compiled with other layers of information in a geographic information system (GIS).
(i) Users- The final product is then presented to the user who apply it to their decision making process.

The electromagnetic spectrum is a band varying from high energy (short wavelengths gamma rays) to lower energy (long wavelength radio waves). Some remote sensing studies use only the wavelengths occurring in the visible light spectrum, while other studies use invisible ultraviolet and infrared radiation. Imaging radar systems used in remote sensing produce and transmit microwaves, then measures the share of the signal returned to the sensor from the Earth's surface (Smith, 2012:4). Remote sensing uses that portion of the electromagnetic spectrum that falls between 103 and 106 nm (Figure 15).

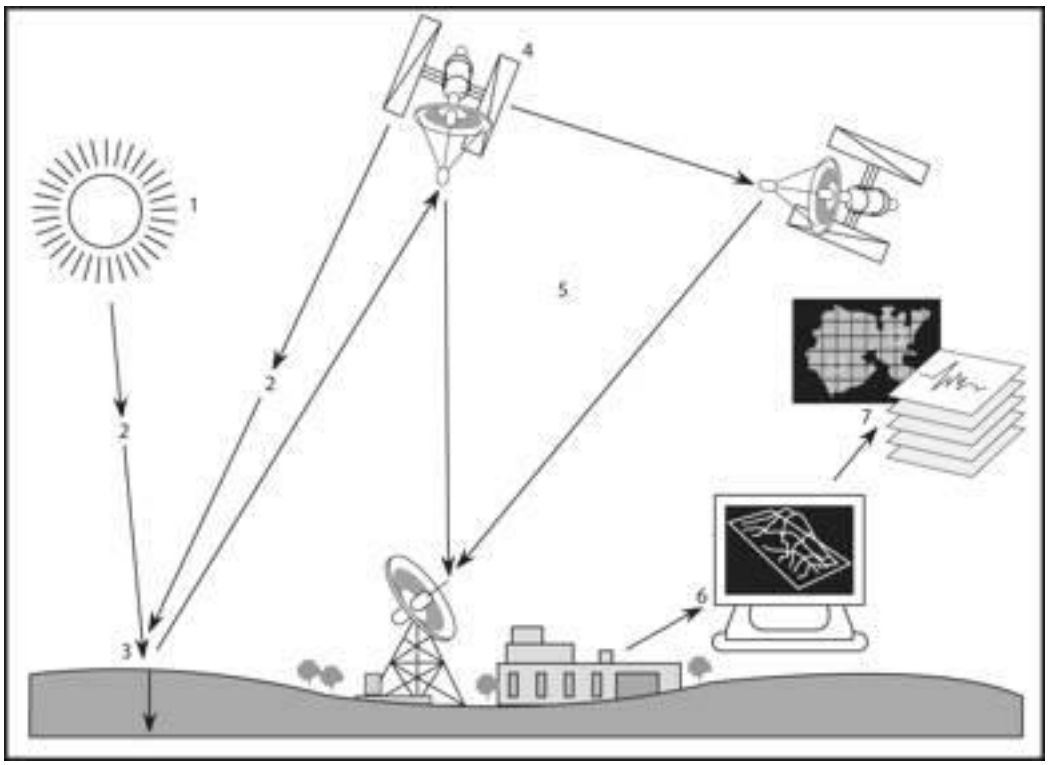

Figure 14: Remote sensing process (Tindall, 2006).

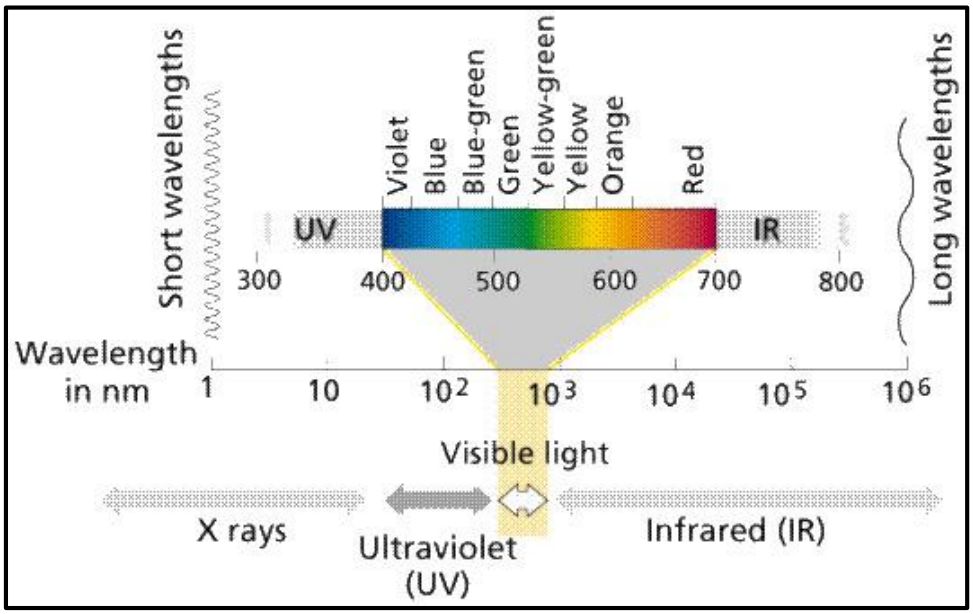

Figure 15: Electromagnetic Spectrum (Dr Wellness, 2013).

A sensor is defined by Fan *et al*. (2015:65) as an instrument that consists of sensors, data processing and communication components, thus, it is a device that scans the environment. Various types of sensors exist:

- Active systems (Van Der Meer *et al*., 2012:649)

Active systems refer to a sensor that supplies its own source of energy or illumination such as RADAR. The process entails transmitting short bursts, or pulses, of microwaves energy in the direction of interest and recording the strength and origin of “echoes” or “reflections received from the objects within the system’s field of view.

- Passive systems (Van Der Meer *et al*., 2012:119):

  Passive systems have an energy source external to the detector. The most common source is the sun. Passive systems are high-energy systems operating in the shorter wavelengths of the electromagnetic spectrum. For most purposes this is the visible and infrared (near, middle and thermal) regions. Passive systems consist of:

  - Reflected solar radiation sensors: This measures solar energy reflected back to the sensor, usually in the visible and near infrared regions.
  - Thermal infrared sensors: These sensors record energy emitted by the Earth’s surface. This energy consists of solar heating energy (short-wave solar energy absorbed and re-radiated at longer wavelengths by the Earth’s surface), geothermal energy, fires and human activities.

- Framing systems

  These are essentially camera systems instantaneously acquiring images from the same geometric vantage point but with different film-filter combinations (Lillesand & Kiefer, 1994:104).

- Scanning systems (Van Der Meer *et al*., 2012:119):

  Scanning systems consist of a detector sweeping across an area (Figure 16). Electromagnetic energy radiated or reflected off the target hits the detector and is converted to an electrical signal. The signal varies with the strength of the energy received. The signal is amplified and stored, or transmitted to a ground receiving station. Most satellite sensors fall within this category such as the push-broom system.

It is assumed that energy of a wavelength less than 3μm is reflected (usually reflected solar energy). Energy emitted by ambient Earth features is of longer wavelength and is assumed to be greater than 3μm.

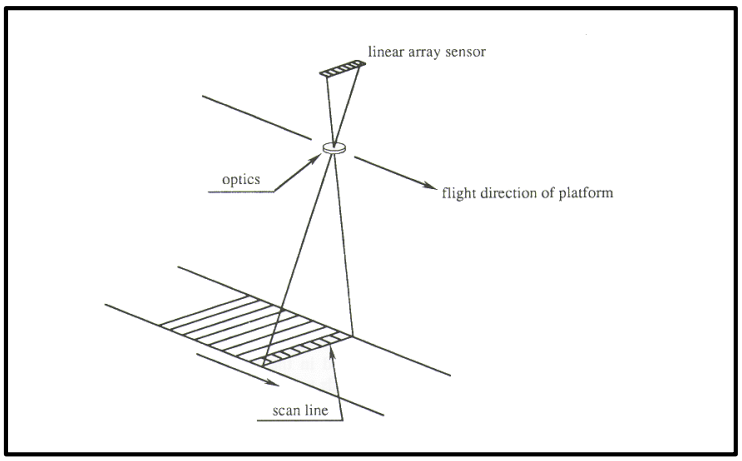

Figure 16: Scanning system (JARS, 1991).

2.5.4.2 Fundamentals of thermal infrared remote sensing

Jensen (2007:6) describes the basics of thermal infrared remote sensing as an object's radiant temperature measured with a radiometer which is not in contact with the object. The radiant temperature is the amount of radiation emitted from an object with a temperature above absolute zero.

The radiation of the object can be seen as "waves of energy". These "waves of energy" are received and converted by the detector into an electrical signal and then into a thermal image (Roelofse, 2011:1). The radiation of objects peaks at wavelengths inversely proportional to the temperature which is the infrared area (Kubiak & Dzieszko, 2012:716).

Thermal infrared remote sensing is influenced by the object's emissivity, which is determined by several factors. The first factor is the colour of the object; the darker the object, the more it will absorb and emit energy. The second factor is the moisture content of the object. A higher moisture content gives the object a greater ability to absorb energy (Jensen, 2007:16). The fact that some objects may still contain water from rain, whereas others contain no water may influence interpretation of infrared images. For this reason rainfall has to be taken into consideration when planning a thermal infrared remote sensing (TIR) survey (Jensen, 2007:16).

The radiation received by the sensor is therefore a combination of surface temperature, surface thermal properties and atmospheric effects. Surface emissivity and atmospheric effects have to be corrected in order to obtain reliable and accurate land surface temperatures (Lillesand & Kiefer, 1994:4)

For most environmental studies, TIR is used to obtain data on how features on the Earth's surface emit and reflect electromagnetic energy. The TIR data produces important information about the

object characteristics. Within this context, a more specific definition is given by Harris (1987:2): "*The acquisition of data and derivative information about objects or materials (targets) located at the Earth's surface or in its atmosphere by using sensors mounted on platforms located at a distance from the targets to make measurements (usually multispectral) of interactions between the targets and electromagnetic radiation*."

As temperature increases, the total energy emitted by the object increases. The spectral distribution of energy emitted is also a function of temperature. As the temperature of the object rises, the highest radiation emitted moves to the shorter wavebands.

Airborne thermal scanners aquire in diffrent wavelength regions depending on the time of day the data is collected. Night time airborne thermal scanner imagery aquire wavelengths between 8-12.5 µm of the electromagnetic spectrum, whereas daytime thermal infrared data aquire in the 3-5 µm wavelength region. A sensor working within the 3-5 µm window is very sensitive to detecting temperatures 600 K (327ºC) and above (surface fires), and sensors working in the 8-14 µm window detect objects with a temperature of 300 K (27ºC) (underground fires) (Zhang, 1998:83).

2.5.4.3 Coal fire detection techniques

According to Zhang (2004:41) coal fires can be detected by a number of features such as emission of smoke, fumaric minerals, pyro-metamorphic rocks, burnt pits, trenches, and surface subsidences and cracks. However, these coal fires can also be detected with infrared remote sensings systems.

Remote sensing research on coal fires was first done in 1963 by a company which produced airborne thermal cameras. The company tested these cameras above a burning coal waste pile (Kuenzer *et al*., 2007:4562).

Numerous techniques can be used in coal fire detection:

- Aerial photos and visible bands on satellite images may be used to detect smoke, the deposition of new materials on the surface (for example, sulphur deposits), and in the case of underground fires, changes in colour of the cap rock and land cracking and surface subsidence (Zhang, 2004:41).

- Infrared images (Kuenzer *et al*., 20017:4561): Short-wave infrared images are used to detect fires hotter than 160°C. Thermal infrared images are the most important in fire detection. Both day and night-time images have been used, though night-time images have the added advantage of eliminating solar heating effects

- Resistivity survey is a geophysical technique which will be discussed in Chapter 2.6.4.

- Landsat (10 - 12.4 µm): Landsat is known as one of the most useful satellites for remote sensing investigations (Harris, 1987:63). Landsat -1, and -3 orbit at an altitude of 900 km and moves at a speed of 6.46 km/sec (Lillesand & Kiefer, 1994:433). The resolution of these bands is between 0.475 to 0.830 µm (Lillesand & Kiefer, 1994:437). Landsat -4 and -5 orbit at a lower altitude of 705 km (Lillesand & Kiefer, 1994:462). Landsat -4 and -5 has a ground resolution of 120 m, which proved ineffectual for very small fires. Landsat -6 was designed to orbit identical as Landsat -4 and -5, however it was improved as it has a resolution of 0.50 to 0.90 µm and a spatial resolution of 15 m (Lillesand & Kiefer, 1994:483). Landsat -7 was designed to have a spatial resolution of 10 m, which allows for good quality image.

- ATSR: ATSR is known as Advanced Spaceborne Thermal Emission and Reflection Radiometer (Lillesand & Kiefer, 1994:514). ASTER is characterised by three scanners and has a resolution of 15 to 30 m (Lillesand & Kiefer, 1994:514). The use of this platform was somewhat unsuccessful, since the thermal band is centred at 11-12 µm and the spatial resolution is 1 km.

- SPOT XS: Satellite Probatoire d'Observation de la Terre (SPOT) was found to be less useful than Landsat TM. SPOT is a polar orbiting platform at an altitude of 825 km and is equipped with a High Resolution Visible (HRV) multi-linear array sensor. The HRV has two modes. The first mode has a pixel value of 20 m and three wavebands in the visible and near infrared. The wave bands are between 0.50 to 0.89 µm. The second mode is the panchromatic mode which has a pixel value of 10 m and a broad wave band of 0.51 to 0.73µm (Harris, 1987:72).

Lillesand and Kiefer (1994:140) defined resolution as an expression of the optical quality of an image produced by a particular camera system.The resolution of the different techniuqes are determined by parameters such as the resolving power of the film and camera lens used to obtain the image, uncompensated image motion during exposure, the condition of the film processing, etc. (Lillesand & Kiefer, 1994:140).

Airborne and satellite remote sensing is becoming more and more available due to the growing number of companies and agencies operating hyperspectral scanners. Table 2 compares airborn and satellite remote sensing.

Table 2: Comparison between airborn and satellite remote sensing techniques.

	Airborn remote sensing	Satelite remote sensing
Spatial resolution (Wessels *et al*., 2013: 248)	60- 120 m	1 -10 m
Cost (Zhang, 2004:28).	Expensive	Low cost
Data gathering (Wessels *et al*., 2013: 267)	Data is only gathered when planned.	Continuous. Data is gathered on a daily basis
Data coverage (Harris, 1987:4)	Flexible	Data acquisition is controlled by the pattern of its orbit
Area coverage (Harris, 1987:4)	Small area coverage	Large area coverage
Time dependent/ independent (Zhang, 2004:49; Harris, 1987:4)	Independent- can be done any time of year and during the day or night	Dependent- Data acquisition is controlled by the pattern of its orbit

Zhang (2004:28) listed the different remote sensing methods used to detect coal fires:

- Advanced Very High Resolution Radiometer (AVHRR),
- Along Track Scanning Radiometer (ATSR),
- Moderate Resolution Imaging Spectrometer (MODIS),
- Russian RESURS-1,
- Bi-spectral InfraRed Detection (BIRD),
- Advanced Space-borne Thermal Emission & Reflectance Radiometer (ASTER),
- Thematic Mapper (TM) and
- Enhanced Thematic Mapper (ETM+).

Surface temperatures can be mapped directly to digital images by means of a lightweight thermal radiometer or thermal infrared camera which are both known to be very precise (Faux *et al*, 2001:2). Thermal infrared remote sensing is done with a Thermal Infrared Radiometer or camera mounted onto an airborne platform. This radiometer works with wavelengths between 3-5 µm and 8-14 µ. Digital images are obtained from the camera. These images can either be used for direct observation or images mosaicked to form a complete image of the area (Faux *et al*, 2001:15).

When the aircraft is flying at a lower altitude, smaller pixels will be obtained (Jensen, 2007:27). This will maintain a good radiometric and spatial resolution. However, when flying at a lower altitude, less of the environment will fit into a single image, this will then result in flying more lines, to obtain images of the entire area. Unfortunately, the more lines, the more images and the more difficult it will be to mosaic the images to obtain a complete image of the area.

Errors can easily occur when data is taken in a small aircraft, helicopter or UAVs. According to Deitchman (2009:2) these errors can be caused by a variation in flight speed, the sensor orientation to the ground, the flight altitude and the resolution of the thermal image of the specific airborne collection platform. These errors can affect the quality of the images and make the data difficult to analyse.

It is preferable to take infrared images in the evening because the contrasts between the coal fires and the surrounding objects are then much larger due to the comparatively low temperatures of the surrounding objects (Zhang, 2004:3; Zhang, 1998:44).

2.5.4.4 Image processing technique: Mosaicking

Mosaicking is defined by Li *et al*. (2015: 108) as a process of merging two or more images with overlapping areas into a single view with an indistinguishable seamline. By combining raster images from a specific area, a new large-area image can be created from multiple images with overlapping area (Li *et al*., 2015: 108).

Mosaicking can be done by automatic positioning of georeferenced images or it can be done manually by placing tie points between pairs of overlapping images (Figure 17). Automatic positioning allows the program to mechanically place the georeferenced images in the specific map projection. Manual mode uses a bundle adjustment algorithm to compute a least-squares best fit for all tie points and any available ground control points. Most mosaicking programs will allow the user to aplly contrast enhancements for each raster to set up contrast matching of input objects (Smith, 2006:3).

Information of mosaicking techniques for thermal infrared images is limited, as only a few studies have been done on this topic. However, a study done by Miraliakbari *et al*. (2010) and Li *et al*. (2015) indicates that the mosaicking of thermal infrared images can be a successful method of interpreting these images.

According to Smith (2006:13) distortions is one of common errors in mosaicking. Distortion mostly occurs in low-altitude images such as aerial images. An object pictured in adjacent photos may be displaced from its true position by different amounts and in different directions in each image. When the photos are mosaicked, the two images of the same ground object are not placed at the same location in the mosaic (Smith, 2006:13).

Li *et* al. (2015:108) describes several complications with the mosaicking of remote sensing images, and the solution to these problems. The most frequent complication is the difference in tonal colour which is caused by the changing of angles and the difference of time when the images

were taken (Li *et al*., 2015: 108). To ensure a natural integrated image, tonal adjustments has to be applied. Tonal adjustment ensures that the overlapping region of images remain constant. The average luminance condition of the reference image in the overlapped area is calculated, and the other image is normalized to adjust. The mean value represents the average of the image intensity and the variance of standard deviation represents the volatility of the intensity (Li *et al.,* 2015: 109).

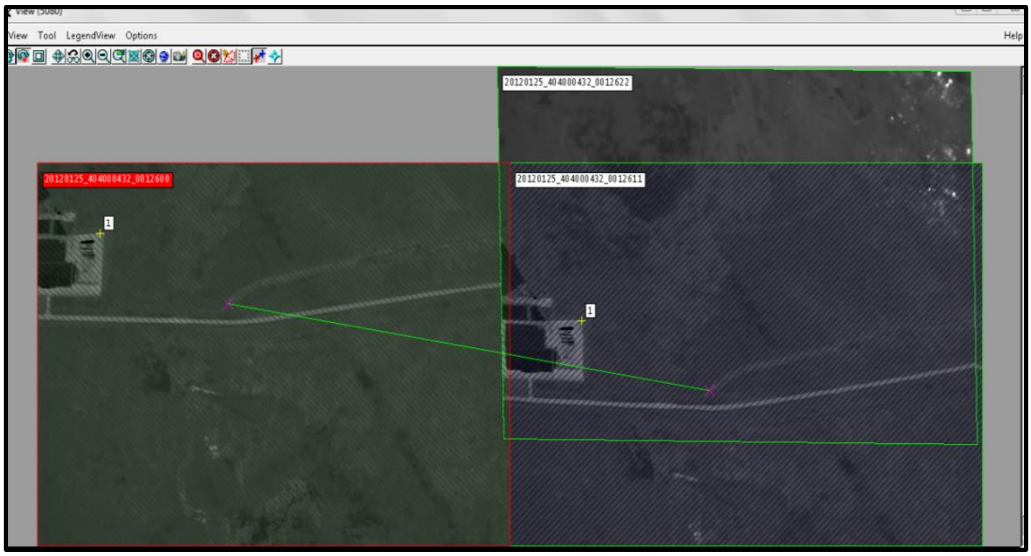

Figure 17: Tie points for manual mosaicking (Screenshot by Schoeman, 2014).

2.6 Subsidence

2.6.1 Causes of subsidence

Hebblewhite (2009:115) describes subsidence as the deformation of ground masses caused by mining activities. The seriousness of the impact of surface subsidence caused by coal mining activities depends on different factors, such as the mining method, geological setting, depth of workings from the surface, the size of the mining void and whether the mine is operational or abandoned (Bell *et al*., 2001:200). According to Engelbrecht *et al*. (2011:80) the composition of the roof material will also influence the appearance of subsidence on the surface. Horizontal underground mining will cause vertical land subsidence equal to two-thirds of the thickness of the extracted layer (Rahn, 1985:325).

The influence that coal seam depth, dip of the coal seam and the angle of the seam has on subsidence was studied by Howladar & Hasan (2014: 3700). Mining at reasonable shallow depth can result in subsidence, and the affected surface area is generally larger than the extraction area (Howladar & Hasan, 2014:3706). Howladar & Hasan (2014: 3706) determined that more subsidence developed when the coal seam depth is less than 200 m, whereas less subsidence develops when the coal bed is deeper than 440 m. It was determined that the dip of the coal bed

do not have a major effect on the amount of subsidence formation. However, it does slightly influence the shape of the subsidence (Howladar & Hasan, 2014: 3706).

The type of method used for coal mining, is one of the most important factors which influence the formation of subsidences (Howladar & Hasan, 2014: 3706). Coal mining methods which are used all over the world include longwall mining, top slicing, sub-level caving and room-and-pillar mining. Longwall mining is frequently used due to large amount of coal extraction. The larger the width of the longwall coal mining panel, the larger the deformation caused by subsidence. The board-and-pillar method is used when the coal bed is thick and has a gentle slope. This method usually results in smaller subsidence (Howladar & Hasan, 2014: 3707).

Subsidence formation maybe enhanced by geological activities such as faults and folds, unconformities and other variations in the overlying and adjoining stratum (Howladar & Hasan, 2014: 3708). The lack of stability forces through mining is able to activate the portion along a fault plane. Faults may also weaken the overlying strata and trigger the subsidence in materials. The presence of joints and fissures may also affect the occurrence of subsidence, however, it is said by Howladar & Hasan (2014: 3709) that these joints and fissures only affect the formation of subsidence on a small scale.

According to Howladar & Hasan (2014: 3709) the floor and roof on the mine are critical factors that can determine if subsidence may form, since subsidence propagate from these areas. If the roof material is weak, it will cause the overlying material to fall and compact which will result in a greater likelihood of formation and severity of subsidence.

Lee *et al*. (2013:648) mentioned that water withdrawal can cause the formation of voids and may result in the occurrence of subsidence due to the change in hydro-geological properties of the strata. As the water is withdrawn, the draw-down of the water level removes the support for the overlaying material, thereby increasing the vertical stress on the overburdening material (Kiernan, 1989:126).

2.6.2 Subsidence in eMalahleni

Underground mining is focused at the maximum mineral recovery (Muaka, 2013:75). According to Muaka (2013:78) 90% of recovered coal from the Witbank Coalfield is from the board-and-pillar technique and the remaining 10% is divided between the pillar-extraction (stooping) and longwall mining techniques.

The No. 2 coal seam in the Witbank Coalfield was initially mined by the board and pillar method from 1908 to 1947. This method left a coal pillar size of 6×6 m remaining to support the roof

material and a room space of 7 m (Figure 18) (Bell *et al*., 2001:197). This method extracted 60% of the coal resources. According to Engelbrecht *et* al. (2011:79) the initial board-and-pillar technique left little or no environmental degradation. However, the pillar robbing method was introduced in 1930 and increased the extraction from 60% to 90% (Bell *et al.,* 2001:197; Engelbrecht *et al*., 2011:79). This was done by mining the pillars which eventually resulted in only four smaller pillars supporting the roof. According to Muaka (2013:77) the displacement of pillars causes an increase in the stress in the remaining pillars which caused pillars to collapse and resulted in surface subsidence.

Pillar failure was caused by the weight of the heavy overburden and the small compromised pillar strength. When one pillar collapses it increases the stress on the next pillar, which then causes more pillars to collapse, and then the collapsing and sagging of the roof material which eventually forms a surface subsidence. Coal fires can weaken the strength of coal pillars as it burns the coal as fuel (Zhang, 2004:24).

Longwall mining is an underground mining method where a slice of coal (3 to 4 km long and 250 m to 400 m wide) is mined. This method is prone to sagging due to the minimal support for the roof material. The longwall mining technique recovers 80% of the coal resources. The subsidence formed due to longwall mining is referred to as controlled subsidence (Engelbrecht *et al*., 2011:80). According to Lee *et al*. (2013:647) longwall mining results in more subsidence than the room-and-pillar method due to the larger amount of coal extracted.

Bell *et al*. (2001:197) identified 15 m to 20 m deep voids in eMalahleni's old mine workings. These voids resulted in crown holes at the surface with diameters between 5 and 10 metres. Engelbrecht *et al*. (2011:88) identified subsidence basins of approximately 33000m^2. The subsidence developed over a large area, restricted the expansion of the town of eMalahleni to the north and land was rendered unsuitable for agricultural purposes (Van Tonder, 2011:57).

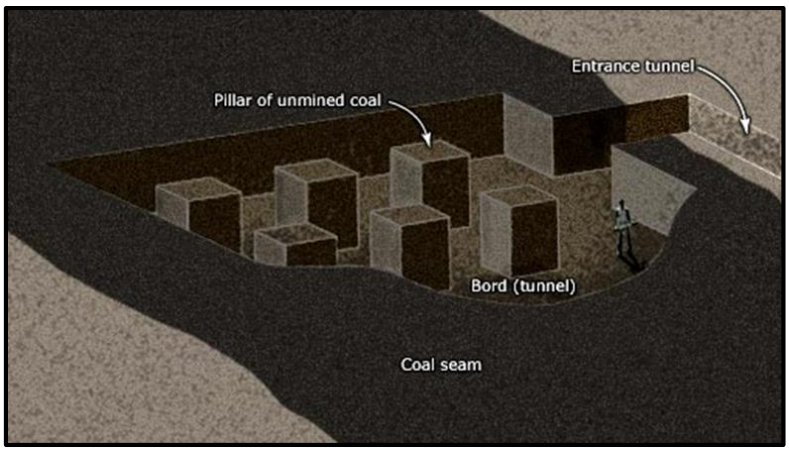

Figure 18: Board-and-pillar mining (Sherwood & Philips, 2012).

2.6.3 Environmental problems associated subsidence

Subsidence generally occurs with minimal warning and causes damage to ecosystems, water systems, land use and anthropogenic structures (Dinger *et al.,* 2007:22). Subsidence may cause severe damage to infrastructure such as roads, dams, pipelines and buildings. Subsidence events can also pose a substantial threat to the health and safety of people (Engelbrecht *et al*., 2011:77).

Hydrological pathways may be impacted due to the influences of subsidences, such as an increase in groundwater recharge of water ponds in an area affected by subsidence (Engelbrecht *et al*., 2011:77). Polluted surface water can also enter aquifers through subsidence (Singh, 1989:47). Furthermore, groundwater which moves through mining cavities can become polluted and contaminate the natural environment as it is discharged into wetlands, streams and dams (Bell *et al*., 2001:197).

Subsidence increases the entry of water and oxygen into old mine workings, which results in increased oxidation rates which can lead to spontaneous combustion of coal and the oxidation of sulphates to form AMD (Bell *et al*., 2001:205).

2.6.4 Detection and analysing of subsidence

According to Engelbrecht *et al*. (2011:77) it is important for mining companies to know where subsidence occurs, how the ground is moving and how fast subsidence is developing. With this information, decisions can be made on infrastructure development as well as remedial actions and prevention strategies (Engelbrecht *et al*., 2011:77).

Seismic investigation can be used for the detection of subsidence, such as the study done by Venkatanarayana and Rao (1989:63). The study was done by preparing time-distance plots and calculating the velocities and thickness for different layers by releasing seismic waves into the earth and collecting the seismic reflection data. The results indicated different seismic velocities which specify the different structures of the layers (Venkatanarayana & Rao, 1989:63) (Figure 19). Seismic waves behave similar as light waves which makes it possible for them to bend and reflect at boundaries of different rock layers. Seismic waves travel with different speeds through different rock types due to the density and the rigidity of the rock. Thus, the speed at which the wave moves through the rock, gives an indication of the density and the composition of the rock (McCarthy & Bruce, 2005:28).

The electromagnetic geophysical technique is known to be a relatively easy method to use (Pazuniak, 1989:266). EM is based on the principle that magnetic fields can be generated from electrical currents and vice versa (Poteet, 1989:273) (Figure 20). The EM instrument contains

coils for transmitting and receiving electromagnetic fields (Pazuniak, 1989:266). The transmitting coil sends an electromagnetic field into the ground which creates a secondary field which is measured by the receiving coil (Pazuniak, 1989:266). The EM measures the sub-surface conductivity which indicates possible cavities (Pazuniak, 1989:266). The ease with which an electromagnetic field can be transmitted through material is quantified by conductivity (Poteet, 1989:273). According to Poteet (1989:247) voids will have a lower conductivity than rocks.

The geophysical technique known as resistivity can be used to develop a resistivity cross-section for detecting of sub-surface voids (Figure 21) (Pazuniak, 1989:267). According to Poteet (1989:273) resistivity is the reciprocal of conductivity. However the use of resistivity survey is limited due to the large amount of labour needed and the penetration limitation of the method (Pazuniak, 1989:267). The resistivity survey is done by creating a current of known amperage between two electrodes; by measuring the voltage between two additional electrodes, the average resistivity of the subgrade can be determined (Pazuniak, 1989:267). Sheets (2002:9) successfully detected underground mining voids with resistivity.

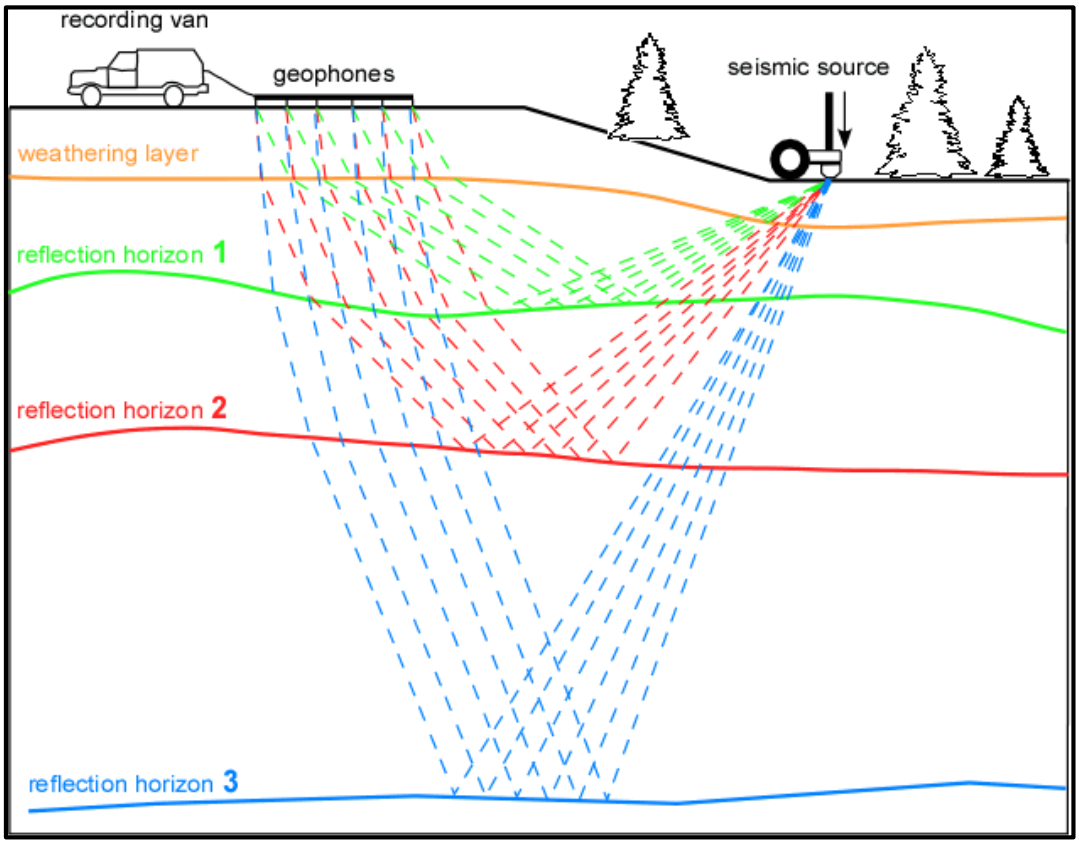

Figure 19: Seicsmic survey done by releasing seismic waves into the earth and collecting the seismic reflection data. (Geoexpert Ag, 2015).

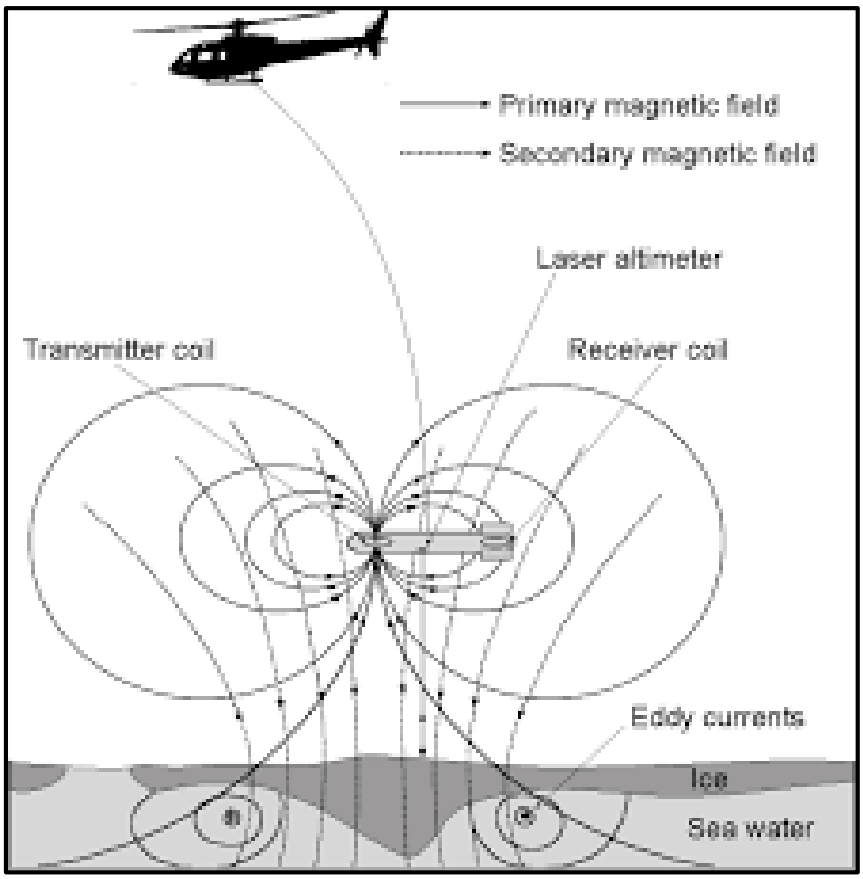

Figure 20: Magnetic fields generated from electric currents by the EM process (Geosiam Geophysical Services, 2015).

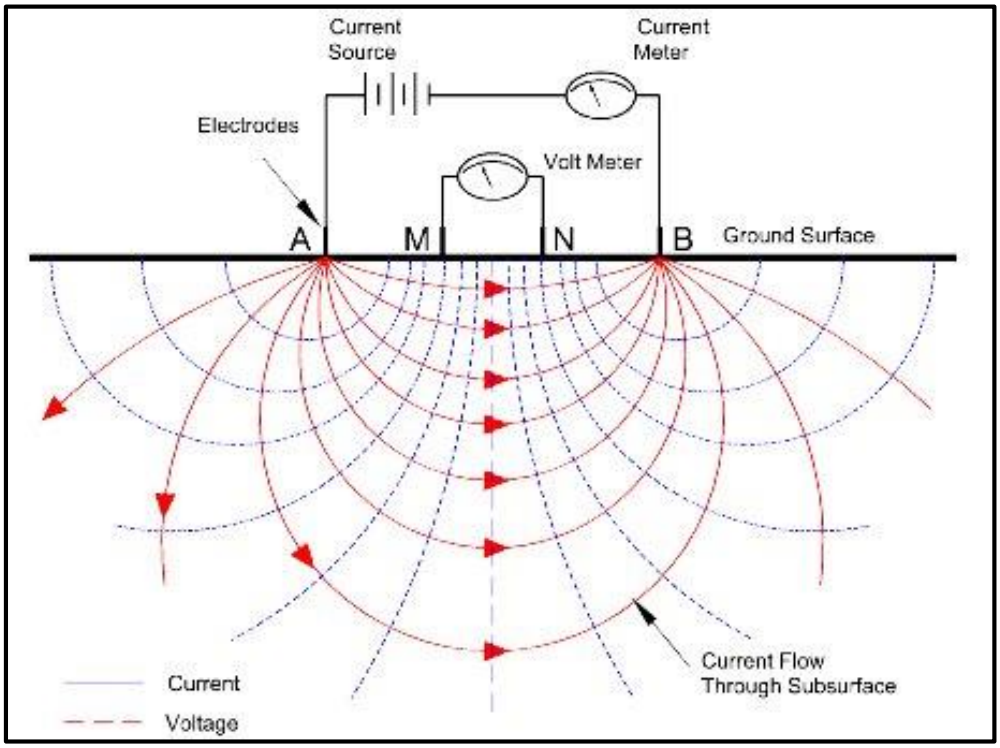

Figure 21: Electrodes creating a current to determine the average resistivity (Geohunt, 2015).

Ground penetrating radar is used to gather information at the boundaries of subsidence structures and their three-dimensional internal geometry (Carbonel *et al*., 2014:214). Ground penetrating radar sends short pulses of electromagnetic radiation into the ground and records the signal strength and time required for the return of the reflected signal (Carbonel *et al*., 2014:215). A reflection signal is produced when the energy pulse encounters a material with a different dielectric (polarization) property (Figure 22) (Geoview, 2012). The dielectric difference between the two materials, determines the amplitude of the reflection (Geoview, 2012). The reflection of the transmitted electromagnetic pulse can indicate if underground voids are present (Munk & Sheet, 1997:6).

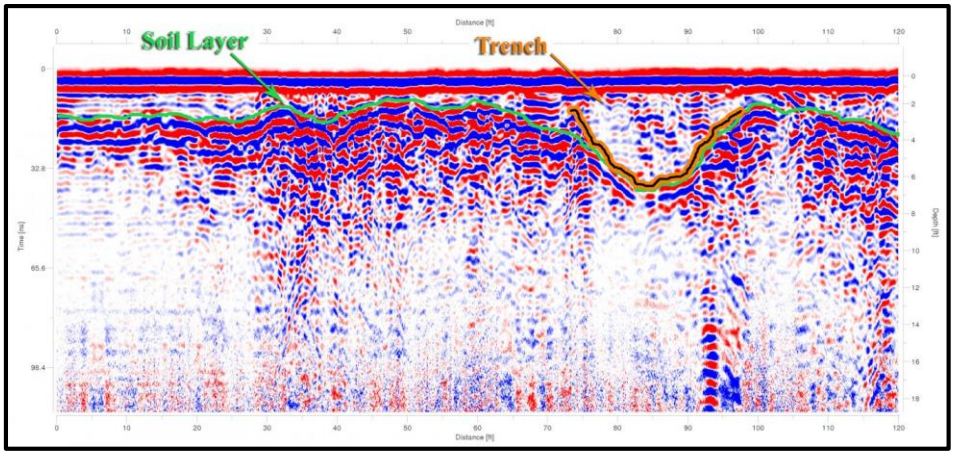

Figure 22: Ground penetrating radar data indicating a sinkhole feature (Geoview, 2012).

Remote sensing techniques such as synthetic aperture radar (SAR) and differential interferometric synthetic aperture radar (DInSAR) processing can be used to observe subsidence, as it provide the capability to gather subsidence measurements over large areas with minimum cost. SAR involves the recording of the phase (time delay) and amplitude (energy intensity) of microwaves from the earth's surface. Numerous satellites have sensors capable of capturing SAR data (Figure 23) (Engelbrecht *et al*., 2011:78). Dinger *et al*. (2007:22) developed an aerial remote sensing technique to locate hidden, underground sinkholes before they collapse. The remote sensing technique was effective in highlighting circular structures which seems to be associated with subsidence occurrence (Dinger *et al*., 2007:29). Dong *et al*. (2015:5523) successfully detected subsidence in East China with the use of InSAR. The results from Dong *et al*. (2015:5523) showed that subsidence increased with 15 cm/year due to underground mining activities.

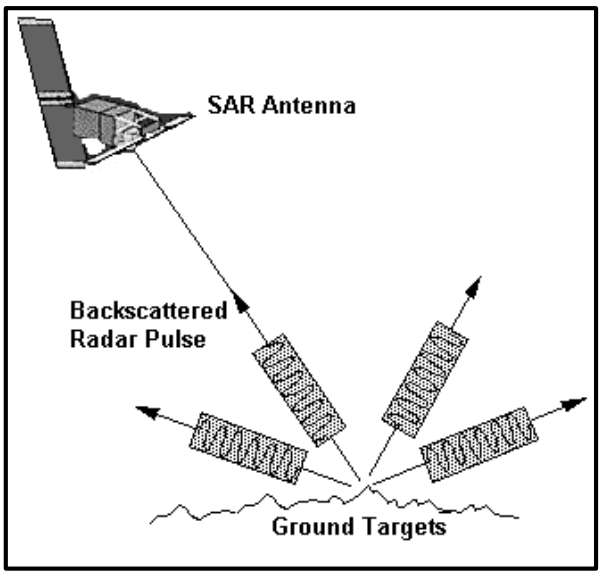

Figure 23: SAR recording backscatter pulses (CRISP, 2014).

Lillesand and Kiefer (1994:722) describe Light Detection and Ranging (LIDAR) as an active remote sensing system which can function in both a profiling and scanning mode. According to Gregersen (2014) LIDAR is a method used to determine the distance to an object by transmitting a laser beam from an aircraft to an object and measuring the time the light takes to return to the transmitter (Figure 24). A LIDAR system flashes up to 400 000 pulses per second at the object (Gregersen, 2014). The pulse is then received by a transmitter as a single or multiple pulses. Single received pulses are from a uniform surface, such as soil, whereas a multiple received pulse is from an area with different heights, such as a forest with high tree tops and lower branches. LIDAR can be used for different purposes such as for the profiling of water depths, which is known to be very accurate (Gregersen, 2014). LIDAR is typically accurate to less than 15 cm in vertical elevation. LIDAR was used by EOMINERS (2013) for the detection of subsidence in eMalahleni. For this study LIDAR can be used to identify areas where subsidence features developed over collapsed underground coal mines.

DEM (Digital Elevation Models) is a technique which can be used for analysing subsidence data in GIS or other digital image processing operations (Lillesand & Kiefer, 1994:340). DEM data is generated with digital profile data, which is orthophoto (orthographic photographs) data which is digitized.

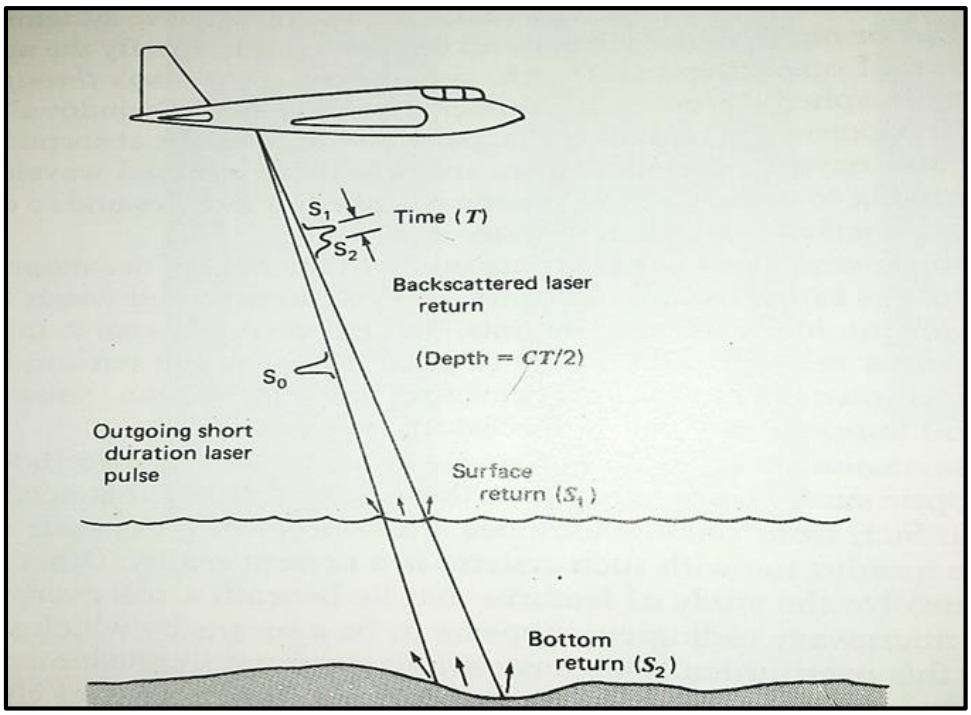

Figure 24: Principle of LIDAR bathymetry (Lillesand & Kiefer, 1994:722).

Orthophotos do not contain the scale, tilts and relief distortions characterizing normal aerial photographs (Lillesand & Kiefer, 1994:335). Orthophotos are produced from a process called deferential rectification which uses overlying conventional photos (Lillesand & Kiefer, 1994:336). By using deferential rectification, photo-scale variation is eliminated. The instrument used to make orthophotos is called an orthophotoscope. However, for this study DEM will be used to identify flow directions for surface water.

Surveying methods such as Global Positioning System (GPS) surveying and spirit levelling can be used to measure and monitor the progress of subsidence development. However, these methods are costly due to the amount of manual labour required for frequent point measurements (Engelbrecht *et al*., 2011:78).

2.7 Acid Mine Drainage (AMD)

2.7.1 Causes of AMD

Coal mining in South Africa generates large volumes of mine waste water that have the potential to harmfully affect an already scarce water resource if not properly managed (McCarthy, 2011:3).

AMD occurs naturally, however, mining activities can encourage the generation of AMD by exposing more sulphates to oxygen and water (Banerjee, 2014:1365; Akcil & Koldas, 2006:1139). AMD originates from mine waste rock, tailings, mining pits and underground workings (Akcil &

Koldas, 2006:1139). The problem occurs not only where operating mines are pumping water for safety reasons but also at closed underground and open-cast workings. Mine dumps with high permeability will allow more oxygen to interact with the sulphate minerals resulting in an increase in the rate of chemical reactions and AMD formation (Akcil & Koldas, 2006:1141).

AMD is formed when sulphur-bearing minerals are exposed to water and oxygen (Akcil & Koldas, 2006:1139). The sulphur in the minerals combines with the oxygen and water which causes the oxidation of sulphur. The oxidation process produces sulphuric acid (H_2SO_4) which is very acidic and is seen as dark reddish-brown water (USGS, 2009). Thus, the primary components needed for the generation of AMD are sulphide minerals, water or humid atmosphere and oxidants which are usually oxygen from the atmosphere (Akcil & Koldas, 2006:1139). Naturally occurring bacteria can quicken the production of AMD by supporting the breakdown process of sulphide minerals (Akcil & Koldas, 2006:1139). Other factors which also increase the rate of AMD generation include: pH, temperature, chemical activity of Fe^{2+}, surface area of exposed metal sulphide, oxygen content and concentration of oxygen in the water phase (Akcil & Koldas, 2006:1141).

Akcil and Koldas (2006:1140) illustrate the generation of AMD by pyrite (FeS_2), which is known to be one of the most common sulphide minerals. The reactions are as follows (Akcil & Koldas, 2006:1140):

- The first reaction is the oxidation of the pyrite into dissolved iron, sulphate and hydrogen:

  $$FeS_2 + 3½\ O_2 + H_2O \rightarrow Fe^{2+} + 2SO_4^{2-} + 2H^+ \quad (1)$$

  The dissolved ferrous iron (Fe^{2+}), sulphate ($2SO_4^{2-}$) and hydrogen ($2H^+$) indicated an increase in the total dissolved solids (TDS) and acidity in the water. The increased TDS and acidity will decrease the pH of the water.

- If oxidizing continues ferrous iron will oxidize to ferric iron (Fe^{3+}) according to the following reaction:

  $$Fe^{2+} + ¼\ O^2 + H^+ \rightarrow Fe^{3+} + ½\ H_2O \quad (2)$$

- At pH levels between 2.3 and 3.5 ferric iron precipitates as $Fe\ (OH)_3$ and jarosite. This precipitation results in less ferric iron in the solution and a lower pH:

  $$Fe^{3+} + 3H_2O \rightarrow Fe\ (OH)_{3\ solid} + 3H^+ \quad (3)$$

- Any ferric iron (Fe^{3+}) from Eq. (2) which does not precipitate from solution through Eq. (3) can be used to oxidize additional pyrite, by the following reaction:

$$FeS_2 + 14Fe^{3+} + 8H_2O \rightarrow 15Fe^{2+} + 2SO_4^{2-} + 16H^+ \quad (4)$$

- By combining Eq. (3) and (4), acid generation which produces iron which finally precipitates as $Fe(OH)_3$ solid can be represented:

$$FeS_2^+ + 3¾\ O_2 + 3½\ H_2O \rightarrow Fe\ (OH)_{3\ solid} + 2SO_4^{2-} + 2H^+ \quad (5)$$

- When combining Eq. (1), (2) and (3), an overall equation is formed for the stable ferric iron which is used to oxidize additional pyrite:

$$FeS_2^+ + 15/8\ O_2 + 6½\ Fe^{3+} + 4½\ H_2O \rightarrow 7½\ Fe^{2+} + 2SO_4^{2-} + 6½\ H^+ \quad (6)$$

Jarosite is known to be a Fe^{3+} bearing precipitate which forms when AMD is generated (Murad & Rojik, 2004:2). However, it is stated by Swayze *et al*. (2008:8) that the dissolution of less-soluble sulphate minerals such as jarosite can cause the generation of AMD.

Backfilled and rehabilitated open-cast coal mines fill with water. When the void becomes filled with water to a depth equal to the lowest point on the rim of the former open pit, further inflow forces void water to decant and discharges on the surface, causing pollution of surface water resources. The decanted water is not only acidic, but typically contains between 2000 and 3000 parts per million dissolved sulphate and a variety of dissolved heavy metals. The emergence on surface of water from the mine void also results in further acid production and the precipitation of red iron oxide. The pH of this water is typically around 2.5, as measured at the Olifants River by EOMINERS (Van Tonder, 2011:38). Evaporation of the water around the seep produces white crusts of calcium sulphate and numerous other sulphate minerals (Epsomite, Hexahydrite, Gypsum, Konyaite, Thenardite, and Halite). The soils around and downstream of such seeps become acidic and saline, and most of the plants die (WWW 2011:45).

2.7.2 AMD in eMalahleni

The Upper Olifants River system provides water to major towns such as eMalahleni, Middelburg, Delmas and Lydenburg (McCarthy, 2011:5). A study done by McCarthy (2011:1) identified large portions of coal deposits which underlie the Vaal River and Olifants River catchments. The Vaal River is the most important river in South Africa, as it supplies water to Gauteng (McCarthy, 2011:1). These coal deposits contain pyrite which has the potential to contaminate the catchments with AMD (McCarthy, 2011:2). As the water seeps into mine workings, it is contaminated by AMD and heavy metals (Bell *et al*., 2001:202). According to McCarthy (2011:1) the mining industry is the main point source of the pollution in the Olifants River.

McCarthy (2011:5) showed that the poor water quality in the eMalahleni Dam, situated in the Olifants River Catchment area, is related to the pollution associated with coal mining in this catchment area. McCarthy (2011:5) highlighted that Eskom imports water for the power stations due to the poor water quality of the eMalahleni Dam.

Fish mortalities have been identified in the Loskop Dam (Figure 25), which forms part of the Olifants River Catchment area (Nkosi, 2001, Driescher, 2008:24). Since 1996 the Olifants River and Loskop Dam have had a history of mass fish mortalities at different times.

Figure 25: Fish Mortalities in the Loskop Dam (Driecher, 2008:24).

The decanting points are caused by the groundwater movement from the ground to the rivers and result in vast seepage zones such as on the western side of T&DB colliery (Stewart & Troksie, 2006:34). The water quality of the decant point is of concern as the pH value is ~2.45 (acidic) and sulphate concentration 10 400 ppm (Janse van Rensburg, 2003:3). Before the water reaches the decant point, it moves through the underground mine workings and is heated by the coal fires in these workings, thus the decant water has a high temperature of 36ºC (Van Tonder, 2011:57). However, these warm decant ponds are easily accessible to local children and used for swimming and bathing (WWW, 2011:48).

2.7.3 Environmental problems associated with AMD

Even though AMD occurs naturally, the acceleration process caused by coal mining can have a profound influence on the local environment and ecology (Banerjee, 2014:1365). According to Banerjee (2014:1365) the impact of the AMD depends on the magnitude of the AMD and the sensitivity of the receiving environment along with other factors such as the degree of neutralization, dilution and/or attenuation.

AMD generally has a pH value of 2.5 which increases dissolution resulting in increased dissolved salts and mobilization of heavy metals (Akcil & Koldas, 2006:1139-1142). AMD can cause long-term damage to water systems, soil and biodiversity due to the low pH, high electrical conductivity and high concentrations of heavy metals such as iron, aluminium and manganese (Akcil & Koldas, 2006:1139 -1140). AMD may impact the groundwater regimes, rivers and other water bodies down-gradient from the discarding point (Penney *et al*., 2014: 244-245).

The production of great quantities of AMD at collieries and the need for cost-effective and environmentally sustainable AMD discarding have created attention in the use of low-quality water from collieries to irrigate agricultural crops (Vermeulen & Usher, 2009:380). Although this will boost the beneficiation of available water and release the increasing pressure on water resources, studies haves shown there is an associated increase in soil salinity (Vermeulen & Usher, 2009:380). Although findings from studies undertaken to assess the impact of irrigation with mine water have shown that irrigation of certain crops would not affect the production thereof (Idowu *et al*., 2008:3), other studies have shown there are critical flaws in the mine-water-irrigation concept (Vermeulen & Usher, 2009:382).

2.7.4 Detection and analysis of AMD

Predicting the potential of AMD can be very difficult and expensive due to the variability of factors influencing AMD, such as mineralogy and site-to-site characteristics (Akcil & Koldas, 2006:1139). Akcil and Koldas (2009:1139) mention that there is no consistent method for classification, measuring and reducing the risk of AMD.

Chemical methods such as cation, anion and alkalinity measurements can be done for the detection of AMD (Banerjee, 2014:1371). Cations and anions of water samples can be analysed using processes such as Inductively Coupled Plasma-Atomic Emission Spectrometer and Ion Chromatography. According to Peeters (2014:2) a Piper plot is a useful visualization method for water chemistry. A Piper plot is composed of two ternary diagrams, one for major anion composition and one for major cation composition. The two ternary diagrams are combined into

a central diamond plot to identify groups and deduce the main hydro chemical processes affecting the water (Peeters, 2014:2).

Banerjee (2014:1365) did a study on the assessment of potential generation of AMD from coal mines in India. The study involved static and kinetic leaching tests on coal mining waste (Banerjee, 2014:1366). The kinetic test was done to simulate mine site leaching by imitating chemical weathering in the laboratory. The data was then used to estimate the reaction rates along with oxidation-neutralization analysis to predict whether AMD may occur (Banerjee, 2014:1367). Another prediction method is acid-base accounting (ABA). ABA predicts the pre-mining drainage quality by establishing the maximum potential acidity (MPA) and neutralization potential (NP) (Foli *et al*., 2015:8471). The net neutralisation potential (NNP) is determined by the balance between NP and MPA (Foli *et al*., 2015:8471).

According to Murad and Rojik (2004:1) AMD precipitate mineralogy can be related to the occurrence of certain minerals to genetic factors such as pH and sulfate concentrations. Mineral sequences may develop as a function of local changes in genetic conditions and can serve to identify such variations in the field (Murad & Rojik, 2004:1). The creation of goethite and hematite by means of chemical precipitation includes the following reactions (Silva *et al*., 2001:469):

- The first reaction involves the precipitation of iron. Hydrolysis of soluble iron by addition of an alkali to precipitate the metal as an hydroxide. The reaction allows the separation of iron from other metals present in the AMD.

$$Fe^{3+}_{(aq)} + 3OH^{-}_{(aq)} \rightarrow Fe(OH)_{3(s)} \quad (1)$$

- The hydroxide is dissolved in water by the addition of nitric acid to form a complex called iron-hexa-aquo ion.

$$Fe(OH)_{3(s)} + 3HNO_{3(aq)} \rightarrow ([Fe(OH)_6]^{3+})_{(aq)} \quad (2)$$

- The synthesis of goethite from Fe^{3+} can be obtained under alkaline conditions by the precipitation of the ferric nitrate solution (iron-hexa-aquo-ion), producing a precipitate called ferrihydrite ($Fe_5HO_8.4\ H_2O$) by the addition of potassium hydroxide at pH 12.0.

$$([Fe(OH)_6]^{3+})_{(aq)} + KHO_{(exc)} \rightarrow (Fe_5HO_8 4H_2O)_{(s)} \quad (3)$$

- Under these conditions, the initially formed precipitate was dissolved and released an ionic species ($Fe(OH)_4$-) which will form crystalline goethite by nucleation, thus beginning the process of growth of goethite (FeOOH) (Reactions 4 and 5).

$$(Fe_5HO_8 4H_2O)_{(s)} \rightarrow [Fe(OH)_4^-]_{(aq)} \quad (4)$$

$$[Fe(OH)_4^-] \rightarrow FeOOH_{(s)} \quad (5)$$

- The final reaction is the production of hematite. The goethite (FeOOH) can be converted into hematite (Fe_2O_3) by thermal dehydration (loss of water), dehydroxilation (loss of hydroxyl) or oxidation/ reduction (by electron change). The most convenient method to convert goethite into hematite is thermal dehydration (Reaction 6), due to the reaction conditions and stability of the formed product.

$$2FeOOH_{(s)} \rightarrow FFe_2O_{3(s)} + H_2O_{(g)} \quad (6)$$

Goethite en hematite are known to be well crystallized and can therefore be identified with X-ray diffraction (Murad & Rojik, 2004:3). It is mentioned by Murad and Rojik (2004:3) that jarosite is formed under the most acidic conditions (pH of 1.5-3) and the highest sulphate concentration ([SO_4]>3000 mg/l), whereas goethite forms under less acidic conditions (pH <6) and lower sulphate concentrations ([SO_4] <1000 mg/l). According to Silva *et al*. (2011:469) goethite can convert into hematite (Fe_2O_3) due to thermal dehydration, dehydroxilation, oxidation or reduction. The colours of these minerals are usually yellow to reddish-brown and can be seen from airborne imagery.

Due to the acidic conditions which these minerals are associated with, these minerals can be used in remote sensing studies to locate potential AMD (Swayze *et al*., 2008:8). EOMINERS detected these minerals by using hyperspectral satellite imagery (EOMINERS, 2013:24). Quental *et al*. (2011:61) approached the detection of AMD with the application of Imaging Spectroscopy (IS), also known as Airborne Hyperspectral imaging Sensing (AHS). Quental *et al*. (2011:69) defined IS as a high-precision method with the ability to classify items on their spectral properties. According to Quental *et al*. (2011:61) IS is used to map mineral assemblages such as sulphates, oxides and oxyhydroxides which are recognisable by particular spectral ranges due to their chemical and structural properties.The areas with high correlation mineralogical assemblage, which are related with low pH, are then mapped as potential AMD areas (Quental *et al*., 2011:61). IS can be used for target remediation as IS locates the source of AMD producing minerals (Cowie *et al*., 2014:746). IS surveys are done by using imaging spectrometers mounted on an aircraft (Figure 26) (HVC, 2012). Every band is composed of continual scan lines acquired by the scanner

along the flight line. IS uses that portion of the electromagnetic spectrum that falls between 0.4 and 2.5 µm (Figure 26).

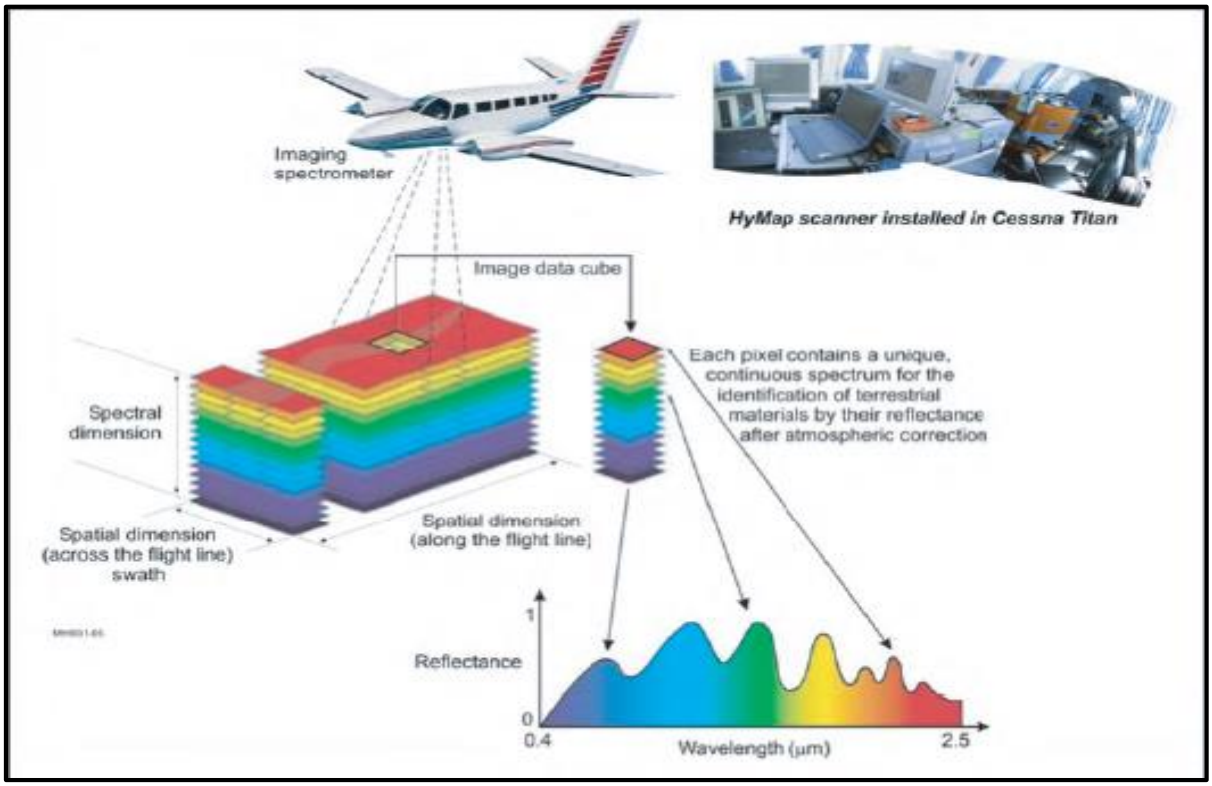

Figure 26: Image indicating the aspects of AHS (HVC, 2012).

2.8 Air pollution

2.8.1 Causes of air pollution

Air pollution is caused by airborne contaminants present in various forms such as gases, vapour or aerosol (dust, aerosols, fumes, smoke, and vapour) (Kovacs *et al*., 2014:1421). These pollutants are released from anthropogenic sources (industries, traffic, domestic activities) or through natural processes (volcanoes, forest fires) (Huang & Gui, 2014:839).

According to Department of Environmental Affairs (2010:4) power stations contributes 73% of the total estimated oxides of nitrogen (NO_x) emission of 978 781 tons per annum and 82% of the total estimated sulphur dioxide (SO_2) emission of 1 633 655 tons per annum.

According to Lloyd (2002:2) all coal contains methane and as mining proceeds, the methane is released into the atmosphere. Lloyd (2002:2) also mentioned that South Africa emits 7 million tons of carbon-dioxide per annum from underground coal mining activities. Mining operations like drilling, blasting, hauling, collection, and transportation also contribute to emissions and air pollution such as the use of explosives which releases carbon monoxide (CO).

The estimated annual emission of fine particle matter (PM_{10}) from metallurgical industries contributes 17% of the total emission (Department of Environmental Affairs, 2010:4). The metallurgical industries also emit 229 tons of NO_2 per annum and 3223 of SO_2 per annum (Department of Environmental Affairs, 2010:5). According to Zibret *et al*. (2012:4455) metal industries contribute to the emission of Fe, Co, Mn and V.

Domestic use of coal such as coal-burning stoves and heated boilers in hospitals and workshops contribute to poor air quality (Banks *et al*., 2011:61). These domestic coal combustion processes are known to be one of the most extreme sources of airborne particulates and gaseous emissions to be inhaled in high concentration (Banks *et al*., 2011:61). Other factors which contribute to low-level air pollution are synthetic fuel production and vehicle emissions (especially leaded petrol) (Banks *et al*., 2011:61).

2.8.2 Air pollution in eMalahleni

According to the study done by Pone *et al*. (2007a:10) the concentrations of toxic gases in the Witbank Coalfield are higher than local and international standards. A study done by Pone *et al*. (2007a:4) determined that 170 million tons of carbon dioxide are emitted from the spontaneous combustion of coal in the Witbank Coalfields. Methane and other volatile gases from these coal fires are considered as a significant contributor to the global deterioration of the biosphere (Finkelman, 2004:20). Discard coal dumps also play a major role in the release of air pollution in eMalahleni as the discard dumps start burning due to spontaneous combustion (Pone *et al*., 2007b:129).

Discharges from coal-fired power stations are an enormous concern for eMalahleni as these stations cause poor air quality in nearby residential area as well as at some distance from the emission point (Banks *et al*., 2011:60). The study by Zibret *et al*. (2013:4460) showed that the metal smelters in and around eMalahleni contribute to Fe, Co, Mn and V emission, whereas coal-fired plants contribute to fly ash which is associated with Al, Sr and Li.

Eskom uses low-grade coal to generate electricity which results in the use of large quantities of coal as fuel for the coal-fired power station (Banks *et al*., 2011:13). By using larger quantities of low-grade coal, more gases are emitted due to the high ash content in the coal (Banks *et al*., 2011:13). None of the coal-fired power stations in eMalahleni have flue gas desulphurisation equipment installed (Banks *et al*., 2011:60). According to Banks *et al*. (2011:60) Eskom will install flue gas desulphurisation at the new Kusile power station which will be build. The Kusile power station will be the first in South Africa to have this desulphurisation technology (Banks *et al*., 2011:60).

Power stations situated in eMalahleni release their emissions far above the steady surface layers through high stacks (Banks *et al*., 2011:58). Plumes do not reach ground level due to the surface temperature inversion occurring at night time. Plumes can reach ground level during summer days due to convection.

2.8.3 Health problems associated with air pollution

Coal mining has always been a dangerous profession with occupational health and safety hazards. Coal workers are likely to suffer from work-related disease such as black lung disease, the non-clinical name for a variety of respiratory illnesses of which coal workers' pneumoconiosis is the most prominent (Khan, 2014).

According to Banks *et al*. (2011:58) the mortality rates calculated for South African urban areas estimate that outdoor air pollution caused 3.7% of deaths from cardiopulmonary disease, 5.1% of deaths from cancers of the trachea, bronchus and lungs, and 1.1% of deaths from respiratory infections in children under the age of five years.

Toxic gases released from coal combustion such as carbon-monoxide can enter into houses through cracks and holes which can result in respiration problems.

Some health impacts related to polutants released from coal fires include (PSR, 2009):

- Respiratory effects: Including asthma, lung disease and lung cancer, and irregular lung development in children.

- Cardiovascular effects: Including artery obstructions leading to heart attacks and death of tissue due to oxygen deficiency, which can eventually lead to permanent heart damage.

- Nervous system effects: Mercury and lead can cause loss of intellectual capacity by acting on the nervous system.

- Pyrite: Causes pneumoconiosis (Harrington *et al*., 2013:1220).

- When CO enters into the bloodstream, it decreases the amount oxygen that is transported to the body's tissue and cells. This is because the haemoglobin in the red blood cells is more attracted to CO than to oxygen.

- Carbon dioxide can be a health risk when the carbon dioxide concentrations are high enough to displace oxygen and cause choking.

- Lead: Lead can cause a decline in intelligence quotient (IQ) and affects the central nervous system. Lead also affects the kidneys, blood-forming system and the reproductive system.

Coal fly ash is created as a by-product from the combustion of coal (Jones *et al*., 2009:3345). Fly ash is formed when incombustible minerals found in the coal are melted. Microscopic glass particles are formed due the very high combustion temperatures of coal. These glass particles can recrystallize and form minerals such as mullite, quartz and hematite (Jones *et al*., 2009:3345).

According to Sambandam *et al*. (2014:801) exposure to coal fly ash is a major health concern as it can be deposited deep into the lung's epithelial cells causing diseases such as pneumoconiosis. Pneumoconiosis is characterized by nonneoplastic granulomatous and fibrotic changes in the lungs and cause various respiratory infections, fatigue and cough (Khan, 2014). These coal fly ash particles are small enough to penetrate through organs, disturbing the basic functions of the organs and causing inflammation of tissue and altering the redox balance towards oxidation leading to cell death (Sambandam *et al*., 2014:802). The potential health effects that fly ash can have on the health of humans depend on the geochemical composition of the coal and the post-combustion process of the coal (Jones *et al*., 2009:3332).

Coal combustion releases sulphur into the atmosphere, which combines with oxygen to form sulphur dioxide (Banks *et al*., 2011:63). Acid rain can change the level of nutrients in lakes and rivers, as it acidifies the water (EPA, 2014). These acidic water conditions can kill aquatic biodiversity. It is also known that acid rain can affect forests, vegetation and soils as it weakens trees and vegetation's defence to diseases (EPA, 2014).

2.8.4 Detection and analysis of air pollution

A cost-efficient method for the sampling of gaseous air pollutants can be done with a hand pump consisting of a Teflon inlet (Pone *et al*., 2007a:4). Gas analyses can be done with gas-chromatography (Pone *et al.,* 2007a:4). Gas-chromatography involves cryogenic pre-concentration of the air samples with liquid nitrogen and then the re-vaporizing of the sample in hot water (Pone *et al.,* 2007:4a*).* The sample is then separated into different detectors, for the detection of different elements (Pone *et al*., 2007a:4).

According to Sugimoto *et al.* (2015:107) air pollutants can successfully be detected by using a polarization particle counter (POPC) that measures the forward scattering and the two polarization components of backscattering for single particles and a polarization-sensitive (532 nm) two-wavelength (1064 nm and 532 nm) LIDAR. The optical characteristics measured using the LIDAR

were consistent with the POPC measurements. POPC consequently provides information on size and non-sphericity of the particle at the same time (Sugimoto *et al.,* 2015:108).

Satellite imagery is a common method used to detect air pollutants (Wanning *et al*., 2014:104). These methods include LIDAR, MODIS and AOT. MODIS capture data in 36 spectral bands ranging in wavelength from 0.4 µm to 14.4 µm and at varying spatial resolutions

Zibret *et al* (2013:4456) studied the atmospheric emmion from different sources by analysing dust samples. According to Zibret *et al*. (2013:4456) the dust acts as a sink of atmospheric particles, therefore the dust mirrors the scale for atmospheric emission from different sources.

2.8.4.1 Collecting of dust samples

Zibret *et al.* (2013:4456) studied street dust to determine the atmospheric emission from different sources such as coal-fired plants and metal smelters. According to Zibret *et al.* (2013:4456) street dust acts as a sink of atmospheric particles, therefore the dust mirrors the scale for atmospheric emission from different sources. Dust can be analysed by ICP-MS and XRF (Zibret *et al.* 2013:4459).

Dust can be gathered by means of dust traps or dust wipes (Van Tonder, 2011:93; Gulson *et al*., 2013:171). Dust traps can be placed in houses and clinics to measure indoor dust amounts and compositions (Van Tonder, 2011:95). The dust trap consists of a microscope glass slide on a Petri-dish which is placed indoors and collected after three months for analysing (Van Tonder, 2011:95). Dust wipe methods, which were used by Van Tonder (2011:97), are known as the Niton method and uses LEAD WIPES from Lynx which meets the ASTM E1792 standard. The method is based on the wiping of a set area, in this case a 10x10 cm surface, with the dust wipe and then to analyse the dust content expressed as ppm/cm^2 with a portable X-ray Fluouresence instrument.

2.8.4.2 Analysing dust samples

Chemical and mineralogical composition of dust samples can be determined by means of and XRF (Salmanzadeh *et al*, 2015:214). X-Ray Fluorescence (XRF) is based on the inherent property of atoms to expel an electron from the inner orbitals (K, L or M) when radiated with a primary beam of sufficient energy (Klein & Dutrow, 2008:322) and the unique fluorescence energy produced by the displaced electrons of the different atoms. ICP-MS is one of the best techniques used to analyse trace elements (Hann *et al*., 2012:115). Mass spectrometry is a technique used to take measurements of atomic and molecular masses (Oxford Dictionary of Geology & Earth Sciences, 2013:362).

2.9 Risk assessment

The scientific concept of risk implies the measurement of the probability of an outcome (event), and the extent (negative consequences) of the outcome (event) (ISDR, 2009:25; Andretta, 2014:1185). This implies that risk has two components, the probability (frequency) of the event, and the probable consequence of the event. Risk can therefore be calculated from the following equation:

Risk = probability (frequency) X consequence (magnitude of the impact) (1)

Hazard can be defined as the probability (likelihood) of the harmful impact (consequence) that includes losses (deaths, injuries, negative impact of livelihoods, loss and destruction of properties) and degradation to the environment (ISDR, 2009:17; Andretta, 2014:1186).

Based on the above, risk can be seen as a function of the potential hazards and the vulnerability of the humans to be affected.

Early warning can be defined as the set of capacities needed for the provision of timely and effective warning information, through identified institutions, that allow individuals, communities and organisations exposed to a hazard to take action to avoid or reduce their risk and prepare for effective response (ISDR, 2009:12).

2.9.1 Risk mapping

The application can be used to spatially identify potential risks by analysing potential hazards and evaluating existing conditions of vulnerability that together could potentially harm exposed people, property, services, livelihoods and the environment on which they depend (ISDR, 2009:26). According to Girgin and Krausmann (2013:957) a risk map is used to display the severity and the impact zone of a hazard.

Scoring is a method used for risk assessment in which the severity of each risk factor is calculated based on a point scale (Hubbard & Evans, 2010:1). On an ordinal scale, factors such as likelihoods are assigned numbers that reflects the order of the factors on an underlying attribute scale (Hubbard & Evans, 2010:2).

GIS is a computer program which aids in efficient development of risk mapping (ACF International, 2010:2). GIS maps are made from one or more layers or collection of geographic objects that are similar. These layers may contain vector features or raster surfaces. Vector features are represented as points, lines and polygons. Raster data is cell-based where a raster data model is represented as single square cells and each cell will have a value corresponding (Morais,

2012). Akinbobola *et al*. (2015:626) successfully created a risk map by using remote sensing data (raster data) and vector data in a GIS.

Chapter 3: Methodology

In order to address the objectives, both primary and secondary data were used. The primary data were generated from field visits. The secondary data obtained from various published and unpublished sources. Secondary data used in this study were mainly provided by the EOMINERS.

In general coal fires can be detected by a Thermal Infrared Spectrometer or a Thermal Infrared camera which captures digital images which requires mosaicking before it can be used in a GIS program. These images can be manually mosaicked into an image to map hazardous areas or through using georeferencing software. The coal fire temperatures can then be classified by using field temperature measurements of the coal fires to verify temperature measurements recorded on the infrared images. A map can then be produced that identifies potential hazardous areas where underground coal fires occur. The hazardous potential can be classified according to the temperatures intervals recorded. TIR data used in this study were provided by the EOMINERS project.

LIDAR can be used to identify areas where subsidence features over collapsed underground coal mines developed (EOMINERS, 2013). The LIDAR data can be used to create risk maps in GIS. LIDAR data used in this study were provided by the EOMINERS project.

AMD produce secondary minerals which can be detected by hyperspectral remote sensing due to the unique spectral signatures of minerals. Water quality parameters can also be used to identify water affected by AMD. The AMD flow path can be determined by using a digital elevation model (DEM) to identify the flow directions of surface water. Water quality, satellite and aerial data used in this study were provided by the EOMINERS project.

Street dust can be used as a proxy for air pollution as street dust is considered a sink for dust containing high levels of metals. Air quality data can then be used to produce a map which identifies areas with potentially high levels of air pollution around sources of the pollution. Street dust data used in this study were provided by the EOMINERS project and from Zibret *et al*. (2013).

An environmental risk map of the study area based on coal fires, subsidence, AMD and air pollution data could then be produced.

Software

Remote sensing analysis was performed using TNTmips 2013 imageprocessing software. GIS analysis was done using ArcGIS 10.2 while Microsoft Office Excel and Access were used for statistical analysis.

Datasets

Secondary data collected during the EOMINERS project field campaigns between 2011 and 2012 were provided to test the dissertation statement. In addition temperature measurements of coal fires were collected in the field during 2013. This data was used to classify and add values to the mosaic TIR images.

The following table indicates the sources of all the data:

Table 3: Sources of data

Data	Type of data	Source of data
TIR images	Secondary data	EOMINERS
Field measurements (Temperatures and GPS coordinates	Primary data	NWU (Adéle Schoeman)
LIDAR	Secondary data	EOMINERS
DEM	Secondary data	EOMINERS
Hyperspectral remote sensing data	Secondary data	EOMINERS
Street dust samples	Secondary data	EOMINERS (Zibret *et al*., 2013)

Research design

The following table shows the strengths and weaknesses of the research designs:

Table 4: Strength and weaknesses of the research design.

Research Design	Strengths	Weaknesses
Secondary data analysis	• All data is available • The TIR data has a high resulotion (good quality).	• Abundant amount of data received. All the data had to be sorted to decide which data would be used. • The mosaicking method used was very challenging • TnTmips was limited to mosaicking only 3 images together due to the size of the TIR data • Time elapsed between secondary data and primary field data gathering may impact on the use of the data for classification purposes.
Primary field data	• Accurate, georeferenced temperature measurements of known underground coal fires were made. • Aerial view of the site allowed for an overview of the entire study area.	• Due to the danger posed by the sites visited, care had to be taken not to spend too much time in the hazardous environment. • Limited funds were available for field visits.
Risk map compilation	• Good quality data was available. • Results will be very useful for municipal planning purposes.	• Software used for mosaicking of TIR images required training. • Mosaicking of images was very time-consuming. • Due to the lapse between collection of primary and secondary data verification might be troublesome.

3.1 Objective Two: Detect burning underground coal fires in the study area.

3.1.1 Data sources and data collection methods

The secondary data, TIR images, field measurements and temperature logs, obtained from the EOMINERS project were collected over an area of approximately 8750 ha.

The data consists of 10 400 digital infrared images of the eMalahleni area. The images were ordered by flight lines of the airplane and the data set for each image recorded includes the date, time, image name, coordinates (longitude, latitude and altitude) and flight information.

A series of overlapping images (~60% overlap between images and flight lines) was acquired over numerous flight lines. During the flight campaign lines were mostly flown in an east-west direction.

The field campaign was carried out during the summer period November 2011 to January 2012. Night time flights were performed with a fixed-wing aircraft which was modified for remote sensing surveys. The area was surveyed by Kopano Energy Resources for the EOMINERS project. (Fischer, 2001:4). The aircraft used had a cruising speed of 140 Kts 100m p/h (160 km/h), operation level service ceiling: 3000 ft (900 m) AGL, maximum endurance of 6 hours, an un-pressurized cabin and a maximum pay-load of 700 kg. Kopano Energy Resource Pty Ltd used a calibrated in-house developed lightweight integrated internal measurement unit (IMU) and GPS system easily fitted to the aircraft to record the roll and pitch which was necessary for the ortho-rectification of the images. The TIR camera system used was a FLIR System with a 320X240 pixel resolution, spectral range of 7.5 to 13 micrometers, and a Field of View (FOV) / minimum focus distance of 24° x 18° / 0.3 m. With a transmission rate of ~7Hz and a stated accuracy of +/- 2ºC +/- 2%, and temperature range of -40°C to +1500°C (optional up to +2000°C) (Fischer, 2011:7). A small computer was attached to the aircraft platform to store thermal imagery and operate the camera. FLIR data was transferred from this computer to a laptop computer for further processing.

A series of overlapping images was acquired for the selected area and the relevant images provided for the use in this project. Kopano developed software specifically for digital processing of remote sensing FLIR imagery. Due to the proprietary nature of the image processing no details of the process can be disclosed here.

The EOMINERS field campaign used rigorous ground trothing which included the installation of a test pad for calibration purposes during the flight campaign as well as the instillation of temperature data loggers in a small impoundment towards the centre of the flight area (Fischer, 2011:7). The temperature loggers were used to construct in-stream temperature profiles and to verify FLIR thermography data (Fischer, 2011:7).

During the field visit in March 2013 the Raytek hand-held non-contact laser sight IR thermometer was used for temperature measurements of selected sites in the study area (Figure 27). Measurements were taken of potential hotspots as well as fissures in Blesboklaagde to the east of the R544 road (Figure 28). The measurements were made from centimetre-wide fissures and holes of up to seven metres in diameter.

The IR thermometer is a light-weight thermometer which can be held by one hand. The IR thermometer has a red laser for aiming at an object to obtain accurate temperature measurments (Mint Gadgets, 2012). Data recorded for hotspots included location (Garmin GPS), size and depth of hotspots.

Figure 27: Measuring of temperatures from a small hole at the study area (Photo by CJ Roelofse, 2013).

Descriptive information was recorded, geographical position determined by means of a Global Positioning System (GPS). A Jabiru aircraft was used for an over-flight for visual inspection of the study area and surroundings. A Canon EOS400 digital SLR camera was used to obtain oblique aerial photographs of the study area as well as documenting the points where field temperature measurements were taken. SLR and digital photographs provide a point of reference for thermal images by assisting with geo-referencing and providing a better understanding of surrounding features.

Most of the area is privately owned, thus access to underground coal fire sites were limited and data were therefore mainly collected on Blesboklaagte.

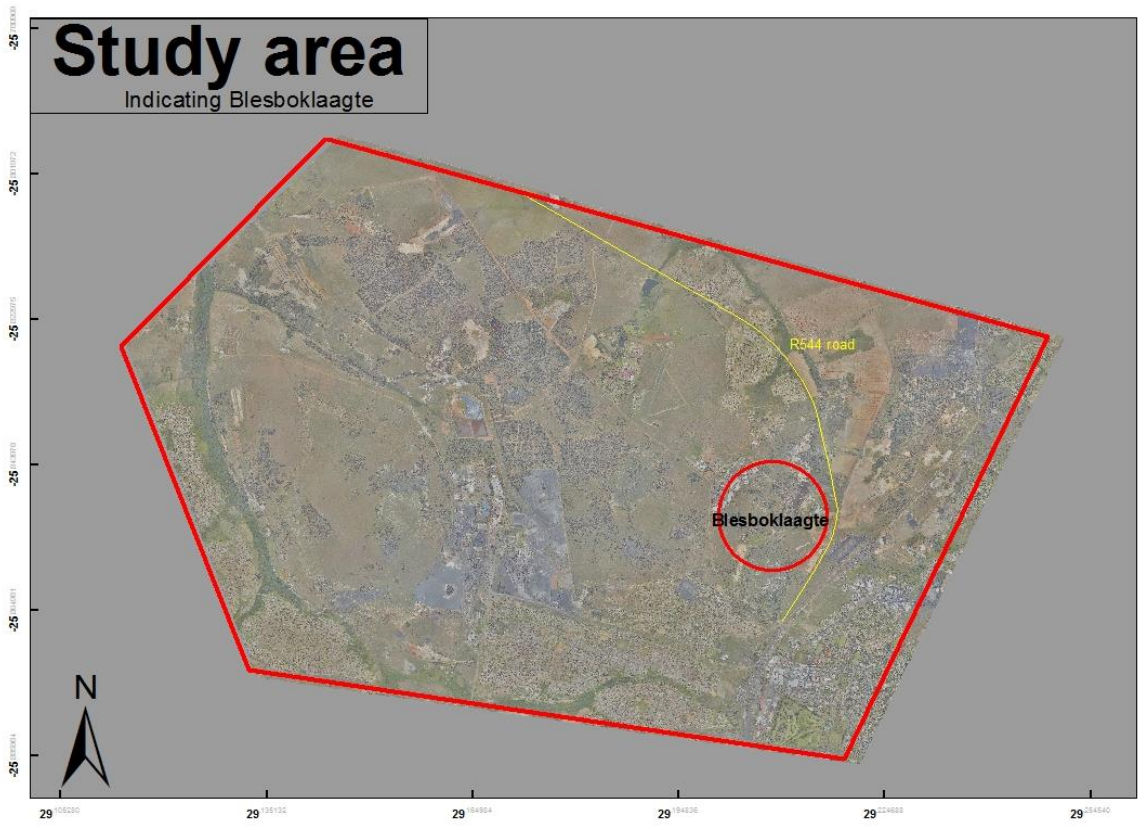

Figure 28: Aerial photo indicating Blesboklaagte whithin the study area.

3.1.2 Methods of data analysis

Due to the 60% overlap in the TIR images a large number of images were acquired. Before the TIR images could be analysed some images had to be eliminated to limit the number of images

A mosaic of the selected images had to be constructed to provide a seamless image which covers the entire study area. This was done with the TNTmips 2013 (MicroImages, 2013). Mosaicking was done by defining a minimum of three tie-points for two bordering photos which resulted in a 25% to 50% overlap between images. This was done with all the photos to form a complete image of the study area.

The geometric distortions in the mosaicked image had to be eliminated. The elimination process was done by overlapping the mosaicked image over a geo-referenced high resolution aerial photo of the area. The overlapping process was done by identifying clear objects on the mosaic image and the colour photo. The overlapping process removed the distortions by replacing objects in the image to their true positions. The overlap process also geo-referenced the mosaicked image.

As seen from the field data in Table 9, there is a vast variation in temperature measurements from different subsidences in Bleskoblaagte. The temperatures vary from 35.5°C to 495°C. The high temperatures are considered a clear indication of underground coal fires.

The mosaicked geo-referenced images were classified into three temperature classes linked to potential for coal fires:

- highest temperatures (+200 ˚C) - listed as high potential for coal fires;
- lower temperatures (48 ˚C - 75 ˚C)- listed as medium potential for coal fires;
- lowest temperatures (35 ˚C) - lower than the second class but above background values listed as low potential for coal fires.

3.2 Objective Three: Locate potential subsidence in study area area.

3.2.1 Data sources and data collection methods

LIDAR data were provided by EOMINERS. Limited information was obtained on the gathering of LIDAR data. The only information provided was that the LIDAR data was collected at <1m spatial resolution over the 8750Ha area.

3.2.2 Methods of data analysis

The shape file of the LIDAR data provided by the EOMINERS project was used to create a subsidence map. By changing the interval size and the colour ramp, subsidence areas where underground coal mining occurred could be seen more easily in ArcMap (Esri Developer Summit, 2015).

Subsidence features were indicated on the map. Separate maps were constructed for the different subsidence features. Each map includes a classified LIDAR image of a specific subsidence feature and an aerial photo of the same subsidence feature. By including an aerial photo with the LIDAR image a visual comparison could be made and the effects of the subsidence on the surrounding area could be determined.

To indicate the relationship between coal fires and subsidence, maps for individual high risk subsidence areas were created by means of map layering in ArcGIS 10.2. The LIDAR layer was overlapped with the classified coal fire data. The maps therefore indicate the co-occurrence of subsidence and coal fires.

3.3 Objective Four: Identify AMD sources and pathways in drainage systems in the study area.

3.3.1 Data sources and data collection methods

EOMINERS provided digital geo-referenced World View 2 images. The images indicate the occurrence of sulphidic iron minerals. A 1-m Digital Elevation Model (DEM) image provided by EOMINERS was used to map the surface water flow paths.

3.3.2 Methods of data analysis

Data received from EOMINERS were used to compile two AMD related maps, one indicating sources of AMD and the other AMD pathways. Potential AMD sources were identified by using a geo-referenced aerial photo to categorise features such as coal dumps, smelters, subsidences and warm decants as well as areas where water quality parameters indicated AMD contamination.

Three geo-referenced TIF layers containing data of AMD producing minerals was received from EOMINERS, consisted of high resolution World View 2 satellite images. The three layers included the occurrence of sulphidic iron minerals such as goethite, hematite and jarosite. Areas with accumulation of sulphidic iron minerals were identified by overlapping a geo-referenced aerial photo with the TIF layers. The areas with accumulation of these minerals where marked with a feature point. All the feature points where then saved as a new AMD source layer.

Drainage channels and the potential downstream flow paths were mapped using digital elevation model (DEM) data from EOMINERS. The DEM layer is a three dimensional representation of the study area. A layer representing all the rivers in the study area was overlapped with the DEM layer. By overlapping these layers, the downstream paths of the rivers could be determined (water flows from higher to lower areas).

Finally the Flow path layer was overlapped with the AMD source layer to produce an AMD pathway map (EOMINERS, 2013:25).

3.4 Objective Five: Identify areas with high levels of air pollution

3.4.1 Data sources and data collection methods

Street dust can be used as a proxy for air quality impacts as the retention time for elements in street dust is 250 days (Zibret *et al*., 2013). However, factors such as severe rain storms influence the quantity of the dust as it remobilizes in dry weather conditions.

Of the forty-six dust samples collected by Zibret *et al*. (2013) around eMalahleni only eleven samples fall within the study area (Figure 29). The eleven street dust sample points of the study by Zibret *et al*. (2013) are located on the eastern and southern part of the study area. Two sample points were taken in separate industrial areas which is located close to smelters. The remaining sample points are distributed over residential area, farms, roads and commercial areas.

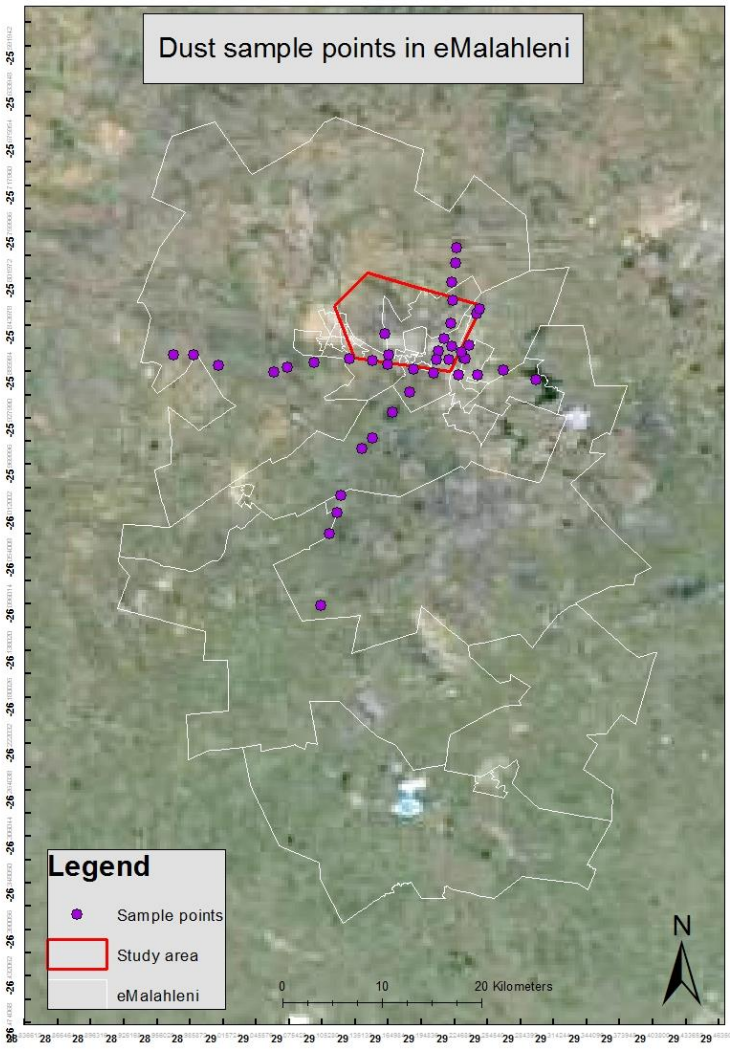

Figure 29: Google Earth image indicating the study area and dust sample points.

3.4.2 Methods of data analysis

The main air pollution sources in eMalahleni associated with coal mining activities are the particulates from the smelting industries and fly ash from coal power stations and other coal burning activities. However, before the air pollution data could be analysed, the chemical elements which are associated with coal mining had to be identified and seperated from the other pollution sources. The chemical elements which are associated with smelting industries and coal combustion were identified by using literature from previous studies.

The data received from the EOMINERS project and Zibret *et al*. (2013) was received as a shape file which could be added onto ArcGIS 10.2.

The Kriging estimator function in ArcGIS 10.2 was used to analyse the air pollution data. Kriging is an interpolation method in which the neighboring measured values are weighted to derive a predicted value for an unmeasured location (Mehdad & Kleijnen, 2015:1804). Weights are based on the distance between the measured points, the prediction location, and the overall spatial arrangement among the measured points (Bohling, 2005:3).

To obtain the best Kriging models in GIS raster layers were first created for each element based on the best selected model during the Kriging application stage. The data was classified into nine classes on resulting a map, to produce pollution zoning. The pollution zoning map was used to identify dust pollution zones in the study area.

3.5 Objective Six: Produce a risk map for the study area

3.5.1 Data sources and data collection methods

All analysed data which was used in objective two to five, was used to create a final environmental risk map for the study area.

3.5.2 Methods of data analysis

The risk map was compiled by calculating the risk value for different risks in the study area which was detected in objective three to five. The risk was calculated by the following formula:

Risk = consequence (magnitude of the impact) X probability (frequency)

The numeric values were assigned for the consequence by rating each factor to the following scale (Table 5):

Table 5: Rating scale for consequences.

Consequence	Harm caused	Score
Negligible	Minimal injury and damage	1
Minor	Minor injury and damage	2
Moderate	Moderate injury and damage	3
Major	Major injury and damage	4
Catastrophic	Incident leading to death catastrophic damage	5

The numeric values were assigned for the probability by rating each factor to the following scale (Table 6):

Table 6: Rating scale for probability.

Probability	Probability that harm will occur	Score
Remote	Never	1
Unlikely	Occurs rarely	2
Possible	Could occur, however uncommon	3
Likely	Recurrent , however frequent	4
Very likely	Occurs frequently	5

After a score has been assigned for the consequence and probability, the scores are multiplied and the risk rating can be assigned (Table 7).

Table 7: Risk rating.

Low Risk (1-8)	Medium Risk (9-14)	High Risk (15-25)
The area needs to be periodically reviewed to ensure controls remain effective	Additional controls and monitoring need to be implemented	New controls need to be identified and implemented. Risk needs to reduce to a low or medium level.

Table 8 indicates the scoring and risk rating.

Table 8: Scoring for risk ratings.

	Consequence				
Probability	1	2	3	4	5
	2	4	6	8	10
	3	6	9	12	15
	4	8	12	16	20
	5	10	15	20	25

By combining the classification data of the hazard potential for coal fires, subsidences, AMD and air pollution an environmental risk map for a part of the eMalahleni municipal area was

constructed. All analysed data from objective two to five was incorporated as separate layers in ArcGIS 10.2.

The potential hazardous areas which were identified for coal fires, subsidence, AMD and air pollution were assigned a risk rating. Each area was digitised to create a new layer (hazard potential). The risk rating for each area was entered as attributes to the new layer. The new layer was then classified to indicate the low, medium and high potential risks. The final risk map therefore indicates all potential risk associated with coal mining activities.

Chapter 4: Results

4.1 Objective Two: Detect burning underground coal fires in the study area.

4.1.1 Field data

During the field visit in March 2013 white smoke and heat, escaping from several of the subsidence features, were observed. The smoke had a rotten egg-like smell, which is known to be hydrogen sulphide (H_2S) (OSHA, 2005). When H_2S gas is inhaled, it is absorbed by the lungs and affects the oxygen utilization and central nervous system. The severity of the health impact is determined by the level and duration of the exposure. The H_2S is released into the atmosphere, but according to OSHA (2005) the H_2S is heavier than the air. This will result in H_2S gas eventually accumulating in the soil, which will lead to soil contamination and this definitely calls for further investigation to determine the impact of H_2S on the surrounding environment.

Figure 30 is a Google Earth map which indicates the location of field measurements and the temperatures of the specific measurements. The field data that was obtained consists of temperatures differing from 35°C to 495°C which can be seen in Table 9.The table also includes a description of the locality where the temperatures were taken. The description varies from fissures smaller that 2 meters in diameter, to smoker holes larger that 5 meters.

Various statistical values for the field measurements were determined. Firstly, the mean value for the field temperatures was determined:

$$Mean = \frac{\text{Sum of measured temperatures}}{\text{Total measurements}} = 154.92\ ^{\circ}C.$$

The mean indicates the average temperature of the field measurements. The mean was then plotted on a graph which indicates that only three coal temperatures were above the mean value (Figure 31).

Afterwards, the variance was calculated by determining the difference of each coal fire from the mean (Figure 31) and completing the formula:

$$\sigma^2 = \frac{(difference\ 1)^2+(difference\ 2)^2+(difference\ 3)^2+\cdots+(diffrence\ 9)^2+}{\text{Total measurements}}$$

$\sigma^2 = 26410$

Finally the standard deviation (SD) was calculated with the square route of the variance (Figure 31): $\sigma^2 = \sqrt{\sigma^2} = 162.51$

The standard deviation is an indication of which coal fires are within the standard deviation (162.51 and) of the Mean. Thus, all temperatures falling within the standard deviation is seen as “normal temperatures”, whereas temperatures above the SD, is seen as above average. Only one temperature (495 ˚C) is above the SD, which is seen as an anomalous high temperature.

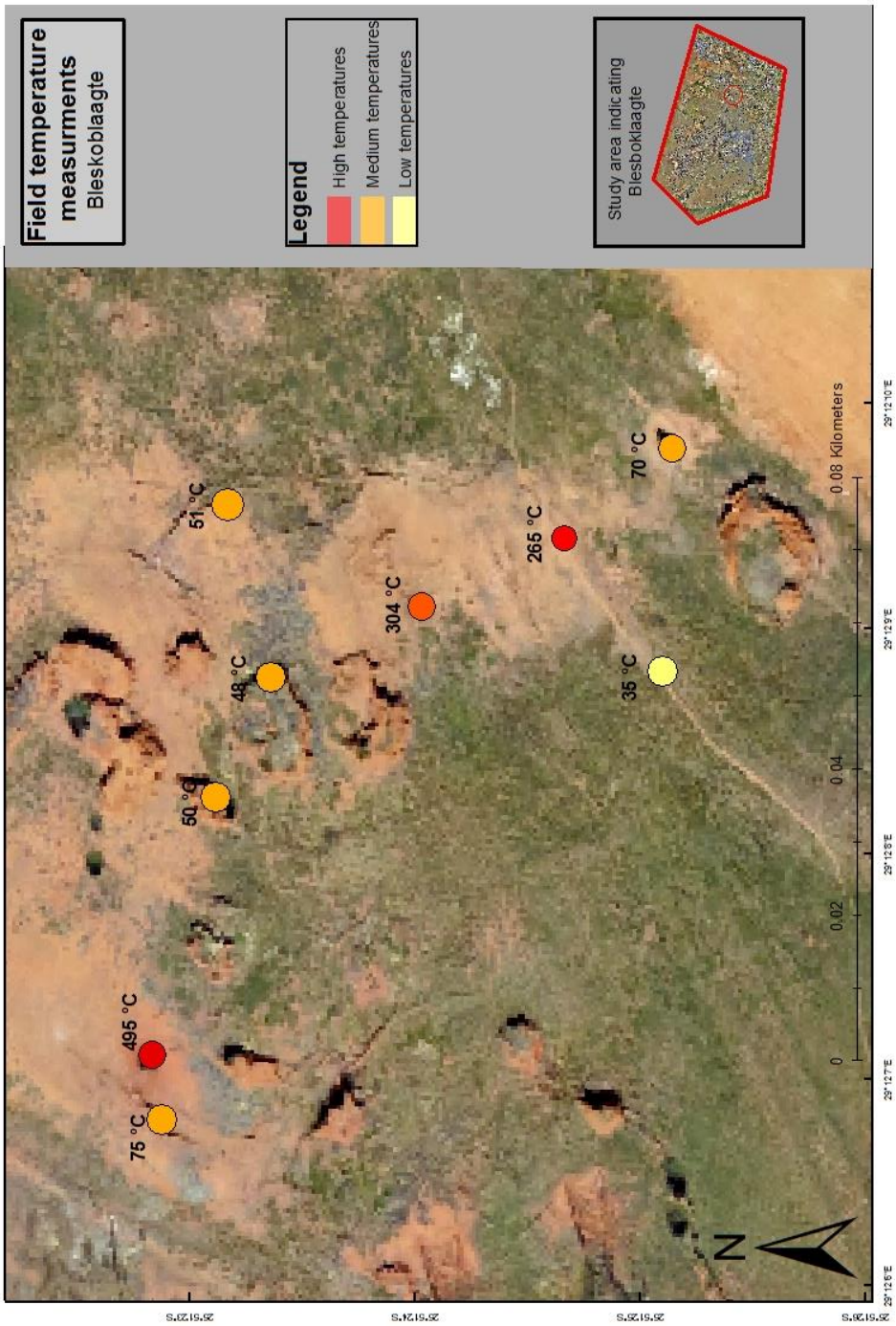

Figure 30: Field temperature measurments in Blesboklaagte.

Table 9: Obtained field temperature measurements.

Temperature (°C)	Coordinates	Description
35.5	S25°51'25.06" E29°12'08.82"	Fissure in sandstone <2 metres. Accumulation of white and yellow minerals.
48	S25°51'23.18" E29°12'08.78"	Smoker hole >5 metres Accumulation of white minerals.
50	S25°51'23.00" E29°12'08.21"	Smoker hole >5 metres Accumulation of white minerals.
51	S25°51'25.27" E29°12'09.76"	Smoker hole >5 metres Accumulation of white minerals.
70	S25°51'24.98" E29°12'09.76"	Fissure in sandstone <2 metres. Accumulation of white and yellow minerals.
75	S25°51'22.64" E29°12'06.91"	Fissure in sandstone <2 metres. Accumulation of yellow minerals.
265.7	S25°51'24.66" E29°12'09.43"	Smoker hole <5 metres. Accumulation of white minerals.
304.1	S25°51'24.05" E29°12'09.14"	Smoker hole >5 metres Accumulation of white minerals.
495.0	S25°51'22.68" E29°12'07.06"	Fissure in sandstone <2 metres. Accumulation of white and yellow minerals.

All temperatures above the mean value fall within the category for high potential coal fires. Whereas, the temperatures below the mean value fall within the medium and low potential coal fire categries.

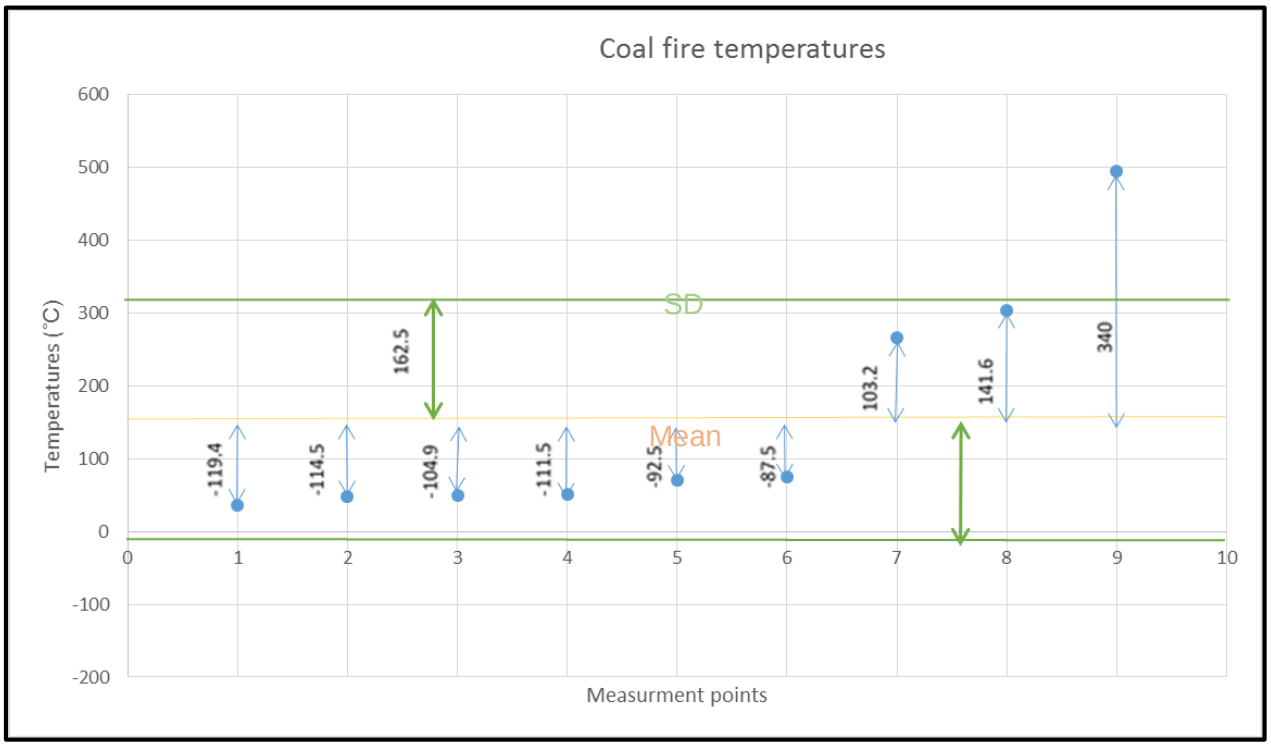

Figure 31: Coal fire temperatures graph indicating the mean and difference of each coal fire from the mean.

Table 10 summarizes the calculated statistics for the measured coal fires.

Table 10: Coal fire statistics.

Mean	154.92 ˚*C*
Variance	26410
Standard deviation	162.51

4.1.2 Secondary data

TNTmips 2013 was initially used to manually mosaic TIR images. However, due to restrictions to the number of raster cells that could be mosaicked, only small areas could be compiled into TIR maps. Thus, the final mosaicked GEO-TIFF image provided by EOMINERS was used in the classification step (Figure 32). The classification of the TIR image into high, medium and low potential for coal fires is shown in Figure 33. The dark orange on the image represents warmer areas (high pixel values), whereas the lighter (light orange and yellow) indicate cooler areas (low pixel values). A mosaicked image for Blesboklaagte, which was used as a case study, was constructed and classified according to the field measurments (Figure 34). The coal fire classification layer was saved as a separate layer and was overlayed onto an aerial photo. The field measurments was then added as a seprate layer to the classified image, and can be seen as individual features.

The classification of the mosaicked TIR image of the entire study area is presented in Figure 33. This image indicates low, medium and high potential for coal fires. The correlation between the occurrence of coal fires and subsidence will be discussed in Chapter 4.2.

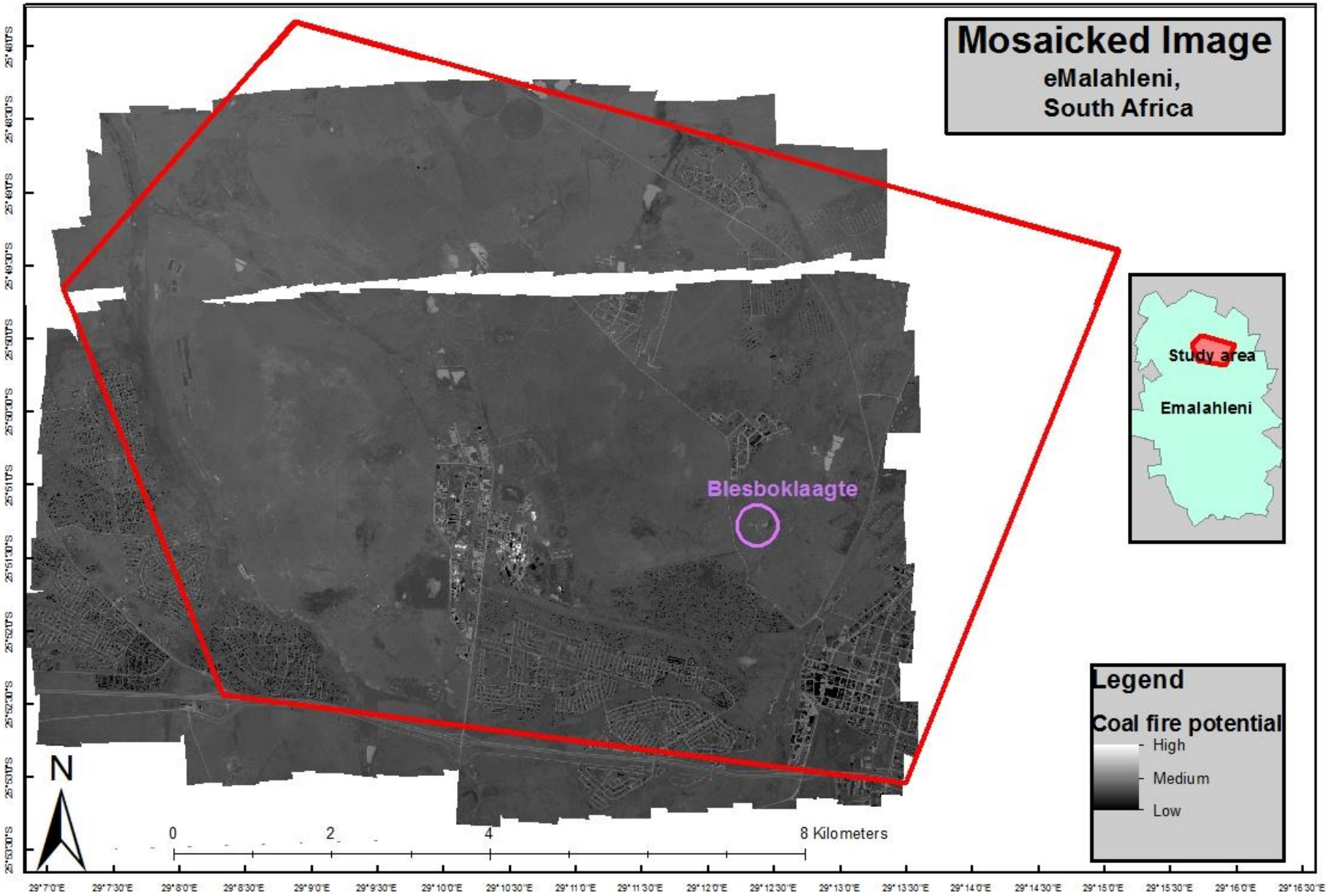

Figure 32: Mosaicked TIR image.

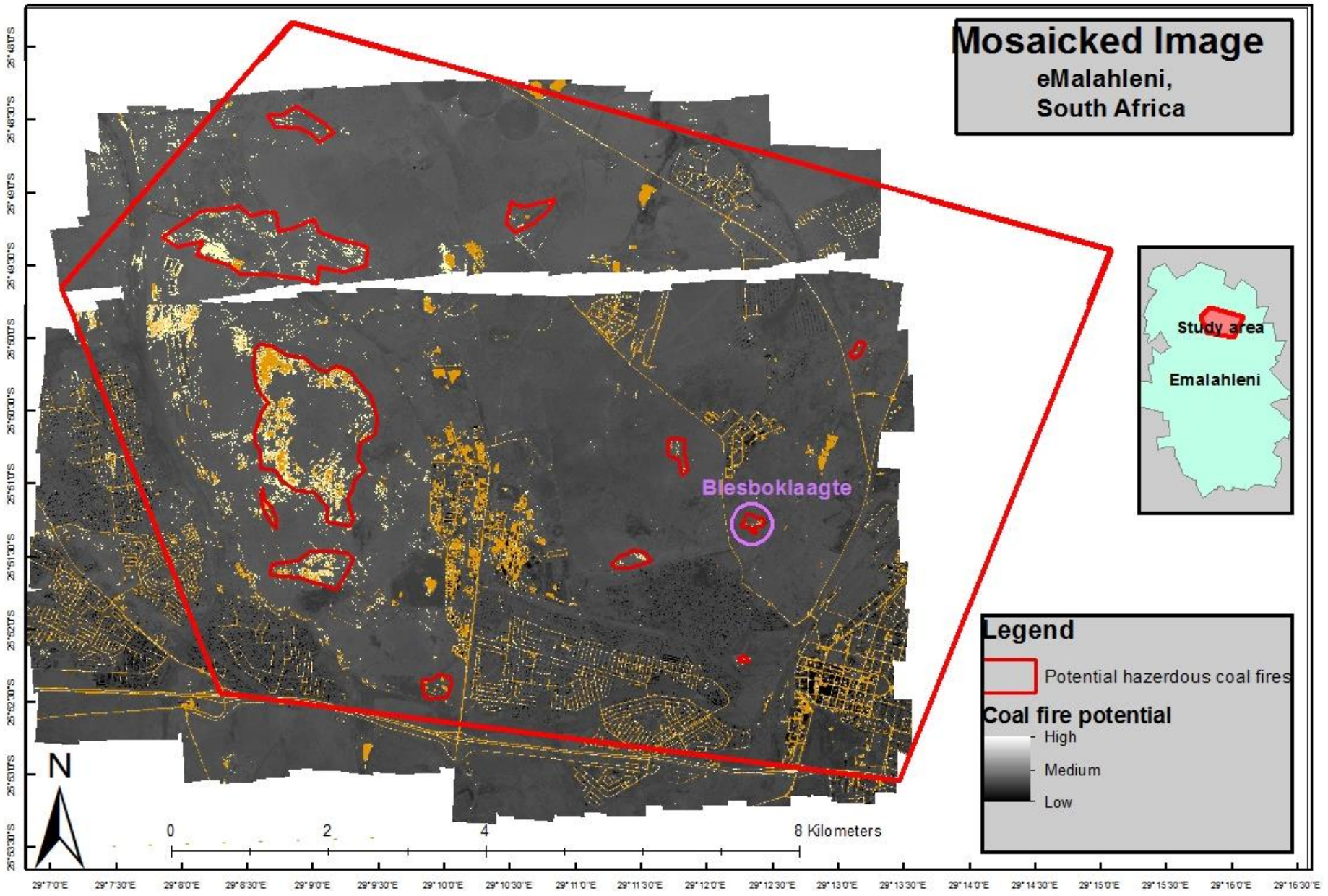

Figure 33: Classified coal fires.

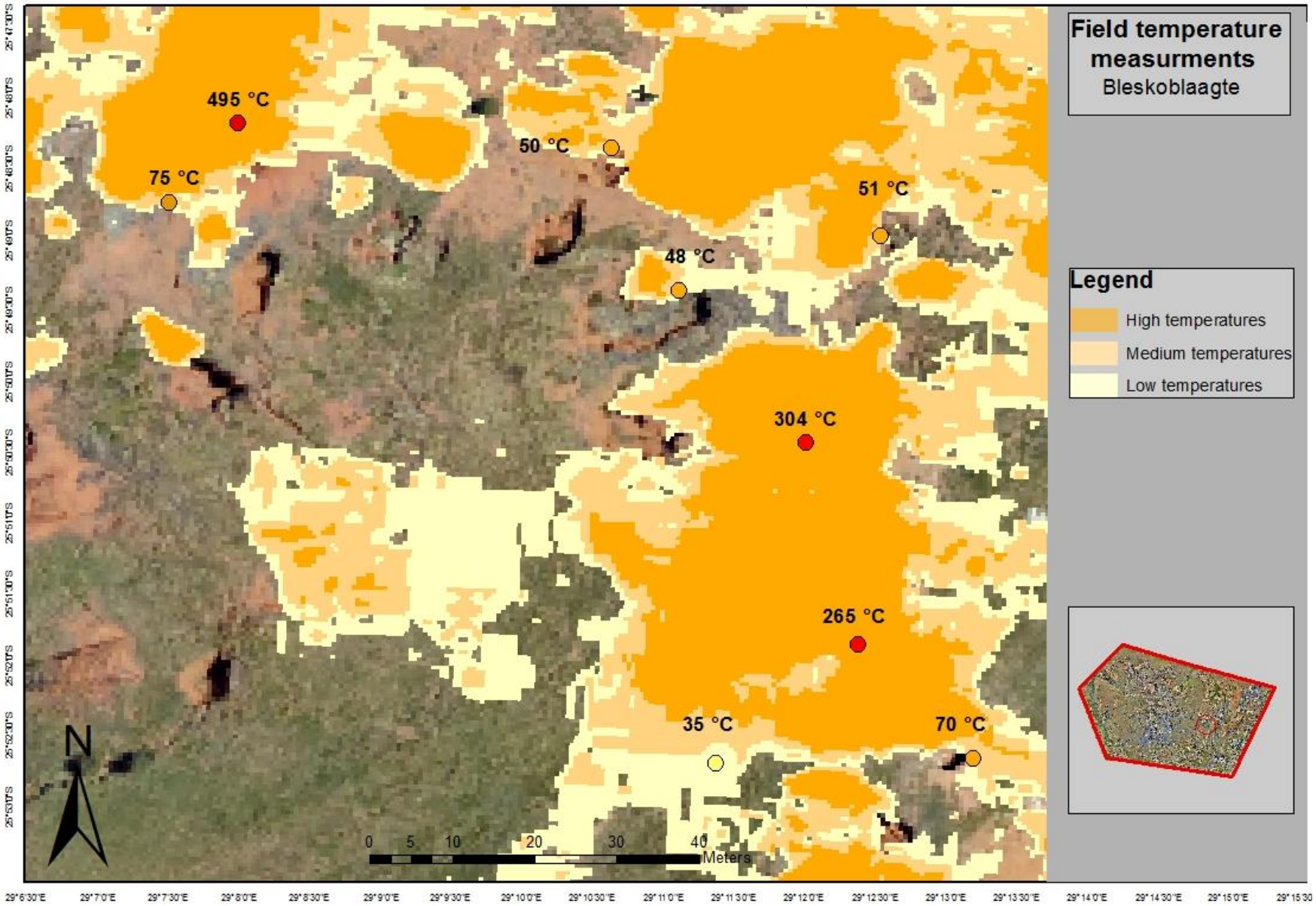

Figure 34: Classified mosaicked image and field temperatures of

4.2 Objective Three: Locate potential subsidence in study area area.

The LIDAR data provided by the EOMINERS project was used to create a map of subsidence areas in the study area (Figure 35).

Different slope angles are indicated with a colour ramp. Dark pixel values indicate no slope, whereas light pixel values indicate a steep slope of up to 90˚. The high resolution elevation data allows subtle structures on the ground (such as subsidences) to be recognised.

Figure 35 shows a high resolution LIDAR map which indicates potential subsidence features. Four high risk areas were identified (red circles). For each identified area, separate maps were constructed to further investigate the areas (Figure 36 to Figure 39). Each map contains a close-up LIDAR image, satellite image and a coal fire insert over the LIDAR image to identify if there is a relation between the subsidence and coal fires.

The first area (Area 1) is located in the south-western portion of the study area and is known as Transvaal and Delagoa Bay Colliery (Figure 36). Subsidence occurs in prominent blocky pattern in an area of 2 km by 3 km. One individual subsidence feature was measured to be approximately 60 m wide.

Area 2 is located on the southern part of the study area in an area known as Kwa-Guqa (Figure 37). Subsidence occurs in noticeable blocky pattern in an area of 1 km by 0.5 km. When comparing the LIDAR image and the aerial photo in Figure 37, it is interesting to note that the areas with little or no slope are the areas used for informal housing, whereas the high slope areas, indicating subsidence occur in between the informal housing sections.

Area 3 is located in the northern part of the study area and is known as Driefontein (Figure 38). Subsidence with a prominent blocky pattern is evident in an elongated area of 2 km long and 0.5 km width.

Area 4 is located on the eastern part of the study area and is known as Blesboklaagte (Figure 39). Subsidence does not occur as block patterns but rather as individual circles of approximately 2 m to 10 m wide.

Area 5 is located along the eastern side of the study area and to the west of the residential area of Jakaroo Park. Subsidence occurs in a noticeable blocky pattern in an area of 0.7 km by 0.3 km.

Although the lighter pixels in the LIDAR image are generally associated with high-lying areas, this is not always the case. In some instances the lighter pixel values may indicate elevations from other sources such as trees, buildings, coal dumps, etc. These areas are indicated with green circles in Figure 35 and named from A to F. These non-subsidence features are indicated and identified in Table 11. These non-subsidence features have thus been eliminated through feature identification from aerial photographs.

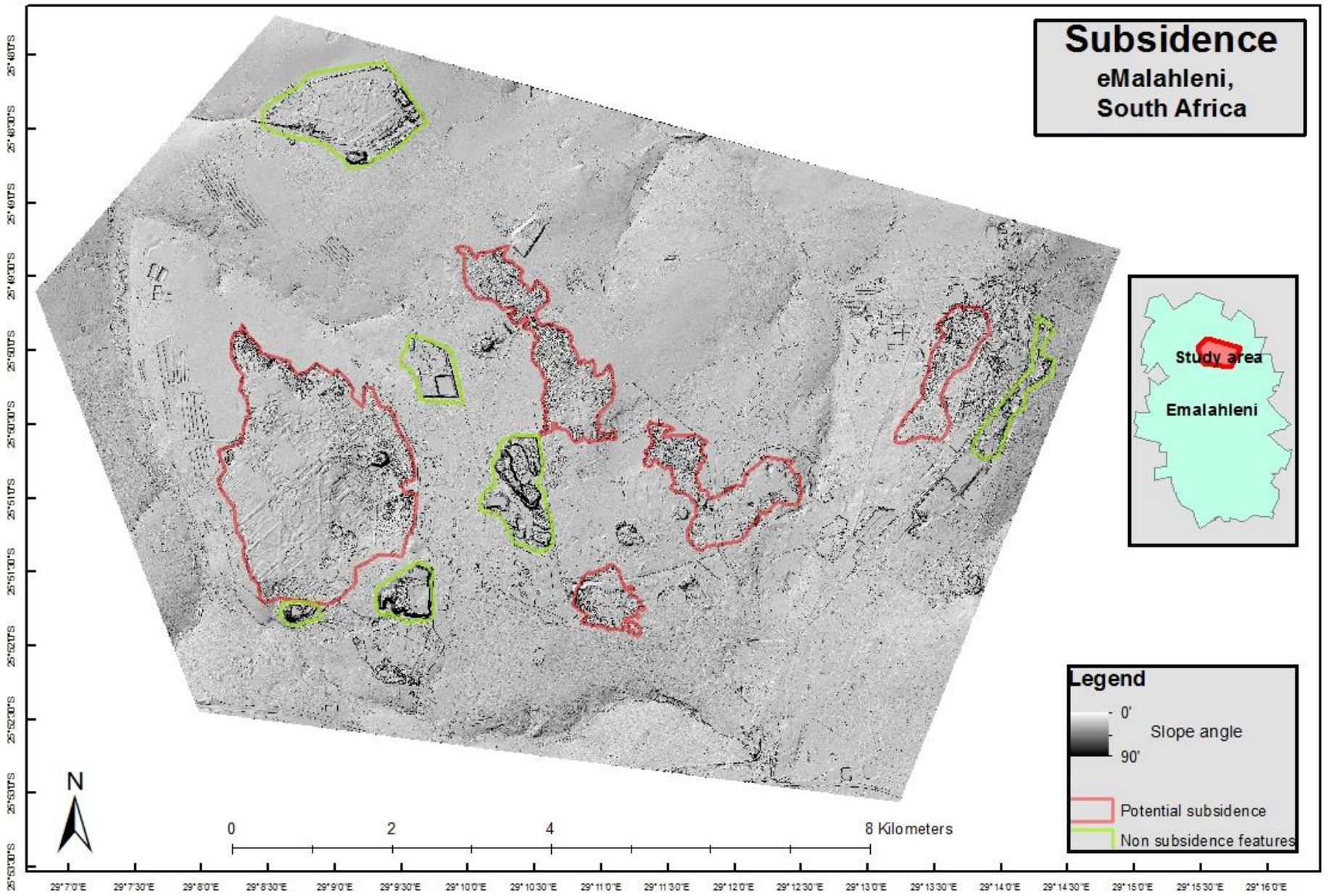

Figure 35: Potential hazerous subsidence.

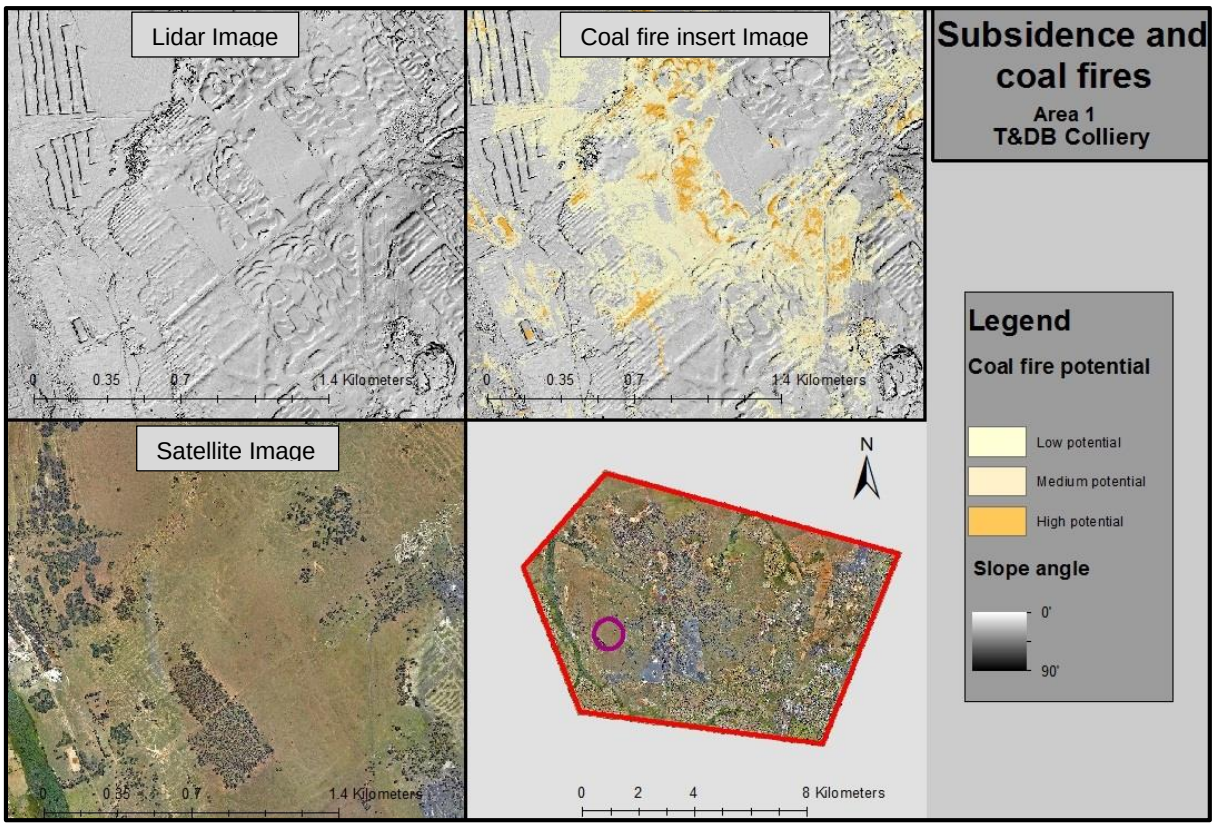

Figure 36: Subsidence in T&DB Colliery.

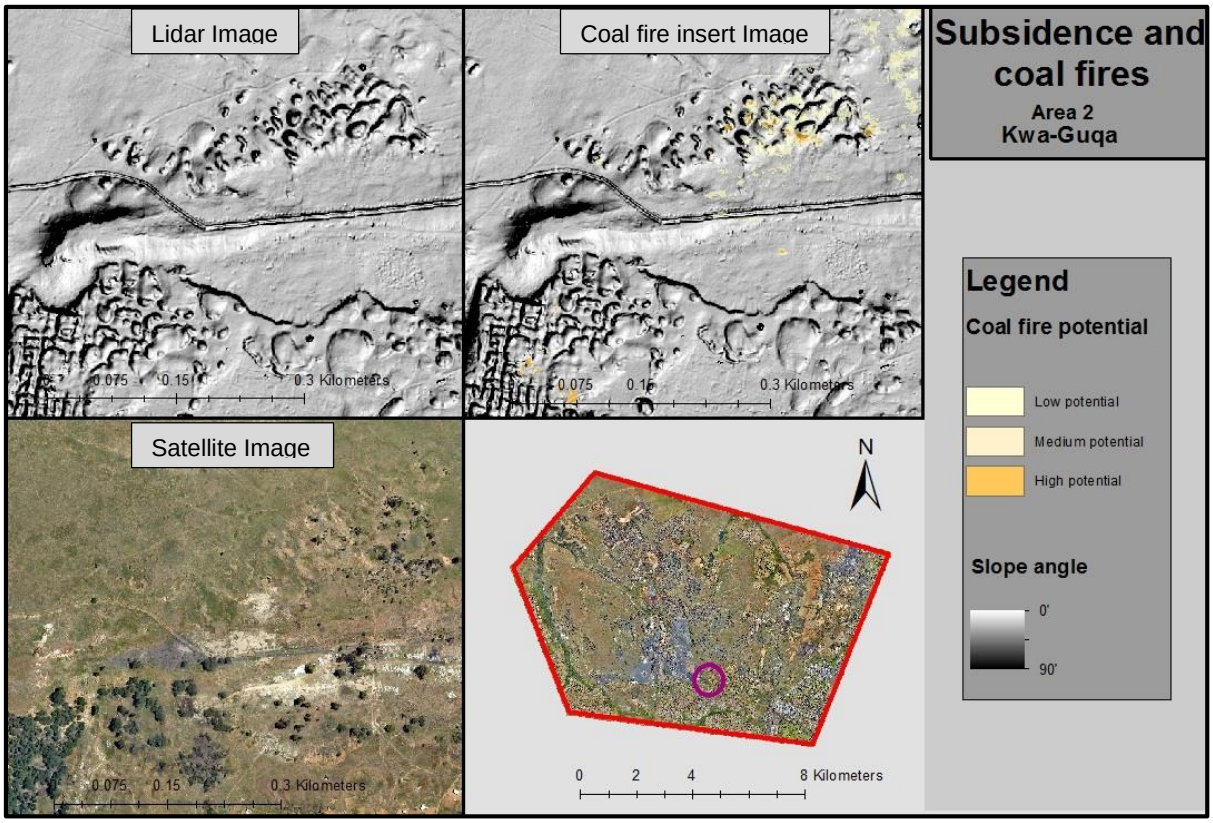

Figure 37: Subsidence in Kwa-Guqa.

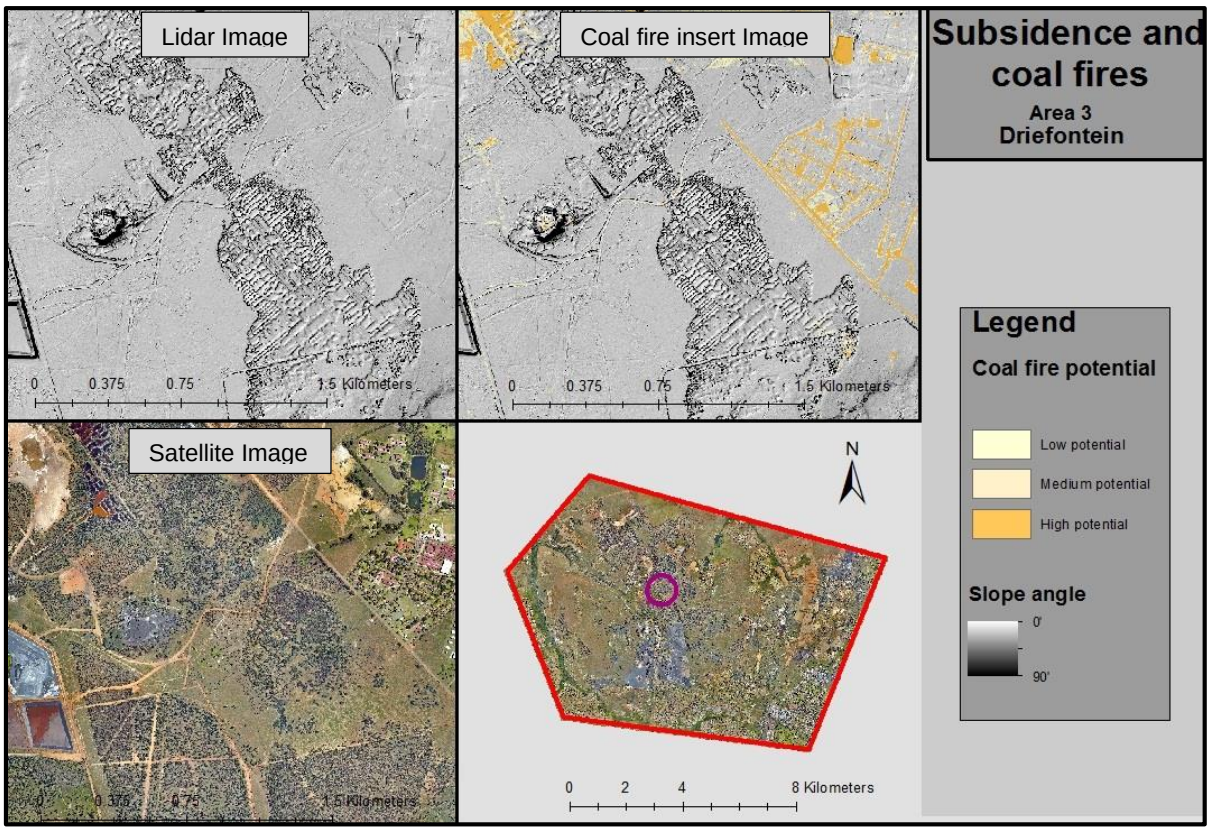

Figure 38: Subsidence in Driefontein.

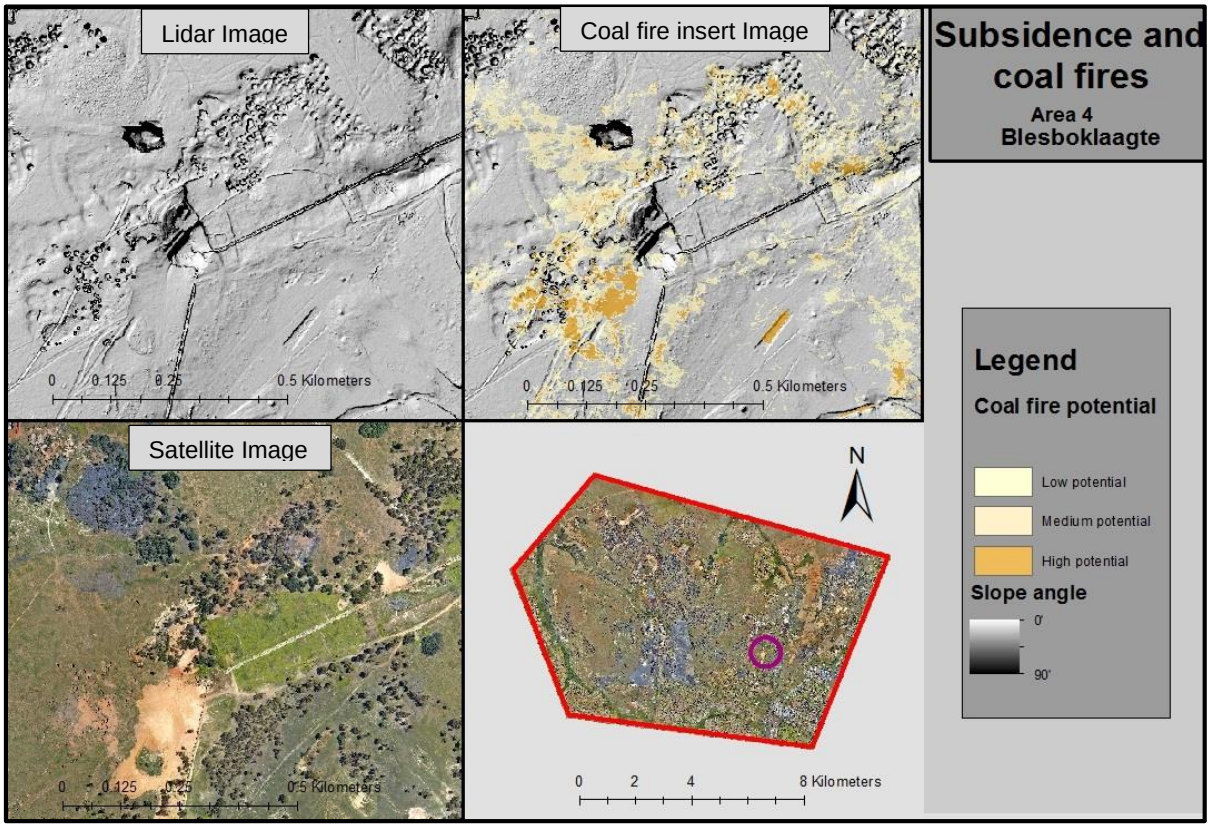

Figure 39: Subsidence in Blesboklaagte.

Table 11: Non-subsidence features

Non-subsidence feature	LIDAR image of non-subsidence feature	Aerial image of non-subsidence feature	Identification
A	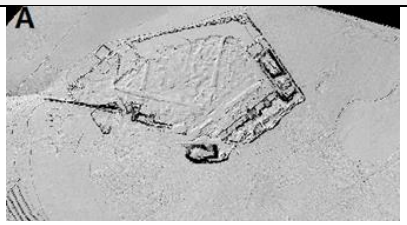		Coal dump
B	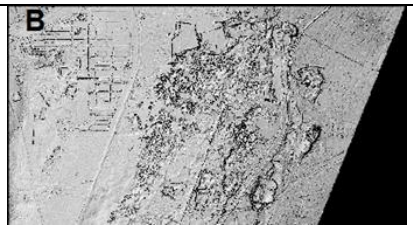		Coal dump
C	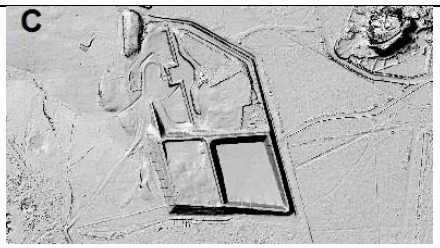		Smelter waste dump
D	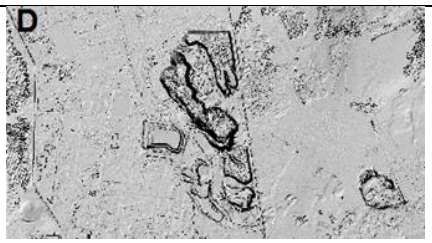		Smelter waste dump
E	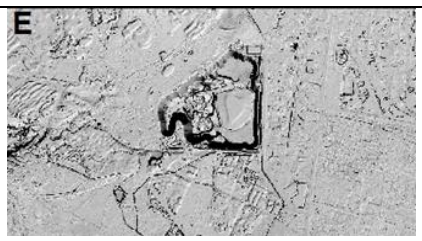		Smelter waste dump
F	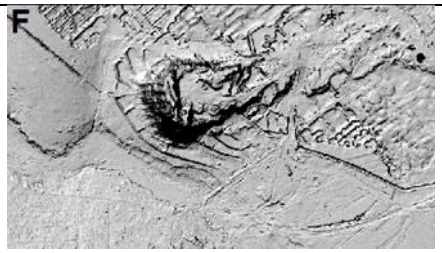		Coal dump

4.3 Objective Four: Identify AMD sources and pathways in drainage systems in the study area.

The interpreted Hyperspectral data layer received from the EOMINERS project was used to compile two maps, an AMD source map (Figure 40) and an AMD pathway map (Figure 41). The potential AMD sources map indicates the different sources such as coal dumps, smelters, subsidence, known AMD areas and warm decant points (Figure 40). The map also indicates AMD-producing minerals. Goethite is indicated as blue, hematite as pink, and jarosite as green with coal shown as light grey.

Drainage channels and the potential downstream flow paths were mapped using the DEM data. The DEM layer indicates elevation with lighter pixel values indicating areas with high elevation, whereas darker pixel values indicate areas with low elevations. A layer representing all the rivers in the study area was overlapped with the DEM layer. By overlapping these layers, the downstream pathways of the surface water could be determined (water flows from higher to lower areas). Thus, the flow of rivers was identified as north and north-west. The DEM layer and surface water pathway was used in the construction of the second map, the potential pathways of AMD in the surface water system (Figure 41). The map displays the possible downstream movement pathways of AMD contamination from numerous identified sources. All the rivers flow towards the Olifants river catchment. AMD-producing minerals occur close to drainage channels, possibly contaminate the surface water in the Olifants river catchment. Figure 42 indicates four close-up images of the Hyperspectral data (A) and satellite images (B) of potential AMD impacted areas. The blue block shows high amount of jarosite accumulated in a decant pond, on the western side of the study area. The purple and green blocks indicate AMD drainage from subsidence in wooded areas. A pond of AMD can be seen in the yellow frame as water flows into masses of broken rock and coal heaps. As the water moves through these discard coal heaps, pyrite is oxidised to produce AMD.

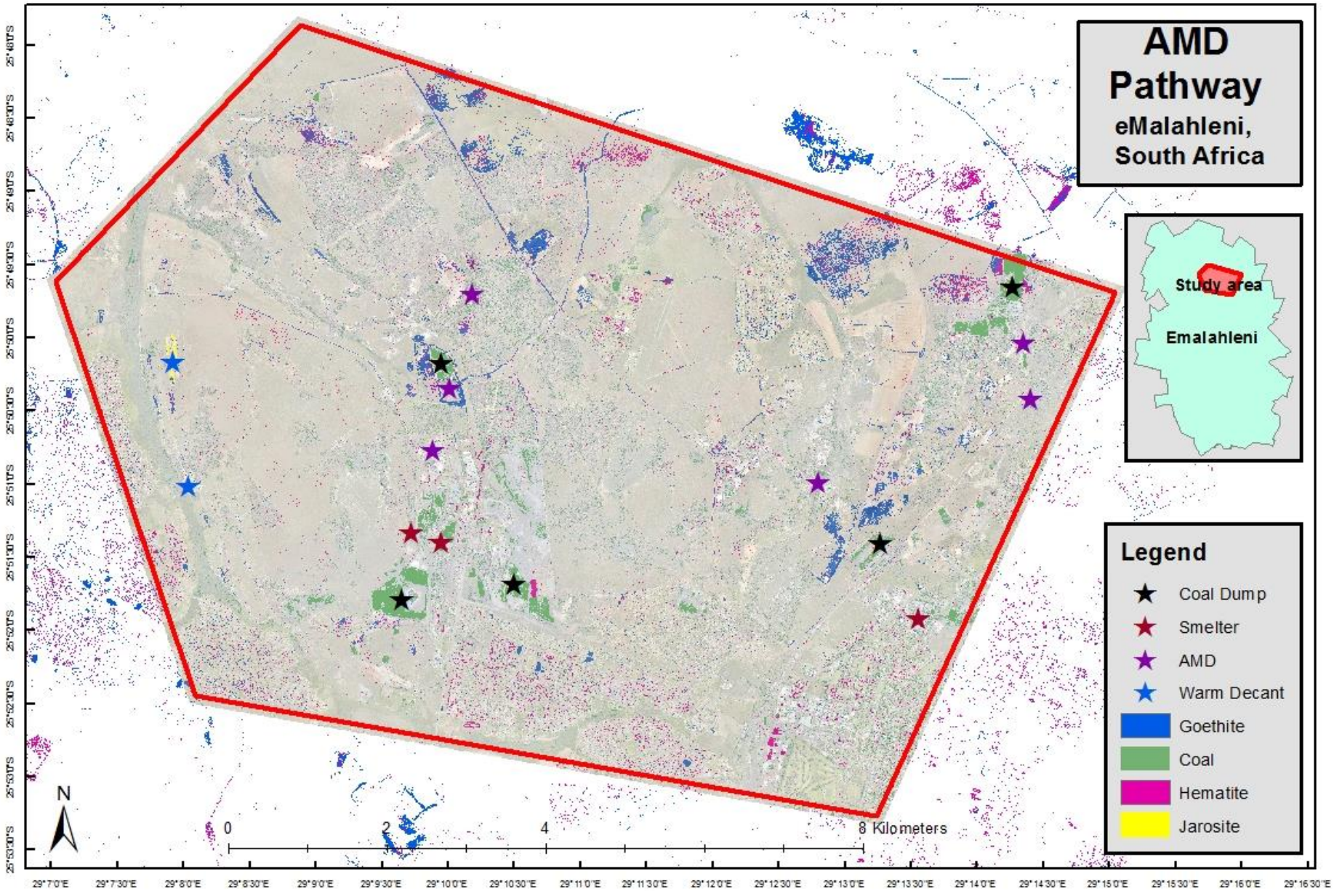

Figure 40: Potential AMD sources.

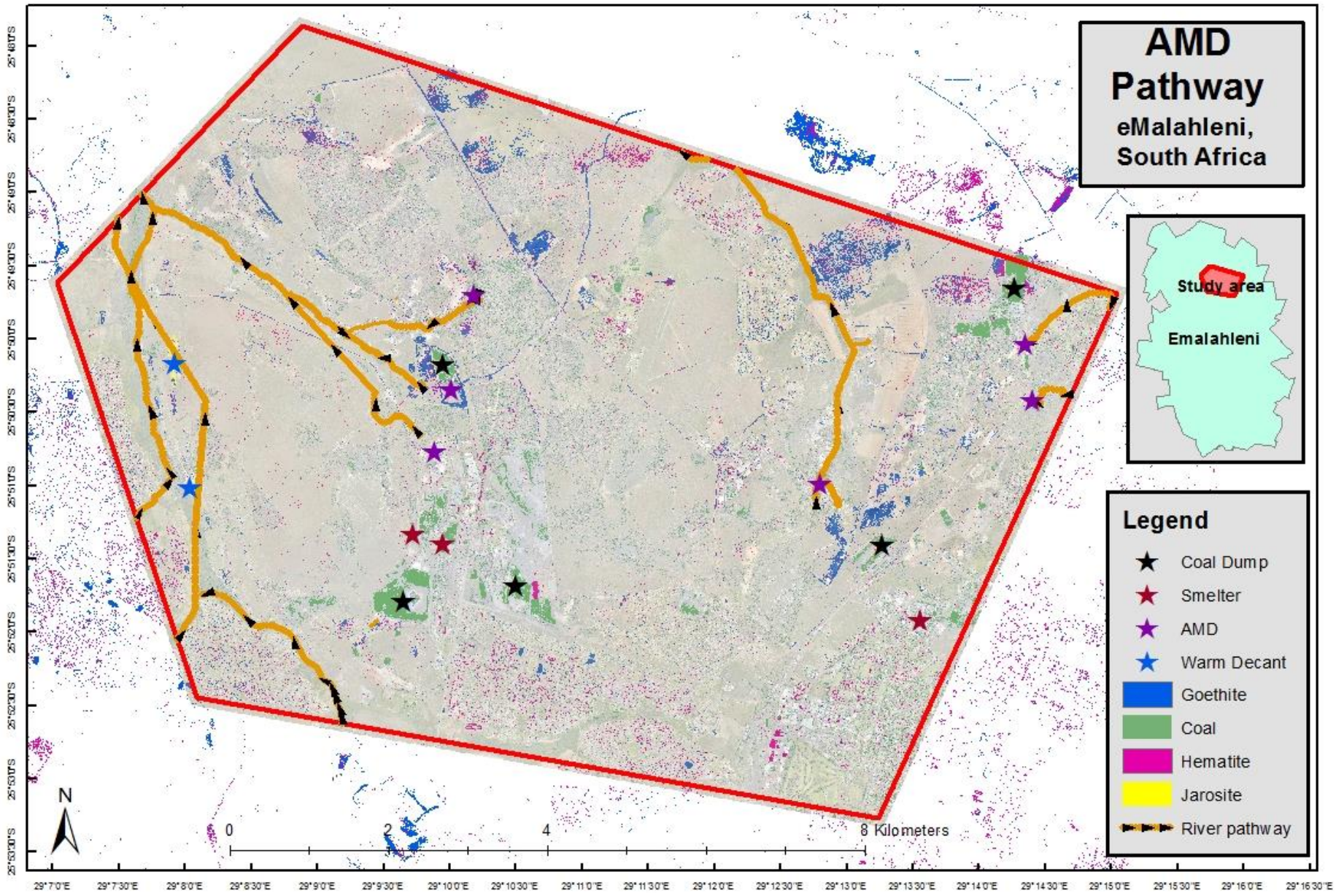

Figure 41: AMD Pathway.

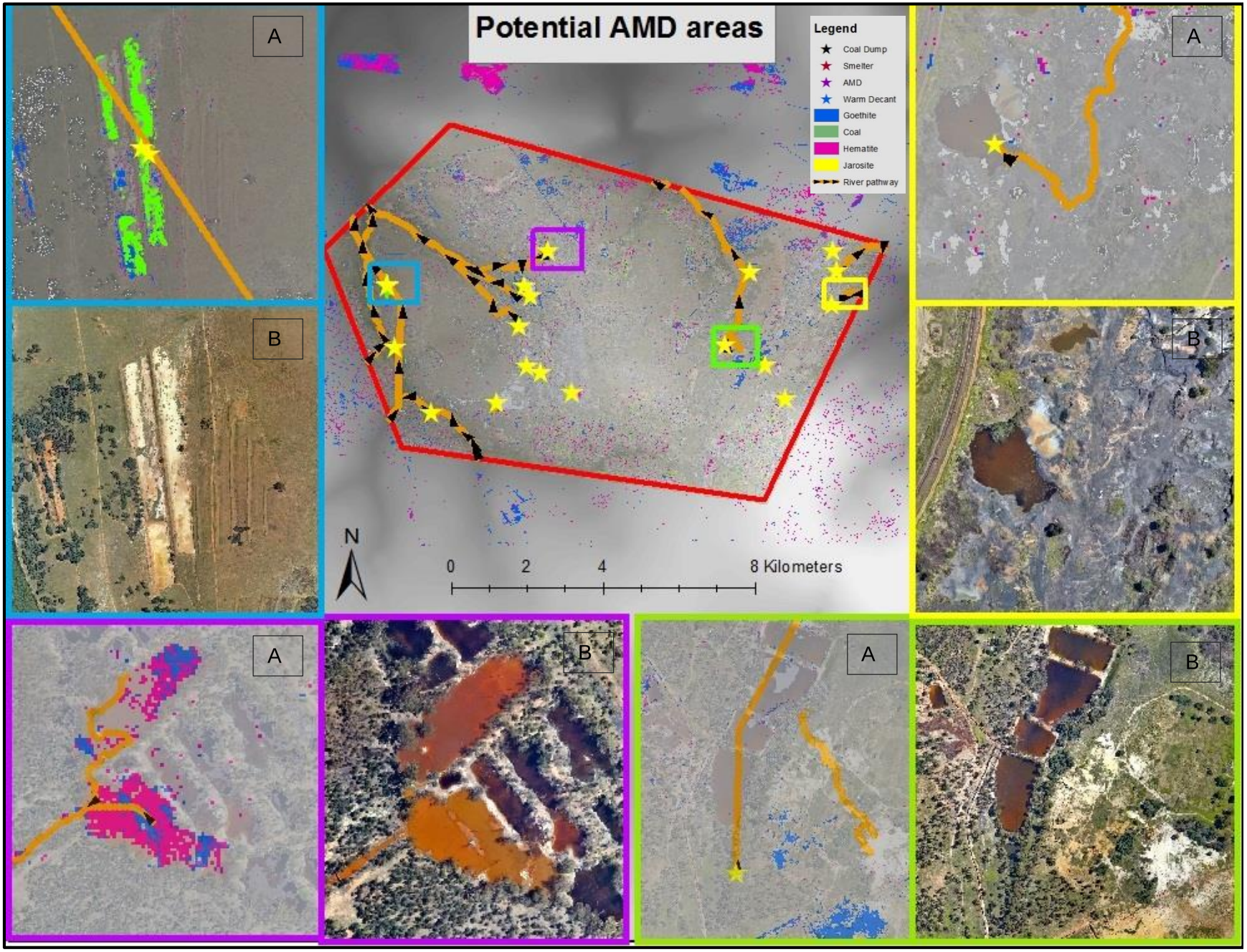

Figure 42: Potential AMD impacted areas (Frames indicated with A is Hyperspectral images and B satellite images).

4.4 Objective Five: Identify areas with high levels of air pollution

Only eleven of the sample points from Zibret *et al*. (2013) fall within the study area (Figure 43). The following elements were selected for this study: Manganese (Mn), Vanadium (V), Chromium (Cr), Lithium (Li) and Barium (Ba) (Table 12). These elements were selected due to their high concentration found by Zibert *et al*. (2013).

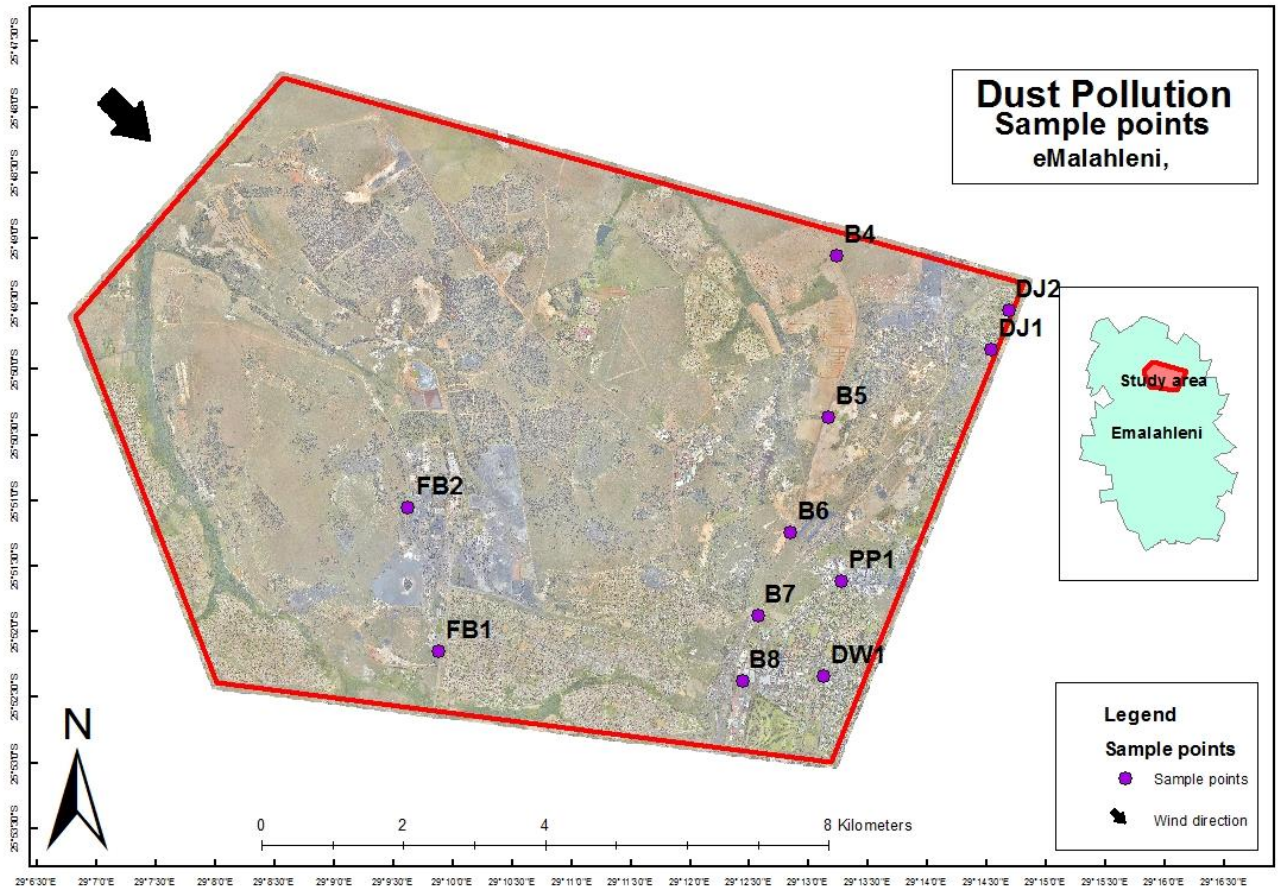

Figure 43: Map of study area indicating sample points for air pollution.

Kriging estimator was used to prepare interpolation maps to examine the dust pollution potential in study area. The Kriging method was used to interpolate, zonate and forecast the probability of data correlation.

Smelting industry air pollutions

Pollutants generally associated with smelting industries include Cr, V and Mn (Zibret *et al*., 2013:4455). Figure 44 to 46 show the classified smelting industry pollution maps constructed by Kriging. Figure 44 indicates enhanced concentration of Cr in the center of the study (FB2) area

where the Ferrobank industrial area occur. The Kriging maps are an indication of the impact this plant has on the air quality in the area. The concentration of Cr decreases with distance from FB2. Also indicate on the Krigged map is the location of the Cr and V smelters in the Ferrobank industrial area.

Table 12: Chemical element results (ICP-MS) for air pollution detection from Zibret *et al*. (2013)

	Mn (mg/kg	V (mg/kg)	Ba (mg/kg)	Li (mg/kg)	Cr (mg/kg)
B4	1143	197.67	211.3	16.13	713.3
B5	1019	163	186	16.1	965
B6	2124	179	309	13.6	1640
B7	918	165	350	9.6	4373
B8	1365	241	286	14.2	7664
DJ1	1117	177	183	12.4	3125
DJ2	610	82	181	24.4	941
DW1	947	240	201	14.8	4204
FB1	1405	896	169	11.4	22490
FB2	5262	1095	121	9.4	43050
PP1	2617	136	591	9.6	3005

Figure 45 and 46 shows concentrations for Mn and V separately. As seen from these figures, the Kriging results are very similar as the source of pollution is located south-west of the study area. The pollution source was identified as Evraz Highveld Steel and Vanadium smelter. Although the Mn and V dust pollution in the study area originates from outside of the study area, some trace could still be found inside the study area.

Fly ash pollution

Pollutants generally associated with fly ash include Ba and Li (Zibret *et al*., 2013:4455). Figure 47 to 48 show the Krigged pollution mapsfor Ba and Li respectively. Figure 47 indicates the highest Ba concentration at PP1. PP1 is located at the Evraz Rand Carbide plant. The Ba concentration decreases with distance from PP1. Figure 48 shows the concentration for Li is extremely high east of the study area and decrease with distance towards the study area. It is clearly seen that the origin of Li dust pollution is from outside the study area and potentially related to the spudomene mine south-east of the study area. Spodumene is common in many lithium-rich pegmatites.

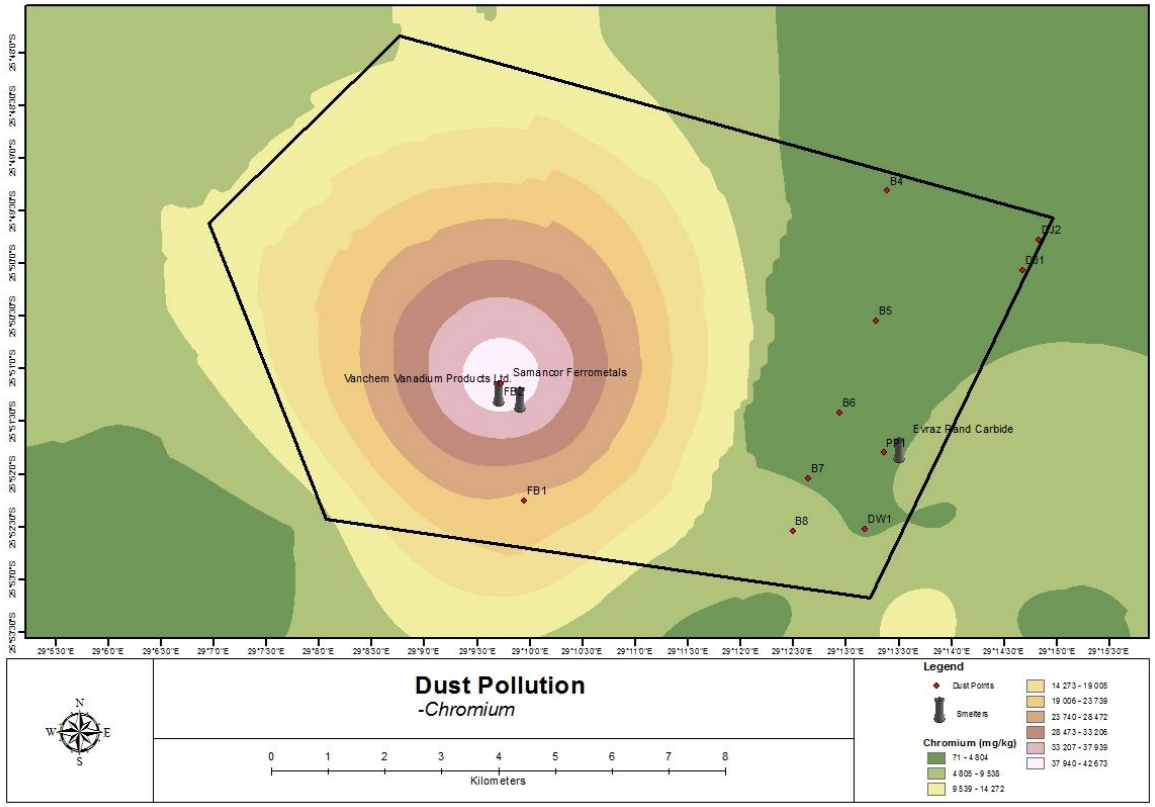

Figure 44: Chromium dust pollution.

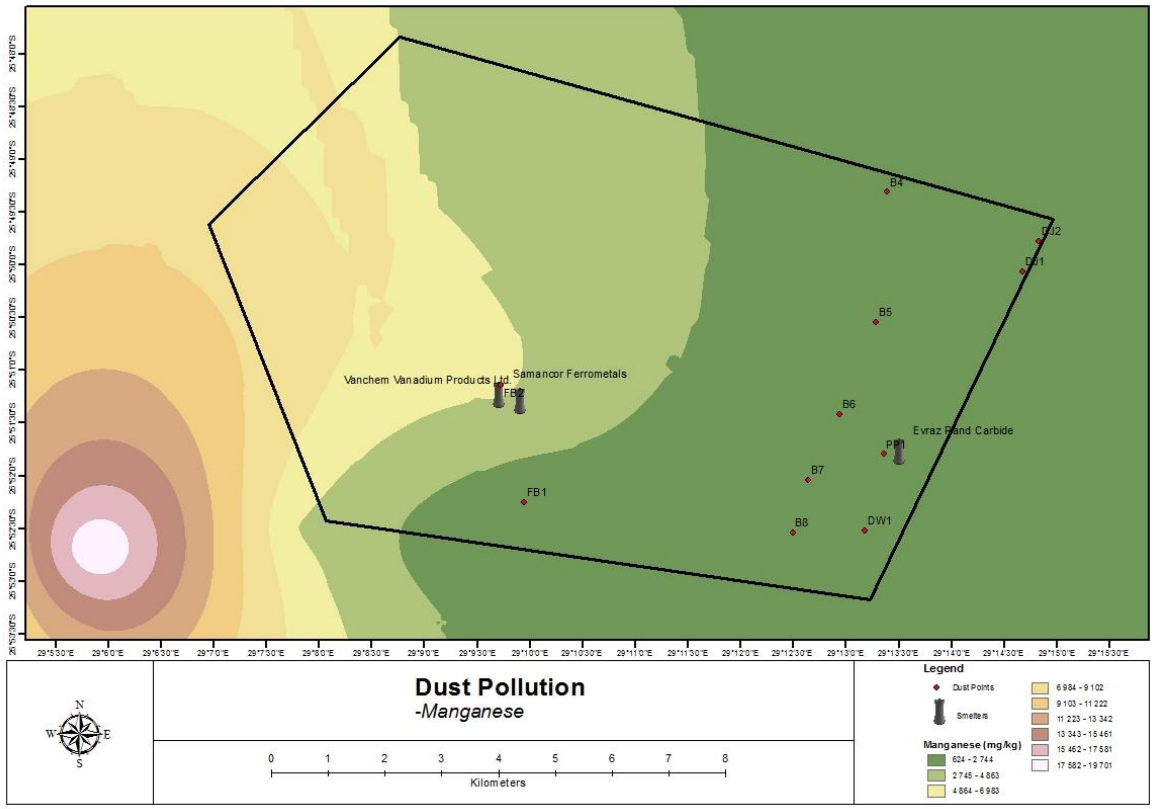

Figure 45: Managnese dust pollution.

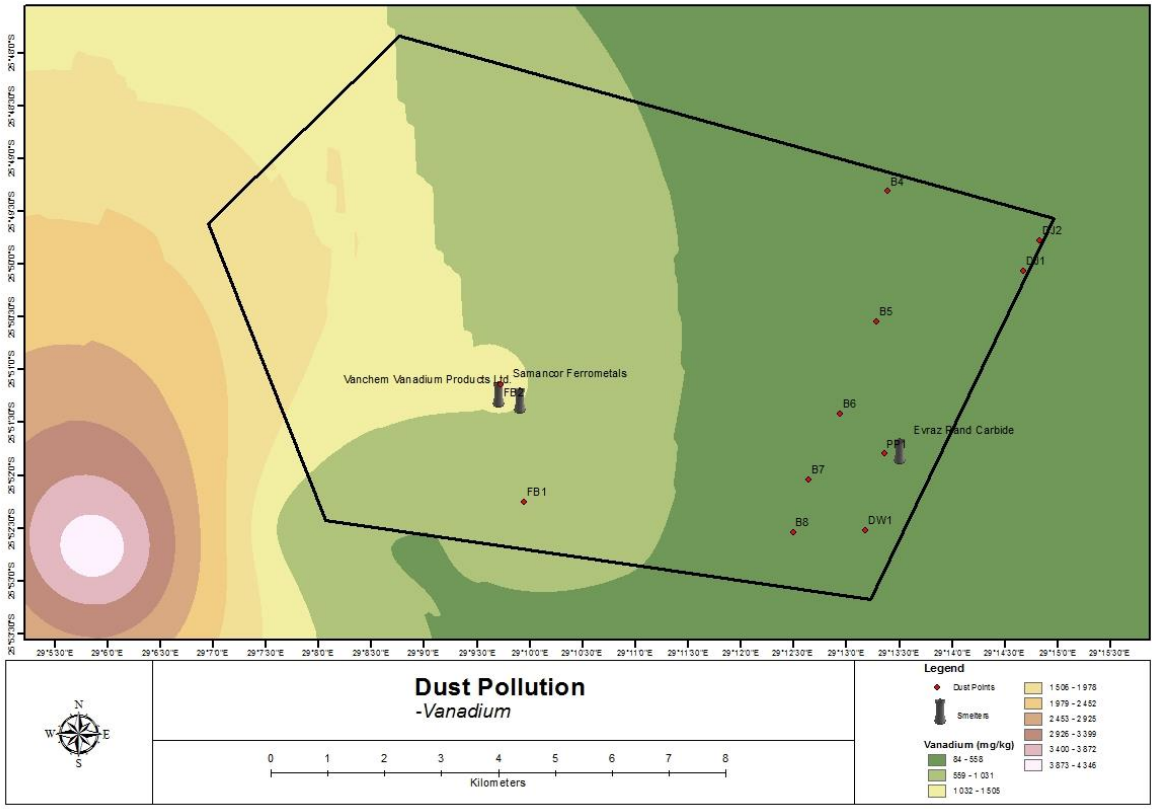

Figure 46: Vanadium dust pollution.

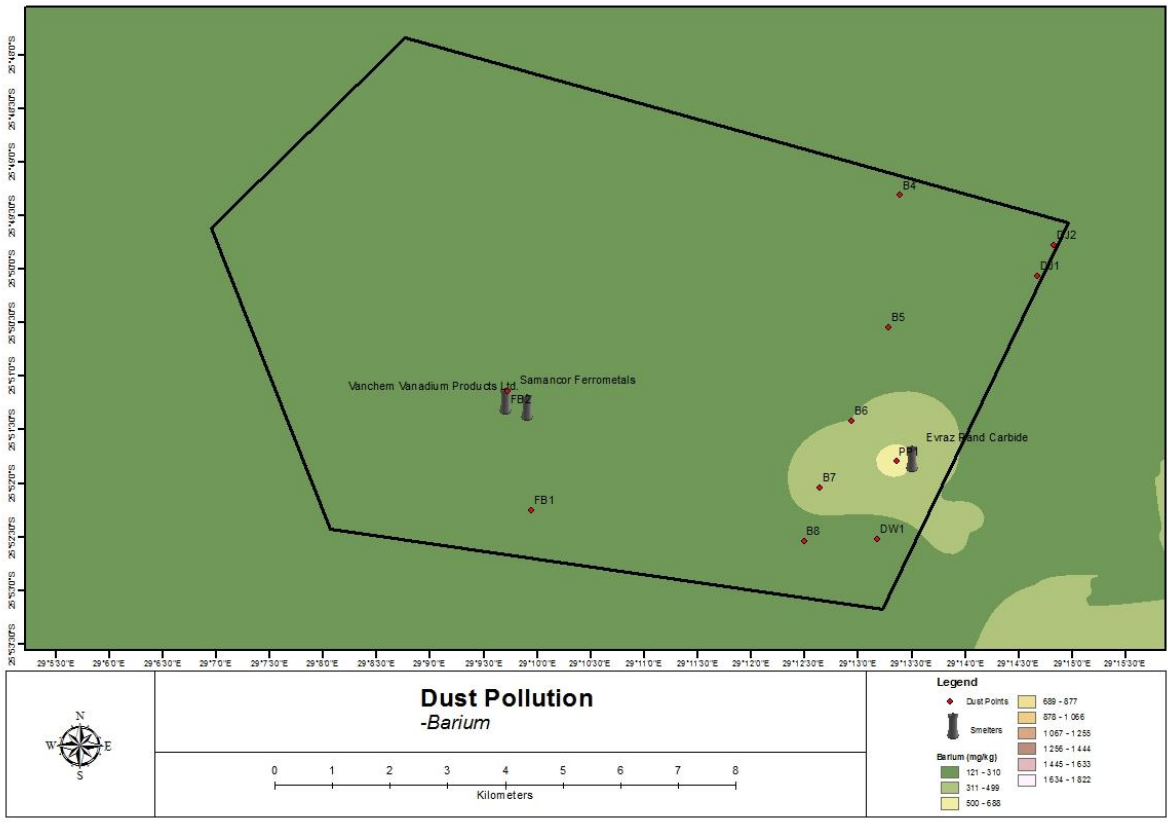

Figure 47: Barium dust pollution.

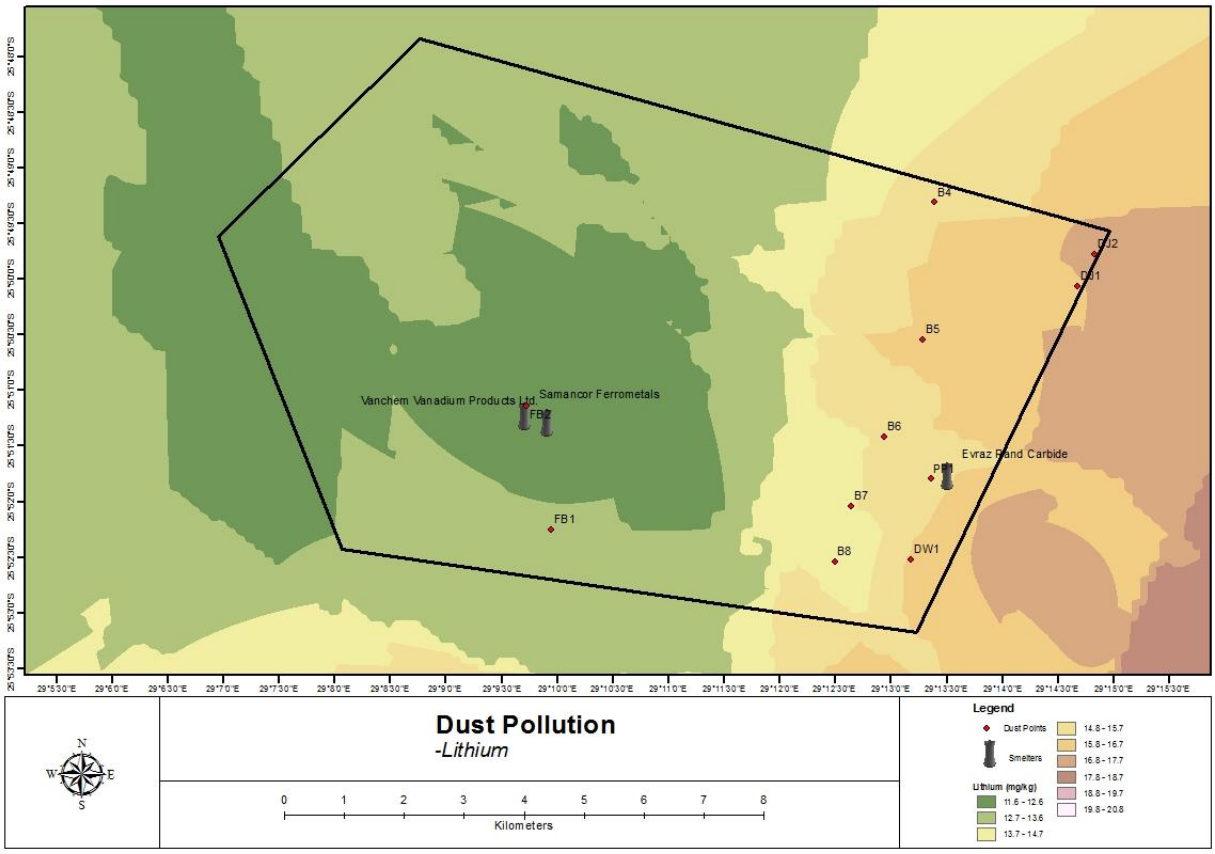

Figure 48: Lithium dust pollution.

4.5 Objective Six: Produce a risk map for the study area

All coal fire, AMD, subsidence and air pollution data were used to construct a risk map for the study area (Figure 49). The map indicates areas with high, medium and low combined potential for environmental risks.

Only one low potential risk area is indicated in the study area which is the Evraz Highveld Rand Carbide. The smelter is a point source for Ba emission in the study area. However, due to the low concentration of emission, the “consequence” and “probability was rated 2. Thus, the risk rating was 4 (low potential).

Cr emission from the Ferrobank industrial was scored as a medium risk potential since the smelters contribute to large amounts of Cr emission which can be inhaled by people in a highly populated residential area around Ackerville and Kwa-Guqa.

AMD pathways and decant points are indicated as medium potential risks. Both the “consequence” and the “probability” was rated 4. Thus the risk rating was 16 (high potential).

Coal fires and subsidence are seen as medium and high potential risks, depending on their location. Coal fires and subsidence at the T&DB Colliery was rated 4 for “consequence” because people from the informal settlement Kwa-Guqa pass over the area daily. The “probability” was rated 4, thus the risk rating was 16 (high potential).

Subsidence and coal fire in Blesboklaagte are shown as a high potential risks. The reason for the high rating is the main road R544 which passes through the area and the industrial workshops. Thus, if a hazard should occur, it could be fatal for people driving on the road and people in the workshops. Damage to the road and high voltage powerlines has been reported previously. The damage to the infrastructures would also be substantial.

Coal fires and subsidence occurring around Ackerville are seen as a high potential risk. The “consequence” was rated 5 since housing occurs in close proximity to subsided areas and the entire area therefore considered to be hazardous due to potential health and safety issues. The consequence could be fatal and major damage can be caused to housing infrastructures. The “probability” was rated 4.

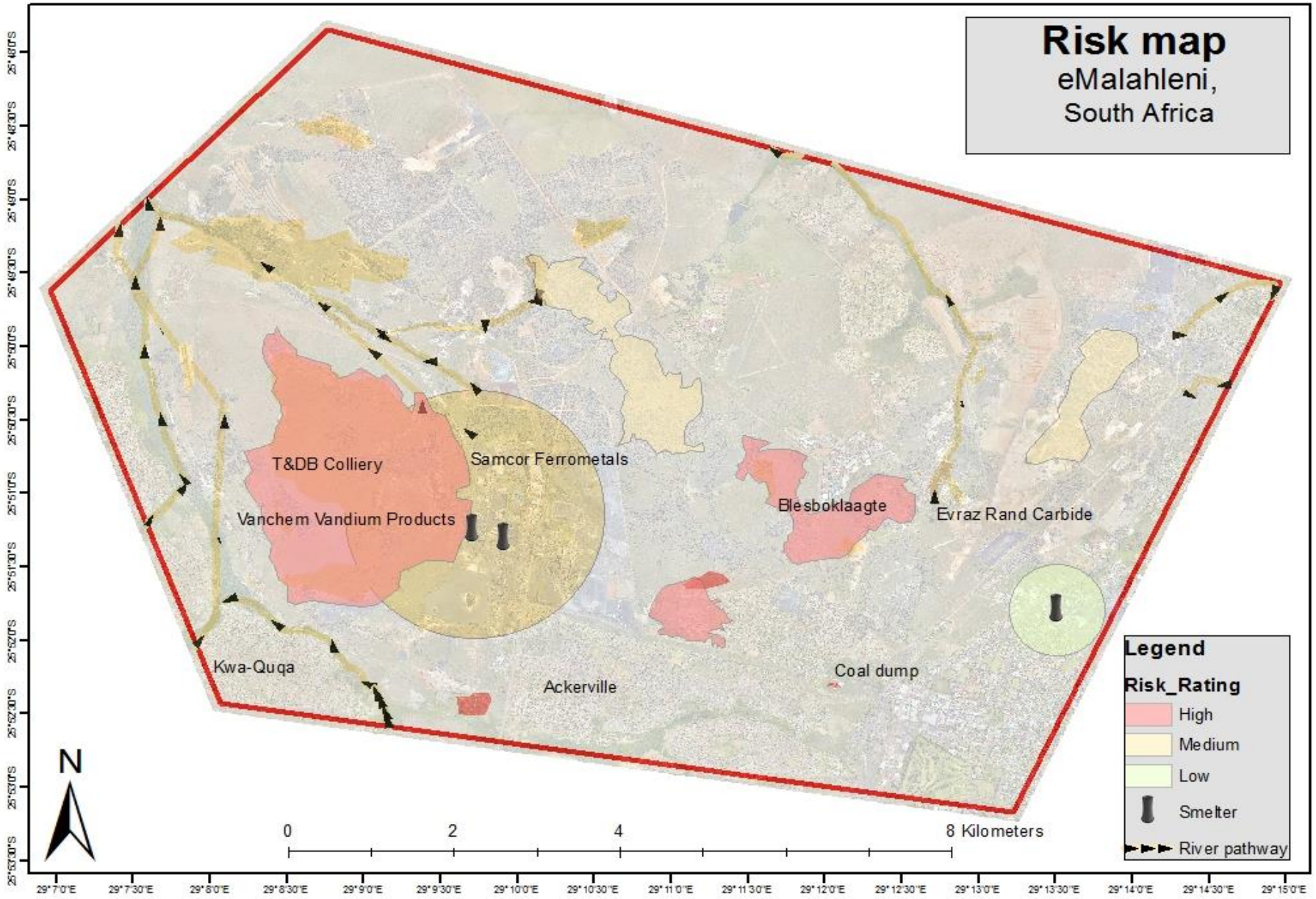

Figure 49: Risk map of eMalahleni Mmunicipal area

Chapter 5: Discussion

5.1 Objective Two: Detect burning underground coal fires in the study area.

White and yellow mineral accumulation was found around fissures and holes developed in areas directly above underground coal fires. These minerals include sulphur and sulphur-bearing minerals such as galena (PbS), orpiment (As_2S_3) and arsenolite (As_2O_3) (Finkelman, 2004:21). According to Annegam *et al*. (2007:133) heavy metals can also be found in these minerals, which can have a possible health impact if these elements were to be mobilized through rain water run-off.

The field data of the Blesboklaagte site showed that the temperatures measured at various points in the area ranged between 35 ˚C and 495 ˚C. The site with the highest temperature was located in the north-western portion of Blesboklaagte, with a temperature of 495 ˚C. This locality represented a subsidence feature of 1 m depth and 2 m wide. The Blesboklaagte measurements were included as a layer on the GIS map (Figure 32) which showed that most of the sites where temperatures above 50 ˚C were recorded during the 2013 field visit corresponded with high temperature events recorded on the 2011/2012 TIR images. It was also noted that areas with high temperatures had little to no vegetation. However, it should be kept in mind that during the latter part of 2012 some rehabilitation occurred to the east of the site which may have affected the temperatures.

The secondary TIR data was collected during the evening to ensure background noises from objects which were heated by the sun were eliminated. Thus, only objects which retained the radiation from the sun and objects with an emissivity would be detected.

The thermal infrared images have a high spatial resolution due to the low altitude at which the plane flew. This means that these images can form a good quality mosaicked image, as similar points on different images can easily be identified. Furthermore, by having high radiometric resolution images, more pixel values can be assigned. The higher the pixel value, the more accurate the temperature observations and values will be (Zhang, 2004:49). The TIR images had a large overlap due to the numerous amount of flight lines. Approximately 27 000 images were taken. From the 27 000 images, only 800 images were selected to ensure an overlap of 30% to 50% on the mosaicked image. The Blesboklaagte area was selected as a training area and images were mosaicked manually by TNTmips, whereas the final mosaicked image of the entire study area was provided by EOMINERS.

The TIR images were not geo-referenced, which made the mosaicking process very time-consuming as all the images had to be linked manually, one by one. However, by manually mosaicking these images, a more accurate mosaicked image was formed. This is because geo-referenced image are generally more distorted due to the movement of the plane.

Interpretation of TIR image data can be complex. The amount and spectral distribution of the radiated energy from an object is a combination of the material's kinetic energy and its surface emissivity. Furthermore, although observations using TIR data focus on specific atmospheric windows, water in the atmosphere between the target and the sensor is one of the largest sources of error. Therefore, due to the unknown variables such as atmospheric interactions, that might affect the recorded emissivity, it was decided to use an alternative method whereby non-radiometrically corrected TIR images are used. This method to assess relative spatial patterns within the TIR image, however, limits the applications for which the data can be used to those not requiring absolute temperature information.

The Blesboklaagte training site where field data measurements were made was therefore used in the classification of the brightness values ranging from 0-255 for the TIR image. Field measurements were taken in the area of Blesboklaagte (red circle) (Figure 28). The supervised classification of the TIR images was done by using the Blesboklaagte field data. The TIR reflectance value recorded for each pixel class was related to the field data and formed the base for the image classification. By using the Blesboklaagte field data the TIR images could be classified into areas of low to high coal fire potential (Figure 32).

The mosaicked image presented in Figure 33 indicates warmer areas where coal fires potentially occur and areas with no potential for coal fires. Areas with no potential for coal fires are shown as dark pixel colours. These areas include vegetated and woody areas, open water as well as low cost housing areas and coal discard dumps. Areas with high pixel values (lighter colours) may represent areas heated up due to coal fires or non-vegetated areas which retained some heat from the sun, such as footpaths, rock outcrops and roofs of buildings.

Image enhancement is concerned with the modification of images to make them more suited to the capabilities of human vision. Visual analysis plays a big role in all aspects of remote sensing. The classification of remote sensing data into false colours is an example of image enhancement.

Twelve high temperature areas were identified (indicated with red polygon) on Figure 33. False colour overlays were used to classify the mosaicked image as shown in Figure 34, into potential coal fires. Low potential coal fires are indicated with a yellow colour, medium potential coal fires with light orange and high potential coal fires with dark orange. All the high potential coal fires are surrounded by medium and low potential coal fire zones. However, the exact point where the coal

fire occurs cannot clearly be identified due to the influence of the heated surrounding air from the coal fire. This suggests that the coal fires in the high potential areas could be the source of the elevated heat signatures observed in the surrounding areas. Medium potential coal fire areas may be related to underground coal fires or due to heated air from a nearby coal fire. Low potential coal fires are most likely to be associated with heated air in an area around coal fires. In most cases, coal fires are a local phenomenon and not large enough to saturate a whole pixel to appear as an anomaly in comparison to the background. The aggregated temperature of a pixel depends on the location, spread, surface type and temperature of the fire/crack and its surroundings.

An alarming finding is that areas identified as a high potential for underground burning coal fires are criss-crossed by footpaths. This suggests that these areas are dangerous as the surface can collapse underneath these footpaths, which can cause serious injuries and even fatalities.

The informal settlement in the south of the study area is also surrounded by areas mareked as medium potential for coal fires (Figure 50). In some instances isolated high temperature areas were identified in the areas where abandoned coal discard dumps occur. The medium and high potential coal fire zones show a blocky pattern in some areas which are linked to the underground board and pillar mining (Figure 51). Several areas with higher than background temperatures were observed around these blocky patterns and possibly linked to seepage points. The high temperatures observed at the decant point and evaporation ponds in the Brugspruit is indications of the high temperature of the decanting AMD.

To the east of the study area, a rectangular object with a high pixel value was identified as an open water body (Figure 52). Other open water bodies in adjacent areas do not show similar elevated temperatures as observed here. This suggests that this water body is heated, either due to warm water entering the water body or due to the water being heated from an underground coal fire.

However, false high temperature areas do occur. These false readings need to be eliminated either through feature identification from aerial photographs or by field verification. These features include linear, rectangular, and irregular-shaped features.

Linear features:

These features represent roads with a higher temperature due to heat energy that was held back by the non-vegetated areas and asphalt surfaces.

Rectangular features: These features include rooftops from buildings and pavements as well as smelters.

Irregular shaped features:

Include open surface water features such as earth dams, sewage works, discard water dams, standing water on discard dumps, collapsed underground mining areas filled with water, rehabilitated areas where ponds formed, evaporation ponds and treatment plant ponds.

Other features which affect surface temperature include exposed bed-rock geology and soil moisture. A good example of this is the higher than background temperatures observed on the exposed sandstone banks of the Brugspruit.

Low temperature features include:

These features include open waters, vegetated and woody areas.

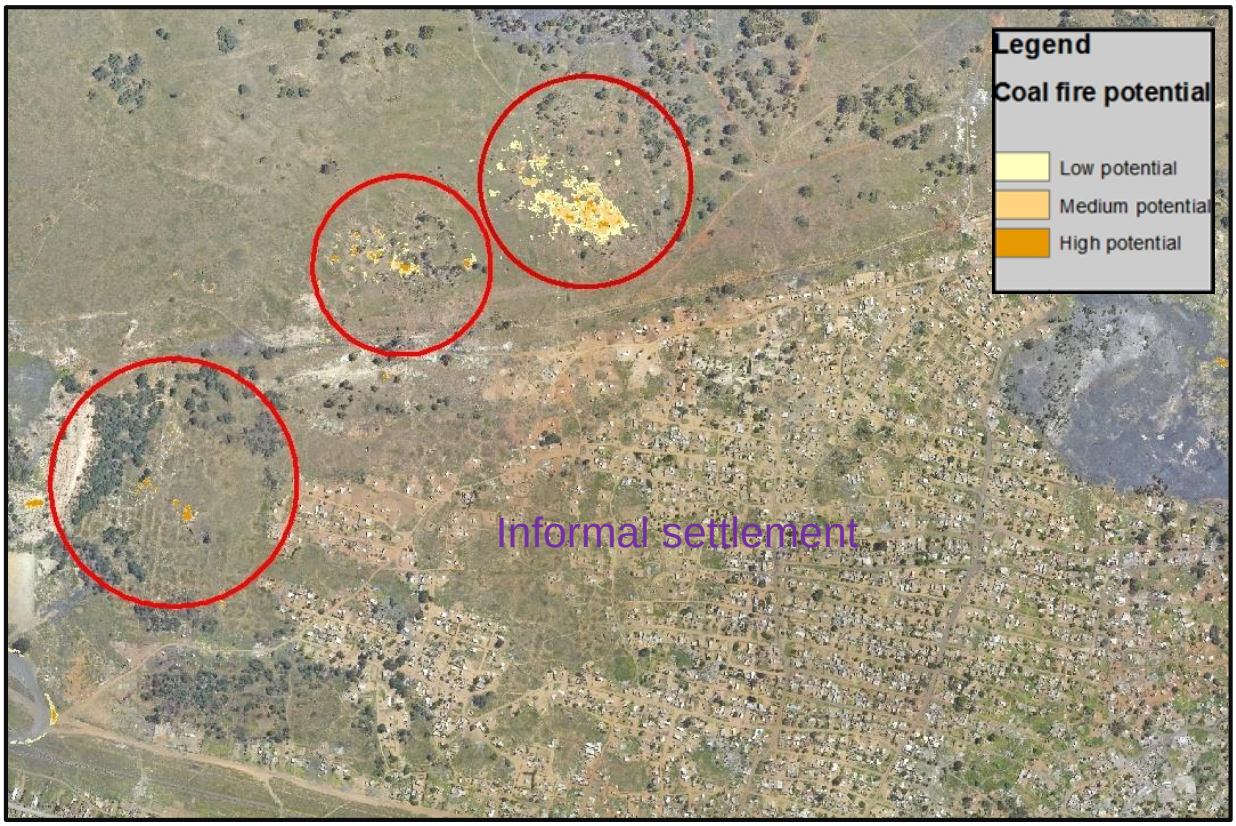

Figure 50: Coal fires surrounding an informal settlement.

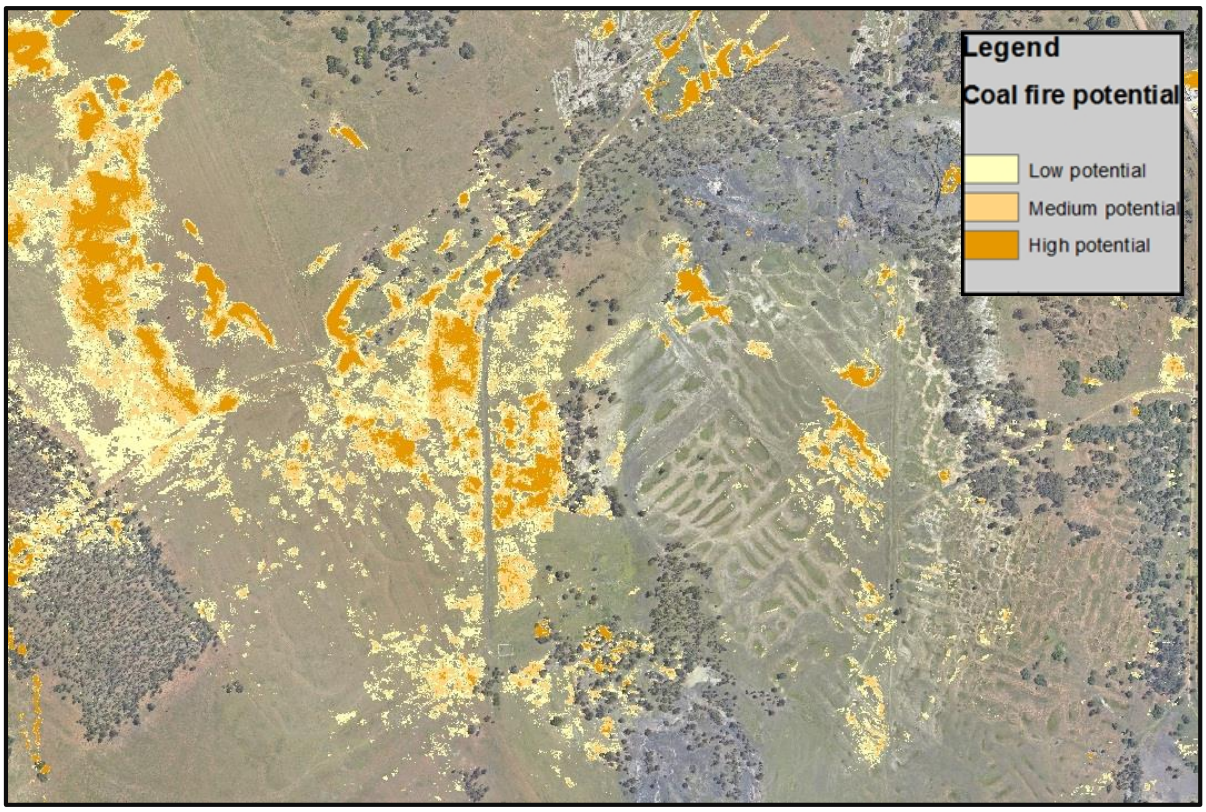

Figure 51: Coal fires occurring in a block pattern.

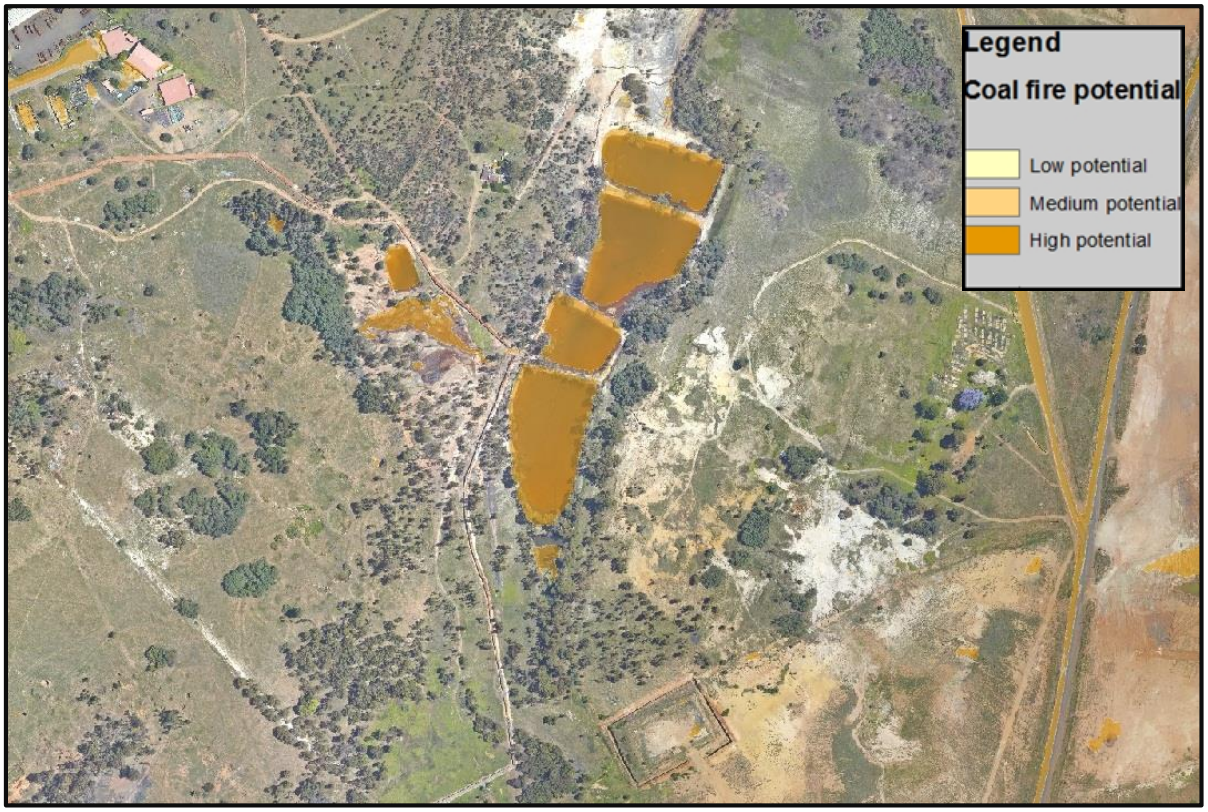

Figure 52: Warm water body.

5.2 Objective Three: Locate potential subsidence in study area.

On the analysed subsidence image as shown in Figure 35, potential subsidences are marked in false colour overlays. Throughout the map in Figure 35, light pixel values can be observed. These pixel values indicate a steep slope angle. The occurrence of steep slopes indicate potential subsidence features.

Four high risk areas were identified with respect to the potential impact that subsidence may have on the environment and infrastructure. These areas are marked with green circles, namely Area 1 (Transvaal and Delagoa Bay Colliery), Area 2 (Kwa-Guqa extention), Area 3 (Driefontein) and Area 4 (Blesboklaagte). In order to more accurately identify subsidence localities, an aerial photo was used for selected high risk areas.

The occurrence of subsidence in Area 1 (T&DB) can clearly be seen in Figure 36. After the original board and pillar mine operations had been abandoned and the roof of the shallow mine collapsed, subsidence formed over a large area. The area is seen as an open field, since it is a hazard for all land uses. Coal fires also occur in the area. Recently the area has been opened for re-mining of the remaining coal left in the original pillars. A clear correlation can be seen between the occurrence of subsidence and coal fires. However, certain subsidence features to the north does not show temperature elevations.

Area 2 is located in the informal residential area known as Kwa-Guqa (Figure 37). The subsidence surrounds an undisturbed area which is stabilised by a coal pillar. It is alarming to notice that areas which are utilized for housing are situated on coal pillars that could collapse at any time and is surrounded by subsidence. Not only can the infrastructure be damaged, but lives could be lost as well. Coal fires occur south of the informal housing.

More subsidence can be observed in Driefontein, south of the airfield (Figure 38). Potential coal fires occur to the south of the subsidence features. However, no clear correlation can be seen between the occurrence of subsidence and coal fires. Secondary roads pass over subsidence that could collapse at any time. Decanting AMD can be seen north-west of Area 3. The water is decanting from subsidences into the Olifants River catchment area. The area could have been rehabilitated since no correlation could be made between the occurance of coal fires and subsidence.

Area 4 is located on Blesboklaagte (Figure 39). The difference in patterns between Area 4 and the other areas, could be due to rehabilitation processes. Coal fires occur in relation to subsidence in the area. It should be noted that during field visitation, subsidence were identified underneath and adjacent to the high voltage power lines.

No correlation can be made between coal fires and subsidence in Area 5, since the mosaicked imgae does not cover the specific area.

5.3 Objective Four: Identify AMD sources and pathways in drainage systems in the study area.

The map presented in Figure 40 indicates all sources of AMD. Coal dumps, smelters, AMD and warm decants are seen as triangles. AMD-producing minerals include goethite (seen as blue), hematite (seen as pink), jarosite (seen as green) and coal (seen as light grey). The accumulation of colours indicates high volumes of the specific minerals.

AMD has been identified in the decant area west of the map, in a large pool above flooded subsidences and throughout the residential area of Jakaroo Park. Jarosite can be seen in small pixel values on the map; however, a large area of accumulation of jarosite occurs to the west of the map. It can be seen from aerial photos, that the area is a decant point. Jarosite is known to be formed under very acidic conditions and high sulphate concentrations. Thus AMD is highly likely to occur in this area.

Coal occurs throughout the map. These areas can potentially produce AMD as the sulphates in the coal can chemically react with oxygen.

Accumulation of goethite, hematite and coal can be seen in some areas on the AMD source map. Figure 53 is a zoomed-in image of a wooded area on the AMD source map. It is clearly seen that the area has a high potential for AMD due to the vast accumulation of the minerals associated with AMD. When placing the aerial photo over this area, it is seen that the area is infact ponds which formed due to AMD formation in the subsidence over the underground coal mine. Water decants from the subsidences caused by previous mining activities. As these pools act as closed basins water is only removed through evaporation, resulting in metals transported into the pools as constituents of AMD largely concentrating in the pools making them toxic pools. Evaporation concentrate the AMD indicator minerals in these areas. It can clearly be seen in the aerial photo that the water in these ponds is yellow-brown, which is an indication of AMD.

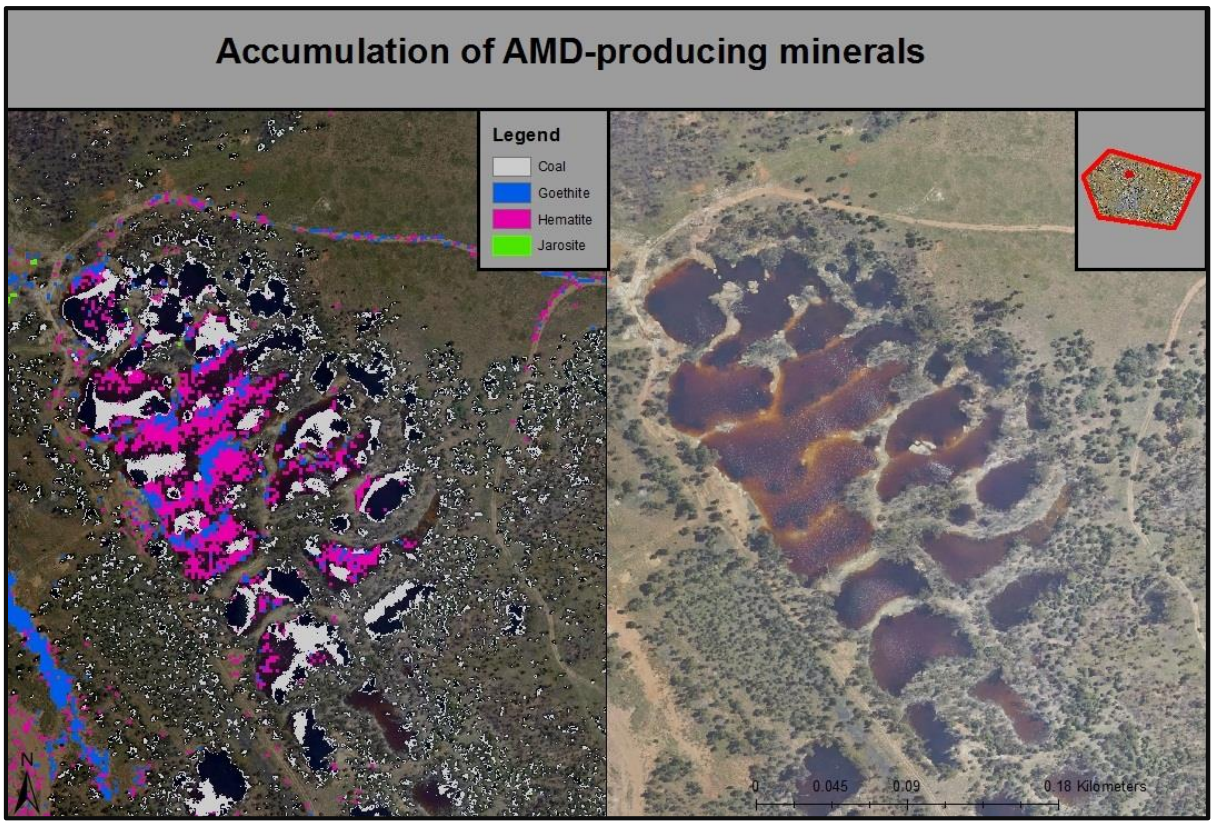

Figure 53: Accumulation of goethite, hematite and coal at ponds of decanting water

The map in Figure 41 indicates all potential AMD sources and where minerals related to AMD occur relative to where surface water flows.

Groundwater movement is from the ground towards the rivers, resulting in huge seepage zones on the western side of the map. This seepage zone is in the area where the decant point is situated. Due to the high potential of AMD in the decant pond, this area is a substantial risk for AMD affecting the groundwater. The decant water which is flowing through the residential settlement of Jakaroo Park flows into the storm water channels. This phenomenon can be seen in Figure 42. The blue block is a zoomed-in image indicating the jarosite present at the decant point, the flow path of the water within the aerial photo. AMD is also flowing in two minor rivers towards the Olifants River.

AMD sources and AMD producing minerals occur in close proximity to rivers, which can result in contamination of the rivers systems. The AMD can lead to devastation of vegetation and the eradication of aquatic flora and fauna. The AMD discharge in streams can precipitate on aquatic plants and micro-organisms, and prevents respiration, killing the plants and micro-organisms.

Subsidence where decanting water occurs in the study area can be seen in Figure 42 inside the purple block. The water in these ponds is high in goethite and hematite, which indicates the presence of AMD. In the zoomed-in aerial photo, AMD can clearly be seen as yellow-brown water

in the ponds. The water from these ponds flows downstream and connects with two other streams, thus, not only polluting one area but the entire catchment.

Water flows freely into and through masses of broken rock and coal heaps. As the water moves through these heaps, pyrite is oxidised and produces AMD. The water then decants to ground and surface water (Figure 42, yellow block). The water moves downstream and connects to the Olifants River cathment, which then further spreads the pollution.

5.4 Objective Five: Identify areas with high levels of air pollution

Remarkably high concentrations of elements were detected with concentrations high above normal averages from the data analysed by Zibret *et al*. (2013). Thus, the extremely high concentrations detected in the study area highlight the severe levels of environmental pollution in eMalahleni.

As seen from figure 43, the sample points only overlap with the eastern side of the study area. The air pollution map is therefore bias. However, to ensure more accurate results, Kriging was done with all 39 samples. It should also be mentioned that no correlation could be seen between the Kriging results and the wind direction.

It is unmistakably clear that the Cr smelter in the Ferrobank industrial area is the main source for Cr pollution (Figure 44). Ferrobank is located in close proximity to residential areas such as Ackervill and Kwa-Quqa which is approximately 1.2 km to 1.5 km from Ferrobank respectively. This is a major concern, as residence from these areas are inhaling high concentrations of Cr. According to ATSDR (2012:5) too high concentrations of Cr can damage male reproductive systems and is also known to be carcinogenic. Another concern is the agricultural lands which are situated in the northern part of the study area. As seen from the Kriging map, the agricultural land has Cr concentrations between 14 273 and 19 005 mg/kg. Cr has a harmful effect on soil microorganisms as the Cr depress their biological activities (Wyszkowska, 2002: 79).

As shown by Figure 45 and Figure 46, the V and Mn pollution source is located outside of the study area. However, V and Mn concentrations in the west of the study area are high. This is also where the industrial area of Kwa-Guqa is situated. High amounts of V which humans are exposed to can cause diarrhoea and it has been determined by the International Agency for Research on Cancer (IARC) that V is probably carcinogenic to humans (U.S. Department of Health and Human Services, 2009:6). Mn is an essential element for all living organisms; however, at such high concentrations, Mn can be a risk to the environment. It is stated by EPA (2013) that chronic inhalation exposure of humans to Mn can affect the nervous system and the respiratory system.

Figure 47 shows that Ba originates from PP1 which is the Evraz Rand Carbide plant. Zibret *et al*., 2013:4465) mentioned that Ba is associated with coal combustion. It can thus be established that the Evraz Highveld Rand Carbide plant is also a source for fly ash. However, the Ba concentrations in the study area is relatively low. Thus, Ba in the study area is not of any concern.

Li concentrations increase towards the east of the study area where a spudomene mine is located (Figure 48). The main concern is the residential area on the east of the study area. This is a major concern, as residents from these areas are inhaling high concentrations of Li. When high amounts of Li is inhaled, it can cause shortness of breath, sore throat, skin irritations, abdominal pain, nausea, vomiting and weakness (Lenntech, 2015).

5.5 Objective Six: Produce a risk map for the study area

The map presented in Figure 49 indicates all potential risks associated with coal-mining activities in the study area.

Only two air pollution sources within the study area were identified in objective 5. The first source is the Evraz Highveld Rand Carbide plant which is associated with the emission of Ba. The source is a low potential risks since the amount of Ba emitted is small. The second air pollution source is the Ferrobank Industrial area which is associated with the emission of Cr. As seen from the Kriging results (Figure 44), the amount of Cr emitted from the source is major and distributed to residential areas close by. Cr is inhaled by residence living in close proximity of the source.

All AMD sources are seen as high potential risks. The AMD follows the surface water pathway and enters the Olifants River catchment. The rivers in the study area is used by residence for swimming and even drinking, which makes the AMD in the area a high potential risk.

The area of most concern is the T&DB Colliery. Due to previous underground mining activities, numerous collapses have occurred, which resulted in additional problems such as the formation of AMD, spontaneous combustion of coal and the further collapsing of coal pillars. When studying an aerial photo of the area, it can be seen that footpaths cross over the area from the informal settlement of Kwa-Guqa to the industrial area (Ferrobank). This is a major concern as residence pass the area daily.

The second area of concern is Blesboklaagte. The Blesboklaagte colliery is situated north-east of the Ferrobank industrial area and partially underlies the informal settlement. Although not shown on the locality map, several low-cost housing developments have been established to the northwest around the local airfield as well as a small industrial area. As seen from Figure 49, the area is associated with coal fires, subsidences and AMD. Previous underground mining activities

in Blesboklaagte have left the area with numerous subsidences and coal discard dumps. A mining licence application for the area is reported to be pending. The remaining coal underground and on discard dumps is scavenged by residents for cooking (Masondo & Lelliot, 2010). However, several incidents where people were injured or died due to burns suffered after falling into burning cavities formed on the coal dumps have been reported (Masondo & Lelliot, 2010). The occurrence of subsidences in the area has caused damage to high voltage electricity pilons which can collapse at any time.

The third area of concern is the residential area of the Ackerville extension. Subsidence and coal fires occur around the housing structures. Residents are building their houses very close to subsidence features. A coal discard dump where spontaneous combusting occurs is just east of the residential area. Houses occur a few meter from the coal dump and can be damaged due to fire. The toxic gases released by the combustion of the coal can be harmfull when inhaled by the individuals.

Chapter 6: Conclusion

Mining in eMalahleni has contributed to the environmental degradation in the area, including spontaneous combustion, subsidence, AMD and air pollution. The study analysed the occurrence of environmental concerns associated with coal mining impacts. This dissertation, is an attempt to focus the attention on the problemsthe problems that surrounds the environmental impact of coal mining in eMalahleni.

The limitations of the study did not influence the quality of the study but increased the time required to complete the study. The results that were obtained from the method support the dissertation problem statement.

All the objectives of the study were successfully achieved.

With respect to objective 1 "*Conducting an extensive literature review on coal mining impacts and the detection of these impacts*": the following conclusion can be drawn:

> The literature review indicated the different concepts of coal-mining impacts, which gives a considerable amount of background on this subject. The literature review also indicated that remote sensing can be used for the detection of coal fires, LIDAR can be used for subsidence detection, hyperspectral data can be used for the detection of AMD producing minerals and that street dust can be used as an indication for the amount of air pollution.
>
> However, due to restrictions to the number of raster cells that could be mosaicked, only small areas could be compiled into TIR maps. Therefore, due to this restriction the final mosaicked image provided by EOMINERS was used in the classification step for the entire study area (Figure 34).

With respect to objective 2 "*Detecting burning underground coal fires in eMalahleni municipal area":*

> Coal fires were detected by airborne TIR remote sensing which is a simple and cost-effective management tool. Airborne TIR images captured at low altitude results in high resolution images. The high resolution allowed good quality images for the mosaicking and classification. The mosaicking and classification allowed for an easy interpretation of the TIR images. Mosaicking of the TIR image was effective and areas that are heated differently were identified in the study area. However, due to restrictions to the number of raster cells that could be mosaicked, only small areas could be compiled into TIR maps. Thus, the final mosaicked image provided by EOMINERS was used in the classification

step. The classification of the mosaicked images was successful as different potential coal fires were located.

With respect to objective 3 "*Locate subsidence in eMalahleni's municipal area":*

Subsidences were detected with LIDAR which is an active remote sensing method used to determine the distance to an object. LIDAR provides a profile of the depth of subsidences. LIDAR images were classified in a GIS programme to locate subsidences in the study area. The LIDAR layer was overlapped with a classified coal fire layer to indicate the relationship between coal fires and subsidence features. The objective was completed as four areas were identified where coal fires occur over subsidences.

With respect to objective 4 "*Identify AMD sources and the AMD pathways in drainage systems in the study area*":

Potential AMD sources were identified by using a geo-referenced aerial photo with respect to category features such as coal dumps, smelters and warm decants as well as areas where water quality parameters indicated AMD contamination. Geo-referenced layers containing hyperspectral data of AMD producing minerals, which were received from EOMINERS, was used to create a GIS layer to indicate accumulation of AMD producing minerals. Drainage channels and the potential downstream flow paths were mapped using data from EOMINERS. The data consist of a digital elevation model (DEM) of the study area. Finally the flow path layer was overlapped with the AMD source layer to produce an AMD pathway map (EOMINERS, 2013:25). The objective was achieved as the map successfully display the possible downstream movement pathways of AMD contamination from numerous sources. It was concluded that all the rivers flow towards the Olifants river catchment. AMD-producing minerals occur close to drainage channels, possibly putting them at risk of contamination.

With respect to objective 5 "*Detect air pollution sources in the study area*":

Air pollution sources in eMalahleni were determined by examining street dust samples which was received from the EOMINERS project and Zibret *et al.* (2013). The data was evaluated by means of Kriging in ArcGIS 10.2. The Kriging results were successful as the point source for Cr was identified as the Ferrobank industrial area where metal and vanadium smelters occur. The Kriging results for Mn and V indicated that that the pollution sources was from the Evraz Highveld Steel and Vanadium smelter. The Ba pollution source was identified as the Evraz Rand Carbide plant. It was concluded from the Kriging

results that the Li pollution originates from a south-easterly direction from outside the study area.

With respect to objective 6 “*Producing a risk map for eMalahleni municipal area*”:

All potential hazardous areas which was identified in objective two to five was digitized to create features. A separate ArcGIS layer was created for the potential hazardous areas. A risk rating was allocated to each potential hazard by scoring the consequence and the probability of the risk. The new layer was then classified to indicate the low, medium and high potential risks. The map successfully indicates all potential risks associated with coal mining activities. It was concluded that T&DB Colliery, Blesboklaagte and Ackerville had the highest potential risks. The T&DB collieries have abundant amounts of subsidences and AMD sources. Most of the rivers in the study area occur in this area which allows AMD to pollute drainage systems further west. Numerous coal-fires were detected in the T&DB collieries. The area is associated with air pollution due to the industrial smelter which is located nearby as well as an informal settlement south of the T&DB collieries. This is a major concern as residents from the settlement walk past the T&BD colliery daily. The second area of concern is known as Blesboklaagte. Coal fires, subsidence and AMD sources were identified in Blesboklaagte. Ackerville extension which is located south of Blesboklaagte is surrounded with subsidence which is a high risk for the residence living in the area, since subsidence can collapse at any moment and cause enormous damage to the residents of the settlement. The results is a contribution towards the understanding of the problems that occur in the eMalahleni municipal area and can be used for future town planning, especially for low cost RDP housing.

Chapter 7: Recommendations

Throughout the study a number of recommendations for future studies were identified:

- TIR remote sensing surveys should be done on a more regular interval. By doing this, the direction of the fire movement, as well as the spreading rate of the fire could be detected.
- It would be more desirable to have more temperature measurements and positions of subsidence to clearly identify a correlation between them.
- A more detailed air pollution study should be performed to more closely identify the sources and impacts on receptors.

Bibliography

ACF International. 2010. Community-based disaster risk reduction project Bicol Region, Philippines. http://www.preventionweb.net/files/13932_ACF1.pdf Date of access: 6 Nov. 2015.

Akcil, A. & Koldas, S. 2006. Acid Mine Drainage (AMD): Causes, treatment and case studies. *Journal of cleaner production*, 14(12): 1139-1145.

Akinbobola, A., Okogbue, E.C. & Olajire, O.O. 2015. A GIS-based flood risk mapping along the Niger-Benue River basin in Nigeria using watershed approach. *Ethiopian journal of environmental studies & management,* 8(6): 616-627.

Andretta, M. 2014. Some considerations on the definition of risk based on concepts of systems theory and probability. *Risk analysis: An international journal*, 34(7):1184-1195.

ATSDR (Agency for Toxic Substances and Diseases Registry). 2015. Public health statement: Chromium. http://www.atsdr.cdc.gov/ToxProfiles/tp7-c1-b.pdf Date of access: 8 August 2015.

Averill, B. & Eldredge, P. 2013. Energy sources and the environment. http://catalog.flatworldknowledge.com/bookhub/4309?e=averill_1.0-ch05_s05 Date of access: 20 March 2014.

Banerjee, D. 2014. Acid drainage potential from coal mine wastes: Environmental assessment through static and kinetic tests. *International journal of environmental science technology (IJEST)*, 11 (5):1365-1378.

Banks, V.J., Palumbo-Roe, B., Van Tonder, D., Davies, J., Fleming, C. & Chevrel, S. 2011. Conceptual models of Witbank Coalfield, South Africa. Earth Observation for Monitoring and Observing Environmental and Societal Impacts of Mineral Resources Exploration and Exploitation, CEC FP7 Project EO-MINERS, (Unpublished).

Bell, F.G., Bullock, S.E.T., Hälbich, T.F.J. & Lindsay, P. 2001. Environmental impacts associated with an abandoned mine in the Witbank Coalfield, South Africa. *International journal of coal geology* 45(2-3):195–216.

Bohling, G. 2005. Kriging. http://people.ku.edu/~gbohling/cpe940/Kriging.pdf Date of access: 18 Nov. 2015.

Bruce, C. 2004. Field guide to rocks and minerals of South Africa. Cape Town: Struik Publishers.

Carbonel, D., Rodríguez, V., Gutiérrez, F., McCalpin, J.P., Linares, R., Roqué, C., Zarroca, M., Guerrero, J. & Sasowsky, I. 2014. Evaluation of trenching, ground penetrating radar (GPR) and electrical resistivity tomography (ERT) for sinkhole characterization. *Earth surface processes & landforms,* 39(2):214-227.

Cellania, M. 2013. 5 Places that are still on fire. *Mental_Floss*, 24 Sept. http://www.mentalfloss.com/article/52869/5-places-are-still-on-fire Date of access: 2 Nov. 2015.

Coaltech Research Association & Chamber of Mines of South Africa. 2007. Guidelines for the Rehabilitation of Mined Land (Unpublished).

Cole, P. 2001. Witbank Airborne Geophysical Survey 2529CC. Report Number: 2001-0109. Council for Geoscience (Unpublished).

Cowie, R., Williams, M.W., Wireman, M. & Runkel, R.L. 2014. Use of natural and applied tracers to guise target remediation efforts in an acid mine drainage system, Colorado Rockies, USA. *Water*, 6:745-777.

CRISP (Centre for remote imaging, sensing and processing). 2014. Synthetic Aperture Radar. http://www.crisp.nus.edu.sg/~research/tutorial/mw.htm Date ofaccess: 3 Nov. 2015.

Deitchman, R.S. 2009. Thermal remote sensing of stream temperature and groundwater discharge: Applications to hydrogeology and water resources policy in the State of Wisconsin. University of Winconsin: Madisn. (Thesis-PhD).

Desk, G. 2004. Case study: Transvaal and Delegoa bay colliery, Witbank, South Africa. http://www.saiea.com/calabash/casestudies/html/delegoabay.pdf Date of access: 18 May 2013.

Dinger, J.S., Zourarakis, D.P. & Currens, J.C. 2007. Spectral enhancement and automated extraction of potential sinkhole features from NAIP imagery: initial investigations. *Journal of environmental informatics*, 10(1):22-29.

Dr Wellness. 2013. Four types of light that can dramatically improve your health. http://www.drwellnesstherapy.com/tanningbeds/article13.php Date of access: 9 April. 2014.

Driescher, A.C. 2008. A water quality study of Loskop Dam and the upper catchment of the Olifants River. University of the Free State, Bloemfontein. (Thesis- MSc).

Engelbrecht, J., Inggs, M.R. & Makusha, G. 2011. Detection and monitoring of surface subsidence associated with mining activities in the Witbank coalfields, South Africa, using differential radar interferometry. *South African journal of geology,* 114(1):77-94.

EOMINERS. 2013. Indicators and earth observation product for the assessment of the extractive industry environment and societal impacts: eMalahleni Coalfield, demonstration site. (Unpublished).

EO-MINERS. 2014a. Mpumalanga Province, South Africa. http://www.eo-miners.eu/test_sites/ts_testsite2_Witbanki.htm Date of access: 26 March 2014.

EO-MINERS. 2014b. Product examples-Witbank. http://www.eo-miners.eu/prelim_results/pr_ppd_witbank.htm Date of access: 16 July 2014.

EPA (United States Environmental Protection Agency). 2013. Manganese Compounds. http://www.epa.gov/ttnatw01/hlthef/manganes.html Date of access: 8 August 2005.

EPA (United States Environmental Protection Agency). 2014. Environmental effects of acid rain. http://www.epa.gov/region1/eco/acidrain/enveffects.html Date of access: 18 Feb. 2015.

Esri Developer Summit. 2015. ArcMap, 10.2. [Computer program]. Esri Developer Summit. 380 New York Street, Redlands.

Falcon, R.M.S. 1986a. A brief review of the origin, formation, and distribution of coal in South Africa. (*In* Anhaeusser, C.R. & Maske, S., *ed*. Mineral deposits of Southern Africa. Johannesburg: The Geological Society of South Africa. p. 1879-1898).

Falcon, R.M.S. 1986b. Classification of coals in Southern Africa. (*In* Anhaeusser, C.R. & Maske, S., *ed*. Mineral deposits of Southern Africa. Johannesburg: The Geological Society of South Africa. p. 1899-1929).

Falcon, R.M.S. 1986c. The Springs-Witbank Coalfield. (In Anhaeusser, C.R. & Maske, S., *ed.* Mineral deposits of Southern Africa. Johannesburg: The Geological Society of South Africa. p. 1869-1984).

Fan, H., Li, J., Chen, N. & Hu, C. 2015. Capabiliy representation model for heterogeneous remote sensing sensors: Case study on soil moisture. *Environmental modelling and software,* 70: 65-79.

Faux, R.N., Lachowski, H., Maus, P., Torgersen, C.E & Boyd, M.S. 2001. New approaches for monitoring stream temperature: airborne thermal infrared remote sensing. http://www.fs.fed.us/t-d/programs/im/rsac_reports/TIR.pdf Date of access: 30 May 2013.

FFF (Fossil Fuel Foundation). 2013. Outlook for the coal value chain: scenarios to 2040. http://www.fossilfuel.co.za/initiatives/2013/SACRM-Scenarios.pdf Date of access: 28 July 2014.

Finkelman, R.B. 2004. Potential health impacts of burning coal beds and waste banks. *International journal of coal geology,* 59:19-24.

Fischer, C. 2011. Field measurement guide of the Witbank TIR Flight Survey in October 2011. (Unpublished).

Foli, G., Gawu, S. & Nude, P. 2015. Arsenic contamination and secondary mineral elavuation in mine drainage using intergrated acid-base accounting and toxicity characterisation leaching procedure: The case of Obuasie mine, Ghana. *Environmental eartch science,* 73(12):8471-8486.

Girgin, S. & Krausmann, E. 2013. RAPID-N: Rapid natech risk assessment and mapping framework. *Journal of loss prevention in the process industries*, 26: 949-960.

Geohunt. 2015. Electrical resistivity survey. http://www.geocities.ws/demon_x17/ersurvey.html Date of access: 15 Nov. 2015

Geoexpert Ag. 2015. Reflection seismic surveying. http://www.geoexpert.ch/reflection-seismic.html Date of access: 15 Nov.2015.

Geosiam Geophysical Services. 2015. Airborne EM Survey. http://geosiamservices.com/services/airborne-services/airborne-em-survey/ Date of access: 11 Nov. 2015.

Geoview. 2012. Ground penetrating radar. http://geoviweinc.com/methods/land/ground-penetrating-radar Date of access: 5 Nov. 2015.

Gregersen, E. 2014. LIDAR. http://global.britannica.com/technology/lidar Date of access: 6 Oct. 2015.

Gulson, B., Anderson, P. & Taylor, A. 2013. Surface dust wipes are the best predictors of blood leads in young children with elevated blood lead levels. *Environmental research,* 126: 171-178

Gutiérrez, F., Galve, J.P., Lucha, P., Castañeda, C., Bonachea, J. & Guerrero, J. 2011. Integrating geomorphological mapping, trenching, InSAR and GPR for the identification and characterization of sinkholes: A review and application in the mantled evaporite karst of the Ebro Valley (NE Spain). *Geomorphology*, 134:144-156.

Hann, S., Koellensperger, G. & Popp, M. 2012. Environmental application of elemental speciation analysis based on liquid or gas chromatography hyphenated to inductively coupled plasma mass spectrometry: a review. *Analytica Chimica Acta,* 688:114-129.

Harrington, A.D., Tsirka, S.E. & Schoonen, M.A.A. 2013. Infammatory stress response in A549 cells as a result of exposure to coal: evidence for the role of pyrite in coal workers' pneumoconiosis pathogenesis. *Chemospere,* 93(6): 1216-1221.

Harris, R. 1987. Satellite Remote Sensing: An introduction. , London: Routledge & Kegan Paul.

Hebblewhite, B. 2009. Outcomes of the independent inquiry into impacts of underground coal mining on natural features in the Southern coalfield- an overview. http:ro.uow.edu.au/coal/90 Date of access: 20 May 2014.

Hocking, A. 1995. Durnacol: The story of Durban Navigation Collieries. South Africa: Hollards Corporate.

HOMEF (Health of Mother Earth Foundation). s.a. Walking-caves-fire. http://www.homef.org/article/walking-caves-fire#sthash.nsBOBjNX.dpuf Date of access: 25 March 2014.

Howladar, M.F. & Hasan, K. 2014. A study on the development of subsidence due to the extraction of 1203 slice with its associated factors around Barapukuria underground coal mining industrial area, Dinajpur, Bangladesh. *Environmental earth science journal*, 72(1): 3699-3713.

Hubbard, D. & Evans, D. 2010. Problems with scoring method and ordinal scales in risk assessment. *IBM journal for research and development,* 54(3): 1-10.

Huang, L. & Gui, B. 2014. Discussion on air pollution and its control measures. *Advanced materials research*, 1010-1012:839-842.

HVC (HyVista Corporation). 2012. Hyperspectral theory. http://www.hyvista.com/?page_id=276 Date of access: 17 Feb. 2015.

Idowu, O.A., Lorentz, S.A., Annandale, J.G., McCartney, M.P. & Jovanovic, N.Z. 2008. Assessment of the impact of irrigation with low-quality mine water on virgin and rehabilitated soils in the Upper Olifants Basin. *Mine water and the environment*, 27(1): 2-11.

ISDR (International Strategy for Disaster Reduction). 2009. UNISDR terminology on disaster risk reduction. http://www.unisdr.org/files/7817_UNISDRTerminologyEnglish.pdf Date of access: 11 Nov. 2015.

ISU (Iowa State University). 2008. Global warming-impact on greenhouse gasses. https://www.extention.iastate.edu/agdm/articles/other/TakMar08/html Date of access: 2 Nov. 2015.

Janse van Rensburg, R. 2003. A long-term acid mine drainage water management strategy for South Witbank Colliery, Mpumalanga. University of Johannesburg. (Thesis: MSc)

(JARS) Japan Association of Remote Sensing. 1996. Pushbroom Scanner. http://wtlab.iis.u-tokyo.ac.jp/~wataru/lecture/rsgis/rsnote/cp2/cp2-11.htm Date of access: 1 November 2015.

Jensen, J.R. 2007. Remote sensing of the environment: An Earth resource perspective. 2nd ed. Upper Saddle River, NJ: Pearson Prentice-Hall

Johnson, M.R., Van Vuuren, C.J., Visser, J.N.J., Cole, D.I., Wickens, H.D.V., Christie, A.D.M., Roberts, D.L. & Brandl, G. 2006. Sedimentary rocks of the Karoo Supergroup. (*In* Johnson, M.R., Anhaeusse, C.R. & Thomas, R.J. The Geology of South Africa. Johannesburg: The Geological Society of South Africa. p. 461-499).

Jones, T., Wlodarczyk, A., Koshy, L., Brown, P., Longyi, S. & BéruBé, K. 2009. The geochemistry and bioreactivity of fly ash from coal-burning power stations. *Biomarkers*, 14: 45-48.

Kiernan, K. 1989. Sinkhole hazards in Tasmania. (*In* Beck, B.F., *ed.* 1989. Engineering and environmental impacts of sinkholes and karst. Netherlands: A.A. Balkema Publishers. p. 123-128).

Klein, C. & Dutrow, B. 2008. Mineral Science. New Jersey: John Wiley & Sons, Inc.

Khan, F.J. 2014. Coal worker's pneumoconiosis. http://emedicine.medscape.cpm/article/297887-overview Date of access: 3 Nov. 2015.

Kovacs, M., Toth, L., Gheție, G., Drăghici, A., Vasiu, T. & Laurențiu, G. 2014. Best management practices applied to prevent and reduce concentrations of dust and gases released from power plants. *Environmental engineering &* management journal (EEMJ), 13(6):1421-1426.

Kubiak, M. & Dzieszko, P. 2012. Using thermal remote sensing in environmental studies. *Transactions in GIS*, 16(5):715-732.

Kuenzer, C., Zhang, J., Li, J., Voigt, S., Mehl, H. & Wagner, W. 2007. Detecting unknown coal fires: Synergy of automated coal fire risk area delineation and improved thermal anomaly extraction. *International journal of remote sensing*, 28(20):4561-4585.

Lee, D., Mojtabai, N., Lee, H. & Song, W. 2013. Assessment of the influencing factors on subsidence at abandoned coal mines in South Korea. *Environmental earth sciences*, 68(3):647-654.

Lenntech. 2015. Chemical properties of lithium- health effects of Lithium- environmental effect of lithium. http://www.lenntech.com/periodic/elements/li.htm Date of access: 8 Dec. 2015.

Li, L., Luo, K., Liu, Y. & Xu, Y. 2012. The pollution control of fluorine and arsenic in roasted corn in "coal-burning" fluorosis area Yunnan, China. *Journal of hazardous materials*, 229-230:57-65

Li, X., Hui, N., Shen, H., Fu, Y. & Zhang, L. 2015. A robust mosaicking procedure for high spatial remote sensing images. ISPRS journal of photogrammetry and remote sensing, 109: 108-125.

Lillesand, T.M. & Kiefer, R.W. 1994. Remote Sensing and Image Interpretation. 3rd ed. Canada: John Wiley & Sons.

Lloyd, P.J. 2002. Coal mining and the environment. Energy research insyitute, Univeristy of Cape Town. (Unpublished).

Mashaba, S. 2012. Saved from mine dump: woman's mud terror finally over. *Sowetan Live*. 25 Jun. http://www.sowetanlive.co.za/news/2012/06/25/saved-from-mine-dump---woman-s-mud-terror-finally-over Date of access: 25 Oct. 2013.

Masondo, S. & Lelliot, J. 2010. Deseted mines a flaring death trap. *Times Live*, 11 Jan. http://www.timeslive.co.za/news/2010/01/11deserted-mines-a-flaring-death-trap Date access: 6 Nov. 2015.

McCarthy, T.S. 2011. The impact of acid mine drainage in South Africa. *South African journal of science,* 107(5/6):1-7.

McCarthy, T. & Rubidge, B. 2005. The Story of Earth and Life: A Southern African perspective on a 4.6-billion-year journey. Johannesburg: Struik Nature.

Mehdad, E. & Kleijnen, J.P.C. 2015. Classic kriging versus kriging with bootstrapping or conditional simulation: Classic kriging's robust confidence intervals and optimization. *Journal of the operational research society*, 66(11):1804-1814.

MicroImages. 2013. TnTmips, 2013. [Computer program]. MicroImages, 13th Street, Lincoln, United States of America.

Miraliakbari, A., Hahn, M & Engels, J. 2010. Development of a Low–Cost Sensor System for Use on Gyrocopters. http://www.isprs.org/proceedings/XXXVIII/part1/03/03_01_Paper_201.pdf Date of access: 30 May 2013.

Mistry, P. 2005. The applicability of remote sensing methods for the detection of fires on coal discard dumps. University of the Witwatersrand. (Dissertation-MSc).

Monroe, J.S., Wicander, R. & Hazlett, R. 2007. Physical geology: exploring the Earth. 6th ed. Belmont, USA: Thomson Brooks/Cole.

Moon, C., Sung, Y., Ahn, S., Kim, T., Choi, G. & Kim, D. 2013. Thermochemical and combustion behaviours of coal of different ranks and their blends for pulverized-coal combustion. *Applied thermal engineering*, 54(1): 111-119.

Morais, C.D. 2012. GIS data explored-vector and rater data. http://www.gislounge.com/geodatabases-explored-vector-and-raster-data Date of access: 15 Nov. 2015.

Muaka, J.J.M. 2013. Investigation into the magnitude and direction of ground stresses in the coalfields and their impact on safety and productivity. University of the Witwatersrand. (Dissertation-MSc).

Munk, J & Sheets, R.A. 1997. Detection of underground voids in Ohio by use of geophysical methods. http:www.pubs.usgs.gov/wri/1997/4221/report/pdf Date of access: 8 Dec. 2015.

Murad, E. & Rojik, P. 2004. Jarosite, schwertmannite, goethite, ferrihydrite and lepidocrocite: the legacy. Paper presented at the Australian New Zealand Soils Conference, 5-9 December. http://www.regional.org.au/au/asssi/supersoil2004/s1/oral/1088_murade.htm Date of access: 1 June 2015.

Nkosi, P. 2001. Dead fish trouble water officials. *News24*, 29 Jan. http://www.news24.com/xArchive/Archive/Dead-fish-trouble-water-officials-20010129 Date of access: 29 October 2015.

Ochieng, G.M., Seanego, E.S. & Nkwonta, O.I. 2010. Impacts of mining on water resources in South Africa. *Scientific research and essays*, 5(22):3351-3357.

OSHA (Occupational Safety and Health Administration). 2005. OSHA fact sheet. http://www.osha.gov/OshDoc/data_hurricane_Facts/hydrogen_sulfide_fact.pdf Date of access: 7 Dec. 2015.

Oxford Dictionary of Geology and Earth Sciences. 2013. 4th ed. United Kingdom: Oxford University Press.

Pazuniak, B.L. 1989. Subsurface investigation response to sinkhole activity at an eastern Pennsylvania site. (*In* Beck, B.F., *ed.* 1989. Engineering and environmental impacts of sinkholes and karst. Netherlands: A.A. Balkema Publishers. p. 263-269).

Penney, K., Mohamedelhassan, E. & Catalan, L.J.J. 2014. Utilization of coal/biomass fly ash and glacial till soil as a flow-through reactive barrier for the treatment of acid mine drainage. *Journal of solid waste technology and management*, 39(4):244-253.

Peeters, L. 2014. A background color scheme for piper plots to spatially visualize hydrochemical patterns. *Groundwater, 52(1): 2-6.*

Pinetown, K.L., Ward, C.R. & Van, D.W. 2007. Quantitative evaluation of minerals in coal deposits in the Witbank and Highveld coalfields, and the potential impact on acid mine drainage (author abstract). *International journal of coal geology,* 70 (1-3):166-183.

Pone, J.D.N., Hein, K.A.A., Stracher, G.B., Annegarn, H.J. & Finkelman, R.B. 2007a. Potential environmental and health impacts of burning coal in Witbank Coalfield, South Africa. (Unpublished).

Pone, J.D.N., Hein, K.A.A., Stracher, G.B., Annegarn, H.J., Finkelman, R.B., Blake, D.R., McCormack, J.K. & Schroeder, P. 2007b. The spontaneous combustion of coal and its by-products in the Witbank and Sasolburg coalfields of South Africa. *International journal of coal geology*, 72(2):124-140.

Poteet, D.R. 1989. Using terrain conductivity to detect subsurface voids and caves in a limestone formation. (*In* Beck, B.F., *ed.* 1989. Engineering and environmental impacts of sinkholes and karst. Netherlands: A.A. Balkema Publishers. p. 271-279).

PSR (Physicians for Social Responsibility). 2009. Coal pollution damages human health at every stage of coal life cycle, reports Physicians for Social Responsibility. http://www.psr.org/news-events/press-releases/coal-pollution-damages-human-health.html Date of access: 8 Oct 2013.

Qi, X., Wang, D., Xin, H. & Zhong, X. 2013. Environmental hazards of coal fire and their prevention in China. *Environmental engineering and management journal*, 12(10):1915-1919.

Quental, L., Sousa, A.J., Marsh, S., Brito, G. & Abreu, M.M. 2011. Imaging spectroscopy answers to acid mine drainage detection at S. Domingos, Iberian pyrite belt, Portugal. *Comunicaçõe geológicas*, 98(8):61-71.

Rahn, P.H. 1985. Engineering Geology: An environmental approach. NJ: Elsevier Science Publishing Company.

Roelofse, C.J. 2011. TIR Airborne Thermography: understanding the basics and limitation TIR technology. Kanopy Kopanao Energy Resources (Pty) Ltd. (Unpublished).

Roelofse, C.J. 2013. Research on Witbank [personal interview]. 25 Feb 2013. Witbank, South Africa. (Unpublished).

Salmanzadeh, M., Saeedi, M., Li, L.Y. & Nabi-Bidhendi, G. 2015. Characterixation and metals fraction of streer dust samples from Tehran, Iran. *International journal of environmental research,* 9(1):213-224.

Sambandam, B., Islam, V.I.H., Raman, P., Bhattacharjee, M., Balasubramanian, A. & Thiyagarajan, D. 2014. Coal fly ash nanoparticles induced cytotoxicity and oxidative DNA damage and apoptosis in change liver cells. *African journal of pharmacy and pharmacology*, 8(32):801-808.

Schmidt, S. 2008. Coal deposits of South Africa - the future of coal mining in South Africa. http://www.geo.tu-freiberg.de/oberseminar/os07_08/stephan_Schmidt.pdf Date of access: 25 Feb. 2014.

Sheets, R.A. 2002. Use of electrical resistivity to detect underground mine voids in Ohio. http://www.oh.water.usgs.gov/reports/wrir/wrir02-4041.pdf Date of access: 7 Nov. 2015.

Sherwood, A & Philips, J. 2012. Coal and coal mining- the nature of coal. http://www.TeAra.govt.nz/en/coal-and-coal-mining/page-1 Date of access: 12 Feb. 2014.

Singer, M. 2010. Changing conception of South Africa coal-based pollution. With special refrence to the Witbank coalfield, 1906-1978. University of Witwatersrand: Johannesburg. (Thesis-MSc).

Singh, Y. 1989. Sinkholes (dolines) in Bhander limestone around Rewa, central India, and their environmental significance. (*In* Beck, B.F., *ed.* 1989. Engineering and environmental impacts of sinkholes and karst. Netherlands: A.A. Balkema Publishers. p. 47-52).

Silva, R., Castro, C.D., Petter, C.O., & Schneider, I.A.H. 2011. Production of Iron Pigments (Goethite and Haematite) from Acid Mine Drainage. (*In* Rüde, R.T., Freund, A & Wolkersdorfer, *ed*. 2011. Mine water-managing the challenges. Aachen, Germany: International Mine Water Association (IMWA). p. 469-473).

Smith, D.A.M. & Whittaker, R.R.L.G. 1986. The Springs-Witbank Coalfield. (*In* Anhaeusser, C.R. & Maske, S., *ed*. Mineral deposits of Southern Africa. Johannesburg: The Geological Society of South Africa. p. 1969-1984).

Smith, R.B. 2006. Mosaicking Easter geodata: tutorial. http://www.microimages.com/getstart/pdf/mosaic.pdf Date of acccess: 8 Aug. 2013.

Smith, R.B. 2012. Introduction to Remote Sensing of Environment (RSE). http://www.microimages.com/documentation/Tutorials/introrse.pdf Date of access: 9 April 2014.

South Africa. 1996. Constitution Act 108 of 1996.

South Africa. 2002. Mineral and Petroleum Resource Development Act 28 of 2002.

South Africa. 2010. Department of Environmental Affairs. Highveld priority area air quality management plan executive summary. Pretoria.

Stratten, T. 1986. Environmental and stratigraphic setting of the Karoo Basin and its mineral deposits. (*In* Anhaeusser, C.R. & Maske, S., *ed*. Mineral deposits of Southern Africa. Johannesburg: The Geological Society of South Africa. p. 1863-1874).

Stewart, M. & Troksie, K. 2006. Proposed power station and associated infrastructure Witbank geographical area, hydrogeological investigation. (Unpublished).

Sugimoto, N., Nishizawa, T., Shimiza, A., Matsui, I. & Kobayashi, H. 2015. Detection of i nternally mixed Asian dust with air pollution aerosols using a polarization optical particle counter and a polarization-sensitive two-wavelength LIDAR. *Journal of quantitative spectroscopy and radiative transfer*, 150(1): 107-113.

Swayze, G.A., Desborough, G.A., Smith, K.S., Lowers, K.S., Hammarstorm, J.M., Diehl, S.F., Leinz, R.W. & Driscoll, R.L. 2008. Understanding Jarosite- from mine waste to mars. (*In* Verplanck, P.L., *ed*. Understanding contaminates associated with mineral deposits).

Tindall, J. 2006. Deconvolution of plant type(s) for homeland security enforcement using remote sensing on a UAV collection platform. https://www.hsaj.org/articles/175 Date of access: 9 Dec. 2015.

Universal coal plc. 2012. Coal mining in South Africa. http://www.universalcoal.com/projects/coal-mining-in-south-africa/ Date of access: 8 Oct. 2013.

U.S. Department of Health and Human Services. 2009. Toxicological profile for vanadium. http://www.atsdr.cdc.gov/toxprofiles/tp58.pdf Date of use: 8 August 2015.

USGS (United State Geological Survey). 2009. Emissions from coal fires and their impact on the environment. http://pubs.usgs.gov/fs/2009/3084/pdf/fs2009-3084.pdf Date of access: 29 Aug. 2013.

Van Der Meer, F.D., Van Der Werff, H.M.A., Van Ruitenbeek, F.J.A., Hecker, C.A., Bakker, W.H., Noomen, M.F., Van Der Meijde, M., Carranza, E.J.M., De Smeth, J.B. & Woldai, T. 2012. Multi-and hyper-spectral geologic remote sensing: A review. *International journal of applied earth observation and geoinformation*, 14(1): 112-128.

Van Dijk, P., Zhang, J., Jun, W., Kuenzer, C. & Wolf, K. 2011. Assessment of the contribution of in-situ combustion of coal to greenhouse gas emission; based on a comparison of Chinese mining information to previous remote sensing estimates. *International journal of coal geology*, 86(1):108-119.

Van Tonder, D.M. 2011. EO-MINERS: Mpumalanga coalfield, South Africa field visit 2011. Earth Observation for Monitoring and Observing Environmental and Societal Impacts of Mineral Resources Exploration and Exploitation (EO-MINERS), 170 pp (Unpublished).

Venkatanarayana, B. & Rao, T.V. 1989. Geological and geophysical investigation for delineating karstic structures in south-western portion of Cuddapah Basin, Andhra Pradesh, India. (*In* Beck, B.F., *ed.* 1989. Engineering and environmental impacts of sinkholes and karst. Netherlands: A.A.Balkema Publishers. p. 59-64).

Vermeulen, P.D & Usher, B. 2009. Operation and monitoring guidelines and the development of a screening tool for irrigating with coal mine water in Mpumalanga Province, South Africa. *Water SA,* 35(4):379-386.

Wanning, W., Yong, Z., JiaHua, Z., Jay, G. & JunLiang, H. 2014. A temperature inversion-induced air pollution process as analyzed from mie LIDAR data. *Science of the total environment*, 479/480: 102-108

Wenhua, P. & Ruxiang, Q. 2014. Coal spontaneous combustion mechanism and research of new flame retardant material. *Applied mechanics & materials*, (513-517):156-160.

Wessels, R.L., Vaughan, R.G., Patrick, M.R. & Coombs, M.L. 2013. High-resolution satellite and airborne thermal infrared imaging of precursory unrest and 2009 eruption at redoubt volcano, Alaska. *Journal of volcanology & geothermal research,* 259: 248-269.

WWW (World Wide Fund for Nature). 2011. Coal and water futures in South Africa- the case for protecting headwaters in the Enkangala grasslands.

http://awsassets.wwf.org.za/downloads/wwf_coal_water_report_2011_web.pdf Date of access: 15 Nov. 2015.

Wyszkowska, J. 2002. Soil contamination by chromium and its enzymatic activity and yielding. *Journal of environmental studies,* 11(1):79/84.

Yang, G., Wu, X., Yang, Y., Lijiang, X., Fang, S. & Jiyong, Z. 2014. Comprehensive treatment of coal waste piles with spontaneous combustion. *Applied mechanics & materials*, (533):384-389.

Zhang, J. 2004. Spatial and statistical analysis of thermal satellite imagery for extraction of coal fire related anomalies. Vienna University of Technology: Gliching. (Thesis-PhD).

Zhang, X. 1998. Coal fires in Northwest China – detection, monitoring and prediction using remote sensing data. Technische Universiteit Delft, ITC Publication No 58. (Thesis-PhD).

Žibret, G., Van Tonder, D & Žibret, L. 2013. Metal content in street dust as a reflection of atmospheric dust emissions from coal power plants, metal smelters, and traffic. *Environmental science and pollution research*, 20(7):4455-4468.